THERMALLY CONDUCTIVE POLYETHYLENE-HEXAGONAL BORON NITRIDE NANOCOMPOSITES FOR HEAT EXCHANGERS APPLICATIONS

A Thesis

by

MEHAMED SALIH ABDELA ALI

Submitted to the Office of Graduate and Professional Studies of
Texas A&M University
in partial fulfillment of the requirements for the degree of

MASTER OF SCIENCE

Chair of Committee,	Ahmed Abdala
Committee Members,	Ioannis Economou
	Bilal Mansoor
	Micah Green
Head of Department,	Arul Jayaraman

December 2019

Major Subject: Chemical Engineering

ABSTRACT

Compared to metals, polymers are less susceptible to corrosion and scale formation caused by high salinity water. Therefore, replacing metals with polymers in heat exchangers that use seawater would result not only in mitigating the corrosion problems but also in substantial cost savings because of the low price and density of polymers. However, the low thermal conductivity of polymers must be significantly increased for their application as heat transfer surfaces. Herein, thermally conductive polyethylene nanocomposites based on hexagonal boron nitride (h-BN) and their 2-D exfoliated nanosheets were prepared by melt blending using twin-screw extruder and dry mixing using ball milling. h-BN was successfully exfoliated to h-BNNS *via* ball milling technique. In addition, h-BN exfoliation was optimized by studying the effect of milling time on the h-BN crystallite size, particle thickness, and h-BNNS yield. Subsequently, the impact of h-BN sheet size, thickness, and loading as well as the h-BN composite processing method on the physical and thermomechanical properties of polyethylene (PE) composites were studied.

It was found that the incorporation of h-BN enhanced the thermal conductivity, thermal stability, and mechanical properties of PE composites. Moreover, milled h-BN/PE composites showed better thermal conductivity and mechanical properties improvement compared to the bulk h-BN/PE composites. After successfully aligning h-BN particles, maximum thermal conductivity enhancement of over 1300 % was achieved. Conversely, the incorporation of h-BN was detrimental to the wettability of h-BN/PE composites. Nevertheless, the wettability of the composites was improved by plasma treatment.

Particularly, the CA of 50 wt. % h-BN/LLDPE composite decreased from 107.6º±2.57º in the untreated to 21.05º±2.34º after the plasma treatment. Furthermore, this treatment showed only slight deterioration with aging demonstrating good applicability. Our results indicate that low cost polymer heat exchanger for seawater desalination can be a reality.

DEDICATION

This thesis is dedicated to my family and friends. Special appreciation to my beloved mom and to the memory of my father who supported me through my academic life.

ACKNOWLEDGEMENTS

I would first like to thank my supervisor Dr. Ahmed Abdala for his continuous support throughout the course of the Master's program. Besides, I would like to thank Dr. Ioannis Economou, Dr. Micah Green, and Dr. Bilal Mansoor for being part of my committee. I would also like to thank my colleagues for the research ideas, support, and encouragement. I would also like to specially thank my colleague Dr. Chaudry for his research guidance as well as experimental support without which this work would not have been possible.

I would like to take this opportunity to show my gratitude and appreciation to the Graduate Office for funding part of my Master's courses and the National Priorities Research Program (NPRP) for funding this project. In addition, I would like to thank QAPCO for their kind cooperation.

I would like to thank Qatar Environment and Energy Research Institute (QEERI) for allowing me to carry out some characterization tests that were essential to this project. I would like to specially thank Dr. Said Mansour, Dr. Ayman Samara, Mr. Omar Al Hassan, Mr. Mohamed Hilal, Mr. Mujaheed Pasha, Mr. Yahya Zakaria, and Mr. Janarthanan Ponraj for their help and support. I would also like to thank Dr. Yiming Wubulikasimu at TAMUQ for providing me training to run the equipment and for helping me analyze the results obtained. Finally, I would like to thank Dr. Patrik and Eng. Asma at Qatar University (QU), and Dr. Lakshmi and Dr. Vasanth at TAMUQ for their kind cooperation.

Finally, many thanks to my parents, family, and friends for their continuous support, help, and encouragement.

CONTRIBUTORS AND FUNDING SOURCES

This project was funded by a NPRP award [NPRP # 10-0205-170349] from the Qatar National Research Fund (a member of Qatar Foundation).

This thesis was supervised by Dr. Ahmed Abdala, Dr. Ioannis Economou, Dr. Micah Green, and Dr. Bilal Mansoor. The TEM, part of the SEM, and DSC analyses were done in QEERI. The SEM, XRD, AFM, TGA, and thermal conductivity analyses were conducted in TAMUQ. The mechanical test was conducted in QU and TAMUQ. The contact angle measurement was performed in QU.

NOMENCLATURE

2D	Two Dimensional
AFM	Atomic Force Microscopy
BN	Boron Nitride
BM	Ball Milling
BMd	Ball Milled
CA	Contact Angle
h	Hours
HDPE	High Density Polyethylene
h-BN	Hexagonal Boron Nitride
h-BN6	Hexagonal Boron Nitride (6 µm)
h-BN35	Hexagonal Boron Nitride (35 µm)
80%h-BN	80 wt. % h-BN-20 wt. % LLDPE
80%h-BN35	80 wt. % h-BN35-20 wt. % LLDPE
IPA	Isopropanol
λ	Thermal Conductivity
LDPE	Low Density Polyethylene
LLDPE	Linear Low-Density Polyethylene
MB	Melt Blending
MED	Multi-Effect Distillation
MSF	Multistage Flash
PE	Polyethylene

SEM	Scanning Electron Microscopy
TEM	Transmission Electron Microscopy
XPS	X-ray Photoelectron Spectroscopy
XRD	X-ray Diffraction

TABLE OF CONTENTS

Page

LIST OF FIGURES

Page

LIST OF TABLES

Page

1. INTRODUCTION AND LITERATURE REVIEW

1.1. Introduction

Inspired by the successful isolation of graphene from graphite by mechanical cleavage exfoliation in 2004, other 2D materials has gained significant interest in the scientific community [1]. 2D nanomaterials such as graphene and hexagonal boron nitride nanosheets (h-BNNSs) have extraordinary and exceptional properties [2], which enables their application in various fields including but not limited to electronics packaging , thermal managements, nanocomposites, and filtrations [3][4][5][6][7][8].

Recently, hexagonal boron nitride nanosheets (h-BNNSs) has been intensively researched. h-BNNSs is an isoelectronic analogue to graphene, usually named white graphene [9]. Similar to graphene, h-BNNSs possess high mechanical, physical, and thermal properties, but unlike graphene h-BNNSs have a wide band gap and better thermal stability [9][10][11]. The combination of these valuable properties play a major role in their various applications, such as a dielectric substrate for electronic devices [5][12], ceramics [13][14], nanocomposites [15], coating [16], lubricants [17], cosmetics [18] and automotive [19]. Driven by the wide range of h-BN applications, the global market of h-BN is expected to grow above $900 million by the year 2023.

This thesis research aims to synthesize thermally conductive polyethylene nanocomposites for utilization as heat transfer surfaces. To do so, h-BN and their 2D nanosheets were incorporated into the polymer matrix via melt blending and dry ball milling. To study the effect of h-BN loading, particle size, and thickness on the nanocomposite properties, h-BNNSs synthesis were optimized by studying the effect of

milling time on the h-BNNSs yield, crystallite size, and particle thickness. Subsequently, the impact of incorporating this material on the nanocomposite properties, including thermal conductivity, thermal stability, tensile strength, and wettability was also investigated.

1.1.1. Motivation

Qatar meets its water demand mostly by the desalination of seawater. For instance, seawater desalination provides 99 % of the total domestic water demand in Qatar [20][21], mainly by utilizing thermal desalination processes such as multistage flash (MSF) and Multi-Effect Distillation (MED) desalination [22]. Metal heat exchangers used in these processes suffers from extreme corrosion, scaling, and fouling due to the high salinity of the Arabian Gulf Sea. These problems are currently mitigated by using corrosion-resistant exotic metals or metal alloys, such as Cu-Ni alloy and Titanium, and by frequent cleaning and scale removal leading to a high capital and operating cost. A less common but a very good alternative to metals are polymers, being relatively resistant to seawater corrosion, fouling, and scaling. Furthermore, other polymer attributes such as lightweight, low cost, and ease of fabrication provide additional benefits, which play role in the reduction of the total cost. However, polymers have poor thermal and mechanical properties. Nevertheless, these properties can be enhanced by the incorporation of thermally conductive fillers inside the polymer matrix.

1.1.2. Overview of Polymer Heat Exchangers

In the past few decades, polymer heat exchangers have been intensively studied due to their corrosion resistance, lightweight, low cost, and ease of fabrication [23][24].

However, the thermal and mechanical properties of polymer is poor and inferior to metals. Therefore, it is desirable to fabricate polymers with enhanced properties that are comparable to metals and their alloys.

In general, the performance of heat exchangers is dictated by their overall heat transfer coefficient (U), which is given by:

$$\frac{1}{U} = \frac{1}{h_i} + \frac{1}{h_0} + \frac{t}{\lambda_i} + \frac{1}{F} \qquad 1.1$$

where 'h_i' and 'h_0' are the inner and the outer convective heat transfer coefficients, (t) is the wall thickness, ' λ_i' is the thermal conductivity, and 'F' is the fouling factor. As shown in eqn. 1.1, U depends on the thermal conductivity, wall thickness, and fouling. However, the thermal conductivity of most polymers is in the range of 0.1- 0.5 W m^{-1} K^{-1} which is approximately 35-500 times lower than that of metals commonly utilized in corrosive environments [24][25]. Particularly, the thermal conductivities of stainless steel, titanium, and Cu-Ni (90/10) alloys are 52-57, 17, and 50 W m^{-1} K^{-1}, respectively [24].

Beside the thermal conductivity, U can be improved by reducing the heat exchanger's wall thickness. Scheffler and Leao reported that 20-50 µm thick high density polyethylene (HDPE) and polypropylene films have approximately 60-105 % of the U value of 1 mm thick Cu-Ni alloy depending on the internal and external convection coefficients [26]. Similarly, Christmann *et al.* indicated that 25 µm polyetheretherketone film resulted in a conductive thermal resistance comparable to 1.5 mm thick stainless steel [27]. In addition, they reported that this film thickness with a proper spacer geometry offers adequate mechanical stability in MED plant. With that being said, the relatively low yield strength of most polymers limits the minimum allowable wall thickness.

Therefore, there is a need to enhance the thermal conductivity and lower the wall thickness to the extent that both high U value and physical integrity of the heat exchanger are achieved.

1.2. Literature Review

1.2.1. Polymer Composites Used for Thermal Management Applications

Polymers and polymer composites are widely used industrially and in our daily life including in electronics, pipes, trash bins, and sport goods. Polymers are macromolecules made of sequences of several atoms or subunits, mainly carbon and hydrogen, linked to each other. Compared to metals or ceramics, polymers have low density and melting point, which makes their processing relatively easy [28]. Moreover, polymers are ductile and flexible, and hence they can be fabricated into complex shapes. Polymer attributes such as light weight, corrosive resistance, electrical resistivity, ease of fabrication, and low cost make them very attractive for many applications [29][30]. One of the most important applications of polymer composites is in thermal dissipation management of electronic devices. Recently, thermal management applications of polymers have remarkably increased, such as in electronics, heat exchangers, appliances and machinery [31]. However, the thermal conductivity of polymers is very low due to their amorphous structure, backbone, defects, and type of bonds. Thus, it is important to address heat transport mechanisms in polymers and their composites.

1.2.2. Thermal Conductivity

Fourier's law of heat of conduction, states that the conductive heat flux is proportional to the temperature gradient [32]. In one dimension the conductive heat flux is written as:

$$q = -\lambda \frac{dT}{dy} \quad 1.2$$

where 'q' is the conductive heat flux, 'λ' is the thermal conductivity, and '$\frac{dT}{dy}$' is the temperature gradient. Heat transfer in solid is mainly quantified by the thermal conductivity, which defines how fast heat energy is transported through a material. The thermal conductivity (λ) can be expressed by:

$$\lambda = \alpha \rho C_p \quad 1.3$$

where 'α' is the thermal diffusivity, 'ρ' is the density, and 'C_p' is the specific heat capacity at constant pressure [33].

1.2.2.1. Mechanism of Thermal Conductivity

In solids, heat can be transferred by electrons, phonons i.e. crystal lattice vibrations, electromagnetic waves, spin waves, or other excitations [34]. The most important parameter of heat transfer in solids is the thermal conductivity. Usually, the total thermal conductivity is written as the sum of all excitation components:

$$\lambda = \sum_i \lambda_i \quad 1.4$$

where *i* represents an excitation component [34].

Electrons are the dominant heat transporter in metals, while phonons are the major contributors in insulators i.e. polymers [29][34]. The thermal conductivity can be estimated by Debye equation:

$$\lambda = \frac{C_v v l}{3} \qquad 1.5$$

where 'C_v' is the specific heat capacity per unit volume, 'v' is the phonon velocity, and 'l' is the phonon mean free path [29][35].

When an atom is heated it gains a vibrational energy (speed), part of the energy is transferred to an adjacent atom inducing a vibrational energy in the adjacent atom, leading to a further propagation which in turns induce another propagation to cover the entire material [35]. These atomic vibrations are called Phonons. Phonons depend on many factors, including crystal structure, dislocations, defects, grain boundaries, and molecular bond [34][35]. Defects, dislocations, and grain boundaries are the major causes of thermal interface resistance. For instance, the irregularities in crystal structure, which can be interpreted as discontinuity of atomic vibrations, are the major causes of phonon scattering, as shown in Fig. 1, [35].

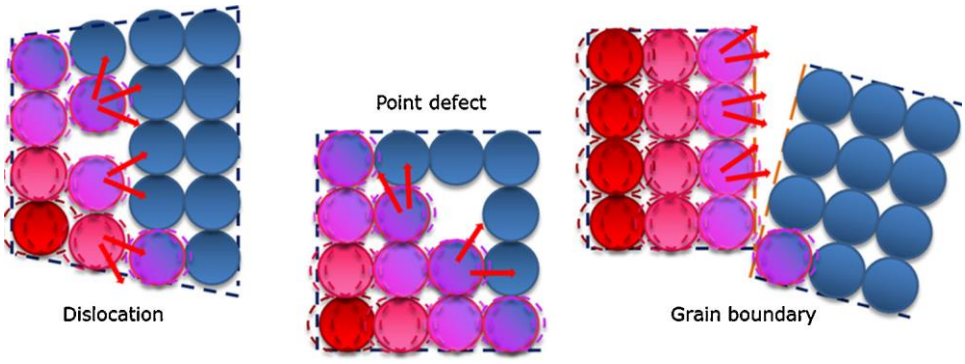

Fig. 1: Phonon scattering due to different defects. Adapted from [35].

1.2.2.2. Thermal Conductivity of Polymers

Polymers are generally insulators with phonons as the dominant heat transporters. Polymers have chains that are connected by weak van der Waals bonds and have very complex morphology that contribute significantly to the phonon scattering [36][37][38][39][40][41]. As a result, the thermal conductivity of most polymers is in the range of 0.1-0.5 W m^{-1} K^{-1} [42]. The thermal conductivities (λ) and the coefficients of thermal expansion (CTE) of typical polymers are summarized in Table 1, as per Huang *et al.* [43].

Table 1: Thermal conductivities (λ) and coefficient of thermal expansion (CTE) of common polymers.

Polymer	$\lambda\ (W\ m^{-1}K^{-1})$	**CTE** $(ppm\ ℃^{-1})$
LDPE	0.33	180-400
HDPE	0.45-0.52	106-198
Polypropylene (PP)	0.14	143
Polystyrene (PS)	0.04-0.14	90-150
Polyethylene terephthalate (PET)	0.29	117
Polymethyl methacrylate (PMMA)	0.15-0.25	90-162
Polytetrafluoroethylene (PTFE)	0.25	126-216
Epoxy	0.17-0.21	81-117
Nylon 6,6	0.25	144
Nylon 1,1	0.36	184

1.2.2.3. Thermal Conductivity of Polymer Composites

The thermal conductivity of polymers is frequently enhanced by the addition of inorganic fillers. Fig. 2 illustrates the major factors that affect the thermal conductivity of polymer composites. Fillers improve the thermal conductivity of polymer composites by forming thermally conductive networks [44] or pathways [42], which act as a bridge for heat transfer.

In principle, the thermal conductivity of polymer composites is affected by both the polymer and the filler thermal conductivities. However, the effect of polymer thermal conductivity is only significant at low filler loading, because of the absence of filler-filler thermal networks. So, heat must pass through both the polymer matrix and the fillers. At higher filler loading, the effect of polymer thermal conductivity is usually neglected due to the formation of thermal networks. It is therefore safe to say that the thermal conductivity of composites depends on the filler loading, filler type, and filler attributes such as aspect ratio, particle size, and particle shape [29][45][46][15].

Filler loading is a first factor when dealing with polymer 'λ' enhancement. The dependence of 'λ' on the filler content is obvious from the fact that fillers have substantially higher 'λ' compared to polymers, and hence their incorporation would definitely improve the resultant composites' 'λ'. The dependence of 'λ' on the filler content is not usually linear, as illustrated in Fig. 3. In Fig. 3, the composites' 'λ' shows a small change at a low filler fraction (below 0.4). Then there is a sudden jump in 'λ' at a filler loading above 0.4. This jump might suggest the presence of thermal percolation threshold, which is a point of sudden increase in the thermal conductivity. Thermal

percolation threshold is caused by the formation of thermal networks and pathways. Kargar *et al.* [47], indicated the presence of thermal percolation threshold in h-BN and graphene/epoxy composites. They specified that the composites' 'λ' dependence on the filler content changed from linear to super-linear above 23 vol. % h-BN and 30 vol. % graphene filler contents.

The intrinsic 'λ' of fillers is indispensable for improving 'λ' of polymer composites. For example, the value of 'λ' of graphene is 5000 W m^{-1} K^{-1} [48] and that of h-BN is 185-300 W m^{-1} K^{-1}[29], which indicates substantial difference in the thermal conductivity of their composites. Kargar *et al.* found that graphene fillers surpassed boron nitride fillers in the thermal conductivity improvements [47]. However, there are limitations on how far 'λ' improves with the increase in the filler 'λ'. Bigg found that there is no significant improvement in the composites' 'λ' as the ratio between the filler and the polymer thermal conductivities exceeds 100 [31]. Fig. 3 demonstrates this by theoretically calculating the composites' 'λ' using Neilson model for spherical particle with packing fraction of 0.637. The result showed no clear improvement in the composites' 'λ' as the ratio of the particle 'λp' to the polymer 'λ_m' was raised above 100 [42].

Filler shape is another important factor. For instance, many fillers have non-spherical shapes. Thus, during fabrications the non-spherical fillers are aligned in different directions which causes anisotropy in the thermal conductivity [29]. Similarly, the filler aspect ratio plays a crucial role in enhancing 'λ'. Bigg indicated that at a given filler

volume fraction, the higher the filler aspect ratio the greater the relative increase in 'λ' [49].

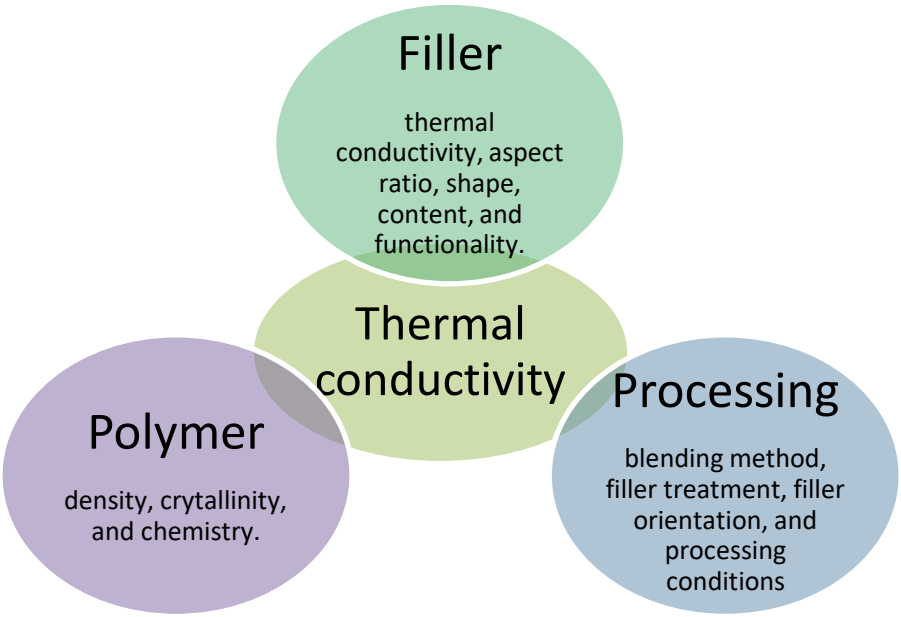

Fig. 2: Factors that affect the thermal conductivity of polymer composites.

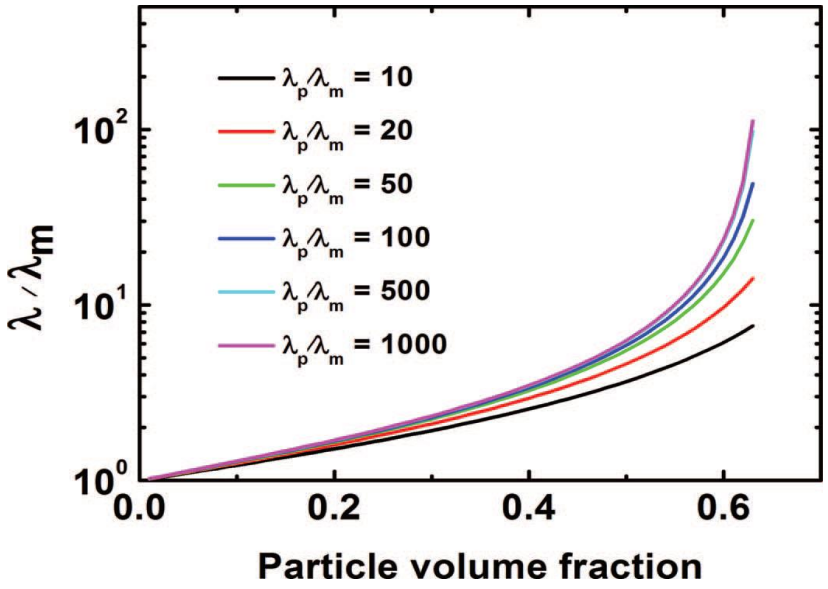

Fig. 3: The ratio of composite to polymer thermal conductivity of different fillers as function of filler contents. Adapted from [42] **copyright line © 2011 IEEE.**

Interfacial interactions between the polymer and filler also play an important role in enhancing the composites' 'λ' [43][29]. For example, enhancing the interfacial interactions can greatly reduce the interfacial thermal resistance, which therefore help improves 'λ'.

1.2.3. Modeling the Thermal Conductivity of Composites

Theoretical calculation of 'λ' is very essential in nanocomposites applications. For instance, this calculation helps in the experimental design by approximating the possible outcomes for a specific set of filler loadings [29]. Many models have been devised to describe the effective 'λ' of the composites including Maxwell Model [50], Rayleigh Model [51], Hasselman-Johnson Model [52], Bruggeman Model [53][29][54][55], Lewis-Nielsen Model [56], and Agari Model [57][58]. Here, Maxwell, Rayleigh, Bruggeman, Lewis-Nielsen, and Agari models are reviewed briefly due to their frequent uses in estimating 'λ'.

Maxwell considered a dilute dispersion of spherical fillers of thermal conductivity 'λ_f' in a big continuous solid phase, a matrix, of thermal conductivity 'λ_m' [50]. Maxwell assumed very small filler concentration (dilute dispersion), and hence there is no filler-filler interaction. The model is written as follows:

$$\lambda_c = \lambda_m \left(1 + \frac{3\,V_f}{\frac{\lambda_f + 2\lambda_m}{\lambda_f - \lambda_m} - V_f} \right) \qquad 1.6$$

where 'λ_c' is the composite thermal conductivity and 'V_f' is the filler volume fraction.

Rayleigh derived his equation by considering spherical fillers arranged in a cubic lattice embedded in a continuous solid phase. Rayleigh's model is expressed as follows:

$$\frac{\lambda_c}{\lambda_m} = 1 + \frac{3V_f}{\frac{\lambda_f+2\lambda_m}{\lambda_f-\lambda_m} - V_f + 1.569\left(\frac{\lambda_f-\lambda_m}{3\lambda_f-4\lambda_m}\right)V_f^{\frac{10}{3}} + \cdots} \quad 1.7$$

Unlike Maxwell, Rayleigh considered filler-filler interaction in his derivation. However, it has been shown that filler-filler interaction is small even at the maximum possible 'V_f' of cubic lattice arrangement [32]. Thus, being simpler Maxwell's model is usually preferred over Rayleigh's model.

Both Maxwell and Rayleigh models fails to fit experimental data at high filler loadings (above 25 vol. %) [59]. At this condition, Bruggeman model give more realistic thermal conductivity predictions. In Bruggeman model, filler interactions are considered using mean field approach making it suitable near the thermal or electrical percolation threshold [29]. Bruggeman model is expressed as follows:

$$\left(1 - V_f\right) = \left(\frac{\lambda_f-\lambda_c}{\lambda_f-\lambda_p}\right)\left(\frac{\lambda_p}{\lambda_c}\right)^{\frac{1}{3}} \quad 1.8$$

Lewis-Nielsen model is a quite popular model for its simplicity and good thermal conductivity prediction at low to moderate filler concentration [56][59]. This model was formed by modifying Halpin Tsai equation for elastic moduli of composites. The model is written as follows:

$$\lambda_c = \lambda_m \frac{1+ABV_f}{1-\varphi BV_f} \quad 1.9$$

$$A = K_e - 1 \quad 1.10$$

$$B = \frac{\frac{\lambda_f}{\lambda_m} - 1}{\frac{\lambda_f}{\lambda_m} + A} \quad 1.11$$

$$\varphi = 1 + \left(\frac{1 - V_f^*}{\left(V_f^*\right)^2}\right) V_f \quad 1.12$$

where 'A' is a shape factor that depends on the filler aspect ratio, 'K_e' is the Einstein coefficient, and 'V_f^*' is the maximum filler volume fraction. The values of 'A' and 'V_f^*' for many systems are readily available in many tabulated data [60]. The inclusion of the shape and the maximum particle packing factors strengthen the ability of this model to fairly predicts the thermally conductivity of most composites especially at low to moderate filler concentration [59].

Agari started from the two extreme thermal conductivity models, series and parallel models, and modified these models by accounting the effect of filler on the polymer matrix and the effect of forming conductive networks [58]. Agari model is expressed as follows:

$$\log(\lambda_c) = V_f C_f \log\left(\lambda_f\right) + \left(1 - V_f\right)\log(C_m \lambda_m) \quad 1.13$$

where 'C_m' is the coefficient that accounts for the effect on the polymer crystal structure and 'C_f' is the coefficient that accounts for the formation of thermal networks [57][58]. The values of these coefficients are determined by fitting the model to an experimental data [61][62][63].

1.2.4. Hexagonal Boron Nitride

Boron nitride (BN) is a compound with equal number of boron and nitrogen atoms [10]. BN does not exist naturally, thus they are synthesized from materials such as boric

acid and boron trioxide [64]. Balmain, 1842, was able to prepare the first synthetic BN compounds by the reaction of molten boric acid and potassium cyanide [10][65]. However, these BN compounds were unstable, thus many methods were devised to stabilize them. This problem minimized their applications in a commercial level, accordingly they were studied in laboratories only. In 1950's, Carborundum and Union Carbide companies were able to produce BN powders and shaped BN in a large scale using hot-pressing techniques [65]. Thanks to the advancement of technologies and the various applications of BN, nowadays the production of BN is economically feasible.

BN can be produced in wurtzite, cubic, or hexagonal structures. The latter two structures are analogous to naturally existing carbon compounds, for instance cubic BN and hexagonal BN are structurally similar to diamond and graphite, respectively [66]. BN is available in the market in both amorphous and crystalline boron nitride forms [67].

Among ceramic fillers, BN and aluminum nitride have the highest thermal conductivities [29][45]. Han *et al.* examined the effect of different fillers on the thermal properties of epoxy resin at 40 °C [68]. The fillers they studied included BN, alumina, diamond, silicon carbide, and silicon nitride, and their particle sizes ranged from micro to nano sizes. Among the fillers investigated, the result indicates that BN was the best filler for improving the thermal conductivity of epoxy resin.

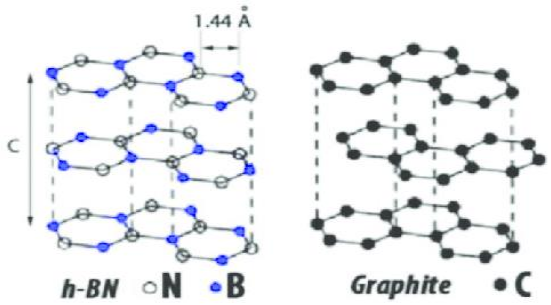

Fig. 4: Schematic diagram of h-BN and graphite. Adapted from [69]**.**

h-BN nanosheets structure are formed by equal number of alternating boron and nitrogen atoms arranged in a honeycomb configuration, hence are structurally similar to graphene [11], as illustrated in Fig. 4. h-BNNSs possess similar properties to graphene such as high thermal conductivity (300-2000 W m^{-1} K^{-1}) [33][30][11], and superb mechanical properties [11][70]. However, unlike graphene, h-BNNSs have electrical insulating property with a bandgap of ~ 5.5 eV [30][71][72] making them excellent candidates in electronics. In addition, h-BNNSs are thermally and chemically stable, therefore are more suitable than graphene in high temperature applications [11] [70] [71].

The thermal conductivity of bulk boron nitride is in the range of 29-300 W m^{-1} K^{-1} [43] and that of h-BNNSs at room temperature, estimated by numerical solutions of phonon Boltzmann transport equation, is more than 600 W m^{-1} K^{-1} [11]. These values are lower than that of graphene, however other attributes such as electrical insulation and thermal stability make them good alternative for graphene in nanocomposite applications.

The in-plane structure of h-BN is made up of nitrogen and boron connected by a strong covalent bond forming one layer, and each layer is connected to its neighboring layers by a weak Van der Waals bonds or forces. This unusual crystal structure of h-BN

is the reason for its anisotropic 'λ'. For example, the in-plane 'λ' of h-BN is ~ 300 W m^{-1} K^{-1},whereas the through-plane 'λ' of h-BN is ~ 2 W m^{-1} K^{-1} [29].

The mechanical properties of h-BNNSs have not been experimentally measured, however, the calculated values of Young's modulus and breaking strength are 0.71–0.97 TPa and 120–165 GPa, respectively [70]. These values are comparable to the experimental values of the Young's modulus and the breaking strength of graphene, which are 1.0 TPa [10][70] and 130 GPa [70], respectively.

Consequently, several techniques have been developed to exfoliate bulk h-BN to a single or few layered h-BNNSs, including but not limited to mechanical cleavage [73], solvent assisted sonication [74][75], chemical vapor deposition [11][73], and thermal exfoliation[76].

1.2.4.1. Synthesis of Hexagonal Boron Nitride Nanosheets (h-BNNS)

1.2.4.1.1. Mechanical Exfoliation

In 2008 Pacile *et al.* were the first to synthesis a few and ten atomic layers of h-BN on SiO_2 or freely suspended [77]. The h-BN layers were peeled off using adhesive tape attached to SiO_2. They succeeded to isolate h-BN layers of thickness varying from 3.5 nm to 80 nm.

Shear force is another approach to mechanically exfoliate h-BN. Lee et al. were able to exfoliate h-BN in aqueous NaOH solution using a ball milling technique [74]. The h-BN particles reacted with the OH^{-1} group which reduced the required shear force to peel the h-BN sheets, as shown in Fig. 5. The combined effect of the reaction and the

mechanical force resulted in flakes with average particle sizes of 1.5 µm and a high yield of up to 18 %.

In another work Tominaga's group investigated the effect of using different mechanical exfoliation methods, such as wet-jet milling (W), ultrasonication (U), and vortex fluid (V) [78]. They found that the particle sizes of the h-BNNS exfoliated by 'W' were approximately the same size as that of the pristine h-BN, meanwhile that of 'U and V' were less than 70 % of the original particle size. In addition, they specified that 'W' resulted in a particle thickness smallest than the other two methods leading to h-BNNSs with a high aspect ratio.

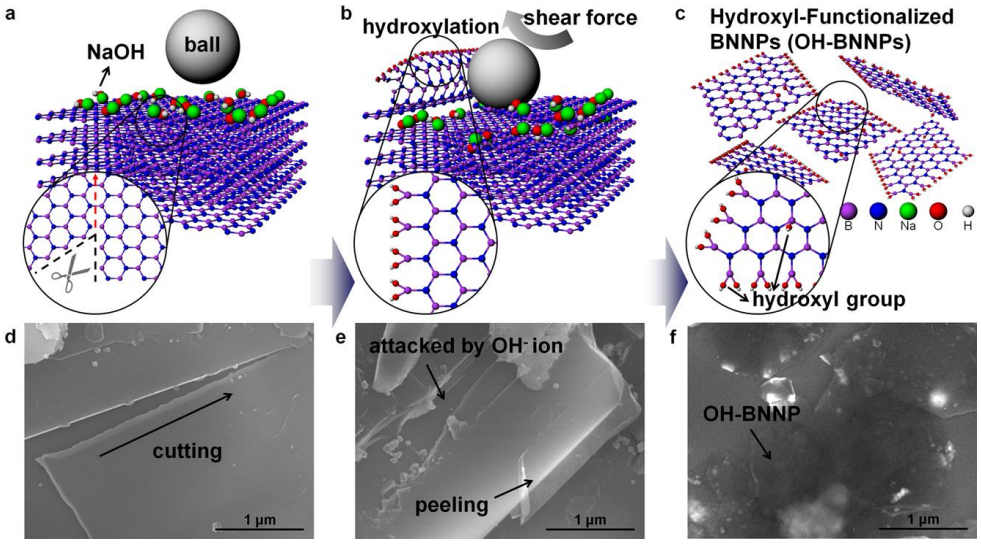

Fig. 5: Schematic diagram and corresponding SEM images of h-BN exfoliation steps. The dissection step (a) and (b), the peeling step (b) and (e), and hydroxylation step (c) and (f). Adapted from [74].

1.2.4.1.2. Liquid Exfoliation

The preparation of a single or a few-layered h-BN by a liquid exfoliation method was first achieved in 2008 by Han's group [79]. In this study, 0.2 mg of h-BN crystals were mixed with a 5 ml of 1,2-dichloroethane solution containing 0.6 mg of poly (m-phenyl-enevinylene-co-2,5-dictoxy-pphenylenevinylene). Then, the solution was sonicated for 1 h to disintegrate and disperse the h-BN crystals into a few-layered h-BNNSs. Subsequently, this led to many similar studies that focused in selecting appropriate solvents that have surface energy similar to h-BN [11].

Coleman *et al.* exfoliated several fillers, such as BN, MoS_2, and WS_2, in a number of solvents of varying surface tension [80]. Their analysis of Hansen solubility parameter theory suggested that successful solvents are those with polar, hydrogen bonding, and dispersive component of the cohesive energy density that match the solubility parameter of the layered materials. Thus, they indicated that N-methyl-pyrrolidine (NMP) and isopropanol (IPA) are the best solvents for the liquid exfoliation of these fillers.

The above studies indicate that the solute-solvent interaction is a vital tool for successful exfoliation. For instance, solvents that form solvent-BN mixture with a minimum Gibbs free energy of mixing are the once favored for BN exfoliation [75]. Many studies have shown that h-BN is favorably exfoliated in NMP, IPA, and dimethyl formamide (DMF) [75].

Zhang *et al.* exfoliated h-BN for the first time using aqueous solution of monoethanolamin (MEA) [75]. In their experiment, 200 mg of h-BN was mixed with a 50 ml MEA or aqueous MEA solution, the mixture was then sonicated for 4 hours in a 6-L

bath sonicator at 50 ℃. In addition, they compared MEA with several classical solvents, including NMP, IPA, DMF, tert-butyl alcohol (BA), and water. The yield of h-BNNSs in the different solvents was 33.7 % (MEA), 12% (DMF), 9.5% (NMP), 8.4% (BA), 4.5% (IPA), and 1.5 % water. Moreover, they have shown that up to 42 % yield of h-BNNSs can be achieved by ultrasonic exfoliation of h-BN in MEA-30 wt % H_2O solution. These results were explained by the similarity in the solubility parameter of h-BN and MEA, for example, the specific surface tension of MEA is 44.8 mJ/m^2 and that of h-BN is 20 ~ 40 mJ/m^2. The pristine h-BN and h-BNNSs exfoliated by MEA solution images are shown in Fig. 6. The lateral dimension of the pristine h-BN was ~ 0.5-5 μm and its thickness was more than 100 nm. The atomic force microscope (AFM) image shows that most h-BNNSs thicknesses are less than 5 nm, implying excellent exfoliation.

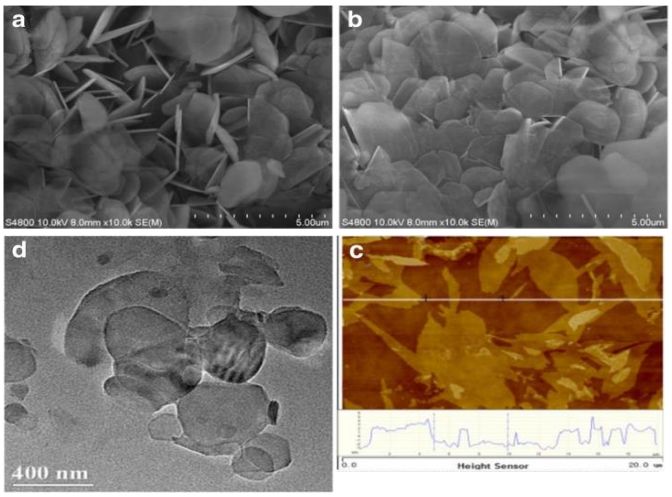

Fig. 6: SEM images of pristine h-BN (a) and h-BNNSs (b), AFM image of h-BNNSs (c), and TEM images of h-BNNSs (d and e). Modified from [75]**.**

1.2.4.1.3. Chemical Vapor Deposition (CVD)

CVD is an epitaxial growth of BN monolayer on different substrates of preferred orientation [10][11][81]. In CVD different precursors such as borazine ($B_3N_3H_6$) [82], trichloroborazine ($B_3N_3H_3Cl_3$) [83][84], and a mixture of ammonia and BF_3 [85], BCl_3 [86], or BH_3 [87] are used as an initiating materials for BN synthesis . The atomic ratio of boron and nitrogen in borazine is 1:1 making it very special precursor, because this atomic ratio helps in avoiding the use of two or more gaseous components as in BF_3-NH_3 or BCl_3-NH_3 [10][33].

h-BN monolayer or multilayer can be fabricated on different transition metal substrates such as Pt (111) [88], Ru (001) [89], Ni (111) [90], Cu (111)[91][92], Pd (111) [93], Fe (110) [94], Mo (110) [95], Ir (111) [96], and Rh (111) [97][98]. For example, in 1990 Paffett *et al.* were able to produce h-BN monolayer on Pt(111) and Ru(001) substrates by the adsorption and decomposition of borazine precursor [99]. The type of precursor and metal substrates are very crucial and play a major role on the resultant h-BN's yield, morphology, orientation, and electronic structure [11].

1.2.4.1.4. Thermal Exfoliation (TE)

In this method, h-BN is simply exfoliated by thermal treatment [76][100][101]. In TE, h-BN is heated in open air at a very high temperature above 800 ° C for several hours, i.e. at or above the oxidation temperature of h-BN. Cui *et al.* oxidized h-BN thermally to form BNO of impressively high yield up to ~ 65 % [100]. This high yield was achieved by the combinatory effects of the thermal treatment (oxidation) and the subsequent hydrolyzation in hot water. Similarly, Ko *et al.* synthesized highly stable h-BNNS, of more

than one month, by thermally treating h-BN powder [76]. However, they reported that their h-BNNS was produced solely due to a physical change, i.e. the h-BN was not oxidized. TE method has many advantages over other exfoliation methods such as low cost, ease of handling, functionalization, high yield, and short processing time.

1.2.4.2. Fabrication of h-BN/Polymer Composites

Polymer nanocomposite can be prepared by chemical and mechanical processes, of which in situ polymerization, melt intercalation, sol gel, and direct powder mixing methods are the most frequently used methods [102]. These preparation methods play essential part in enhancing the properties of the composites. In the following paragraphs in situ polymerization, melt intercalation, and solvent blending methods are briefly discussed.

1.2.4.2.1. In Situ Polymerization Method

In this method, the fillers are mixed with the monomer solution so that the monomer intercalate between the filler layers to cause filler swelling [103] [102] [104]. The resultant is then polymerized using techniques, like initiator, radiation, and heating. Consequently, the polymer chains are formed between the filler layers which induce fillers exfoliation [104] [105], as shown in Fig. 7. The chemical reaction in this method (polymerization) results in a covalent bonding between the polymer and the filler [64]. As a result, fillers are well dispersed inside the polymer matrix leading to excellent composite properties. This method is frequently used for thermosets synthesis, such as epoxy, polyimide and benzoxazine [106]. Sadej *et al.* prepared BN or Si3N4/methacrylate polymer composites by in situ-photo-polymerization [106]. They found significant

improvement in the polymer 'λ' at a very low filler loading. Grafting polymerization is a typical example of in situ polymerization. Jiang *et al.* grafted poly (glycidyl methacrylate) (PGM) on to the surface of h-BN by a free radical polymerization technique to form a PGM grafted h-BN (PGM/h-BN) [107]. The thermal conductivity of the epoxy composites improved by 60%, 203%, and 505% up on the addition of 3, 5, and 15 vol. % of the PGMA/h-BN.

1.2.4.2.2. Melt Intercalation Method

Melt intercalation is a simple, cost effective, and environmental friendly blending method, i.e. no solvent is required, thus it is widely used in industry [105][104]. In this method, the filler is mixed with a molten polymer with the aid of mechanical force such as shear mixer [105][104][103][102], as illustrated in Fig. 8. Melt intercalation is typically used for fabricating thermoplastic nanocomposites [104]. Kahraman *et al.* prepared nano-h-BN/polyurethane composites, a thermoplastic composite, by a melt blending method using twin screw extruder and hot pressing [108]. The composites showed significant improvements on the mechanical, physical, and thermal properties. However, melt intercalation shows reduced filler dispersion compared to solvent mixing [104]. In addition, the high viscosity encountered at high filler loading limits the use of this method at low filler loading only.

1.2.4.2.3. Solvent Blending Method

In this method, the fillers are initially dispersed in a solvent to cause swelling. Subsequently, the polymer solution is added to the mixture resulting in the intercalation and displacement of the solvent [103], as shown in Fig. 9. Finally, the solvent is separated

by either evaporation or coagulation techniques [102]. Zhu *et al.* prepared densely packed BN polymer composites by solvent blending and compression molding methods [109]. The resultant composites displayed anisotropic 'λ', with in-plane 'λ' up to 21.3 W m^{-1} K^{-1}. Similarly, Wang *et al.* prepared poly(vinylidene fluoride)/h-BNNS composites by solution blending and hot pressing [110]. At 4 wt. % filler loading, the in-plane and through-plane 'λ' were 4 W m^{-1} K^{-1} and 0.23 W m^{-1} K^{-1}, respectively. However, solvent blending is economically unfeasible because of the combined cost of the solvents and their separation processes [105], which limit their large scale applications.

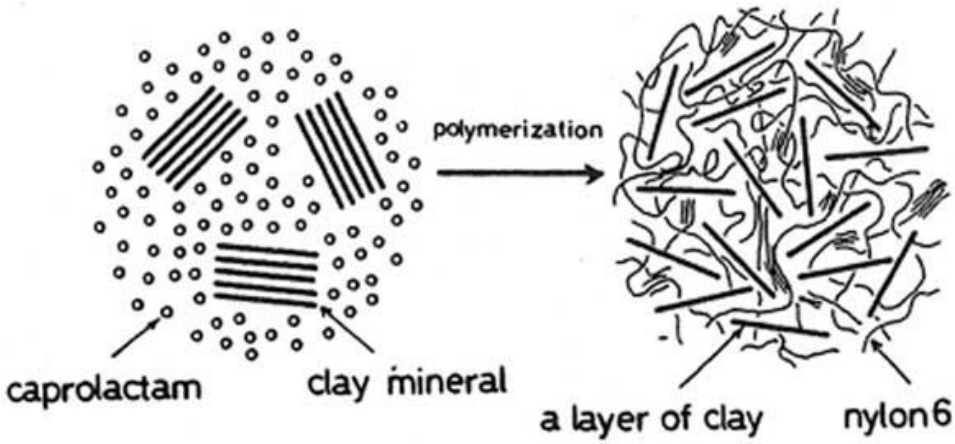

Fig. 7: Nanocomposite fabrication through in situ polymerization method. Adapted from [111]**.**

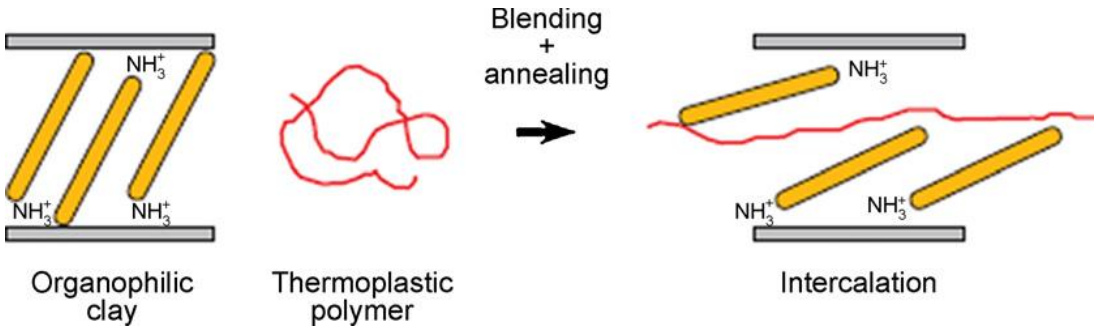

Fig. 8: Nanocomposites synthesis through melt intercalation method. Adapted from [112]**.**

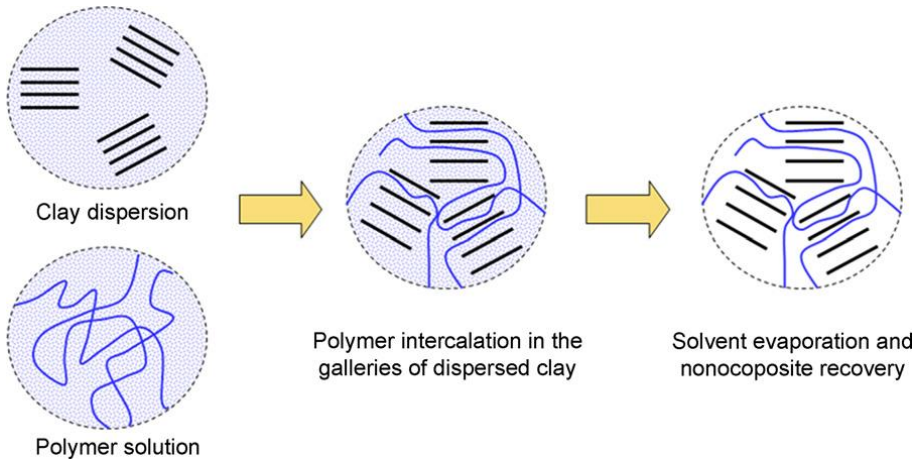

Fig. 9: Nanocomposite fabrication through solvent blending method. Adapted from [112]**.**

1.2.4.3. Thermal Conductivity of h-BN/Polymer Composites

The thermo-physical attributes of boron nitride nanosheets, including superb mechanical properties, high thermal conductivity, and electrical resistivity, account for their frequent applications in polymer nanocomposites [11]. The theoretical value of a single layered h-BN thermal conductivity at room temperature, estimated by numerical

solutions of phonon Boltzmann transport equation, is more than 600 W m^{-1} K^{-1} [11]. However, that of bulk h-BN, calculated is 400 W m^{-1} K^{-1} [11][10] and measured is 100-270 W m^{-1} K^{-1} [70]. The huge difference in the thermal conductivities of bulk h-BN and h-BNNSs are because of the reduction of phonon-phonon scattering in the mono layered h-BN. Nevertheless, the thermal conductivity of bulk h-BN is significantly higher than that of polymers. Therefore, the incorporation of these fillers is expected to improve the thermal conductivity of polymer composites. For instance, at 50 wt.% h-BN content 'λ' increased from 0.22 W m^{-1} K^{-1} to 1.2 W m^{-1} K^{-1} [113]. Equally, Song *et al.* prepared h-BN/polyimide composites with 'λ' of 7 W m^{-1} K^{-1} at 60 wt. % h-BN concentration [114]. Beside filler content other factors, such as filler alignment and treatment, particle size, and aspect ratio, play crucial roles. Kuang *et al.* studied the effect of h-BNNSs orientation on the thermal conductivity of silicon rubber [115]. The thermal conductivity increased from 1.56 W m^{-1} K^{-1} in the randomly dispersed h-BNNSs to 5 W m^{-1} K^{-1} in the oriented h-BNNSs at 30.8 vol. % h-BNNSs loading.

1.2.4.3.1. Factors that Affect the Thermal Conductivity of h-BN/Polymer Composites

Beside the filler intrinsic thermal conductivity; filler content, size, geometry, aspect ratio, orientation, and treatment play very essential role in improving the thermal conductivity. In the following paragraphs, the effects of these factors are briefly discussed.

1.2.4.3.1.1. Filler Content

Generally, the thermal conductivity of composites is a function of filler content or loading. This dependence is usually nonlinear [29]. For example, at low filler loading, i.e. below 35 vol.%, the change in the thermal conductivity is relatively small, whereas at

higher loading, i.e. above 35 vol. %, the change is substantial, possibly because at higher loading more conductive pathways are created [29]. Nonetheless, there is practical limitations to the amount of filler that can be incorporated. For example, high loading might lead to a poor mechanical performance, difficulty in fabrication, and high cost [29][25][44]. In addition, high loading tends to cause filler agglomeration. The consequences of agglomeration is not clear; they might enhance the thermal conductivity or act as an initiator for mechanical failure [25].

Wattankul *et al.* studied the thermal conductivity and mechanical properties of BN filled epoxy (EP) composite as a function of filler loading, mixing conditions, and BN agglomerate sizes [45]. They observed parabolic increase in 'λ' with the increase in filler contents, see Fig. 10. They obtained a maximum 'λ' of 1.97 $W\ m^{-1}\ K^{-1}$ at 28 vol. % loading, mixing speed of 80 rpm, and mixing time of 30 min, followed by sonication. In addition, they observed monotonic increase in 'λ', with the increase in mixing speed, time, and temperature, see Fig. 11. They suggested that mixing actions break down the agglomerates, and hence they increase the filler aspect ratio which improved the thermal conductivity.

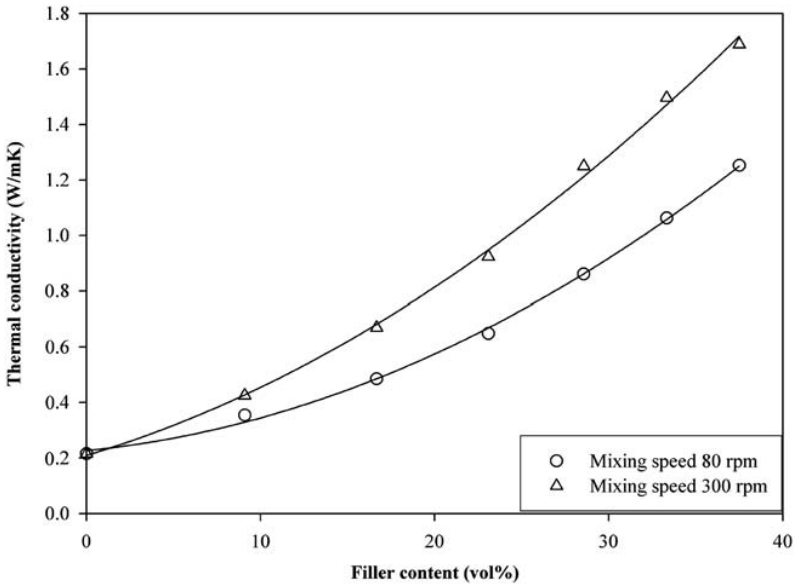

Fig. 10: The thermal conductivity of BN-EP composite at different filler content. Mixing condition: 80 rpm & 300 rpm, 30 min, and 30 °C. Adapted from [45]**.**

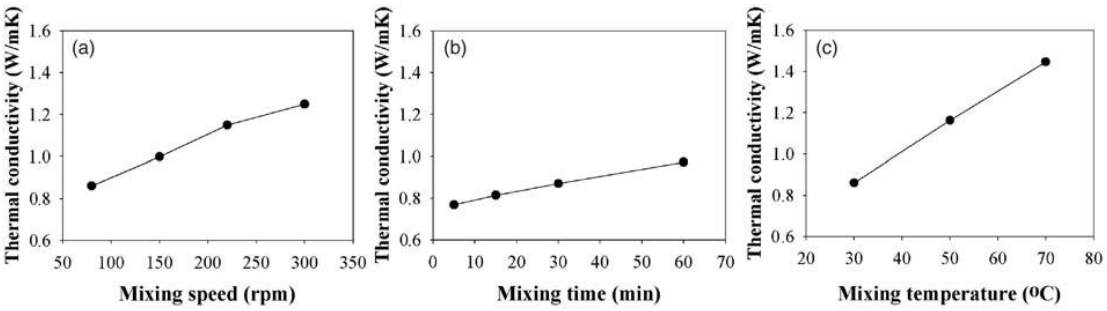

Fig. 11: The thermal conductivity of BN-EP composites at different mixing conditions. (a) mixing speed (30 min, 30 °C), (b) Mixing time (80 rpm, 30 °C), and (c) mixing temperature (80 rpm, 30 min). Adapted from [45]**.**

1.2.4.3.1.2. Filler Size

Generally, composites loaded with large fillers have less polymer-filler interfaces compared to those filled with smaller fillers. Thus, composites loaded with large fillers have lower interfacial thermal resistance producing composite with higher 'λ' [29].

Shin *et al.* investigated the effect of BN content and particle size on the thermal properties of BN and high density polyethylene (HDPE) composites [46]. They found that the thermal conductivity and thermal diffusivity of the composites filled with larger particle sizes were higher than that filled with smaller particles. Likewise, Li *et al.* developed thermally conductive polyimide (PI) composites by incorporating micro and nano-size BN fillers inside the polymer matrix [116]. In their study they investigated the effect of micro and nano size particles alone and their hybrid on the composite 'λ'. They showed that micro sized BN particles (mBN) are better than nano size BN particle (nBN) in improving the composites 'λ', as illustrated in Fig. 12. In addition, they indicated that mBN and nBN hybrids were better in enhancing the thermal conductivity than mBN or mBN alone. These finding were explained by the fact that in the hybrid composites, the micro-size particles form thermal conductive networks and the nano-size particles connect those networks.

However, some researchers have different opinion on the effect of particle size. Fu *et al.* studied the effect of surface treatment and particle size (micro and nano) of Al_2O_3 and BN fillers on the performance of thermally conductive epoxy adhesive [117]. They reported that the composites loaded with nano-particles showed better 'λ', mechanical strength, and electrical insulation compared to those filled with micro-particles. Zhou *et al.* also observed a higher 'λ' value of rubber filled with Al_2O_3 nanoparticles compared to those filled with microparticles [118]. However, they explained this result by the fact that nano particles had higher intrinsic 'λ' than micro sized particles.

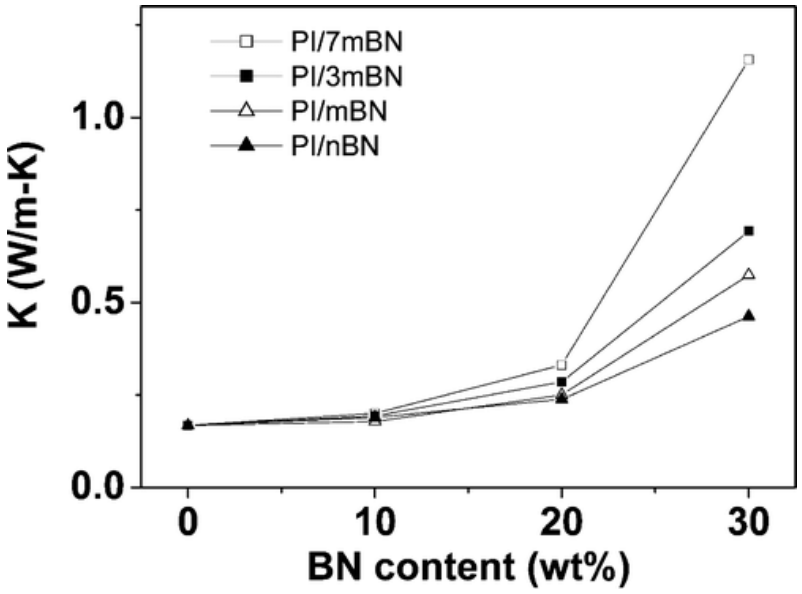

Fig. 12: The thermal conductivity (K) of BN/PI composites of various size at different filler content. (PI/7mBN) 70 wt. % micro and 30 wt. % nano size BN particles, (PI/3mBN) 30 wt.% micro and 70 wt.% nano size BN particles. Adapted from [116]**.**

Therefore, when comparing the effect of particle size on the thermal conductivity, it is very difficult to eliminate other parameters such as surface chemistry, filler morphology, filler preparation, and filler dispersion, which might lead to a different filler properties [29]. For instance, Zhou *et al.* studied the effect of platelet-shaped BN particles dispersion states on the thermal conductivity of HDPE composites [62]. They found that the smaller the particle the better the dispersion and hence the higher the 'λ' value.

1.2.4.3.1.3. Filler Shape

Filler particle shapes also contributes substantially to the thermal conductivity [29][119]. The theoretical and experimental investigations of the effect of filler shapes, such as 0D particles, 1D nanotubes, 2D nanosheets, and other shapes, indicated that

specific shapes tend to form thermal conductive pathways relatively easier, resulting in a higher thermal conductivity [119]. For example, compared to 0D and 1D BN nanomaterials, 2D BN nanosheets have higher thermal conductivity as well as better dispersibility making them more suitable in nanocomposites applications[8].

Lin *et al.* prepared h-BNNSs by liquid exfoliation and studied their effect on the thermal conductivity of epoxy composites [15]. They found that the 'λ' value was improved by 113 % at a very low filler loading of only 5 wt. % of h-BNNSs, whereas 28 wt. % of pristine h-BN was added to get the same result.

1.2.4.3.1.4. Aspect Ratio

Fillers with a high aspect ratio tend to form thermal conductive network at low filler loading, because these fillers reach percolation threshold at low filler concentration [25][120]. Consequently, these fillers enhance the thermal conductivity of the composites by reducing the interfacial thermal resistance [120]. In addition, with these fillers low filler content is sufficient to achieve enhanced composite properties. Moreover, the low filler loading in these systems lead to a better processing due to the low density and low viscosity of these composites [25]. Huang *et al.* investigated the effect of morphology, crystallinity, and content of spherical (s-BN) and flakes (f-BN) boron nitride fillers on the thermal, mechanical, and electrical properties of epoxy composites [121]. They found that the composites filled with f-BN showed significantly improved 'λ' compared to those filled with s-BN, because of the higher aspect ratio and crystallinity of f-BN fillers. For instance, the 'λ' values were 0.933 and 0.464 W m^{-1} K^{-1} at 30 wt. % of f-BN and s-BN loading respectively, as shown in Fig. 13.

1.2.4.3.1.5. Filler Orientation

The nonsphericity of many fillers, including platelet BN, fibers, carbon nanotubes, graphene sheets, wires, and graphite flakes, lead to anisotropic thermal conductivity [29]. Therefore, alignment of such fillers inside the polymers might significantly affect the thermal and mechanical properties of the polymer composites. For instance, the thermal conductivity of platelet BN improves by approximately a factor of 20 when it is oriented parallel to the heat flow (in-plane) compared to when it is aligned perpendicular to the heat flow (through-plane) [122].

Yuan *et al.* oriented BN platelets in to different microstructures using magnetic field and investigated their effect on the thermal conductivity of the resultant composites [123]. They stated that the 'λ'was improved by 44.5 % when the BN platelets were oriented parallel to the heat flow and was lowered by 37.9 % when the BN platelets were aligned perpendicular to the heat flow. Equally, Sun *et al.* reported a maximum 'λ' of 3.09 $W\ m^{-1}\ K^{-1}$ at BN loading of 18 vol.% when BN plates were aligned in polycarbonate (PC) composite using hot-pressing [124]. They stated that such arrangements provide thermal pathways for phonon transport which significantly reduce the thermal resistance, thereby and enhancing the thermal conductivity. Fig. 14 (a) and (b) show the thermal conductivity and the thermal conductivity enhancement of BN/PC composites for horizontally oriented BN (HoBN/PC) and randomly oriented (RoBN/PC). The better performance of HoBN/PC compared to RoBN/PC shown in Fig. 14 (a) and (b) is illustrated in Fig. 14 (c) by the presence of thermal pathways in HoBN/PC composites.

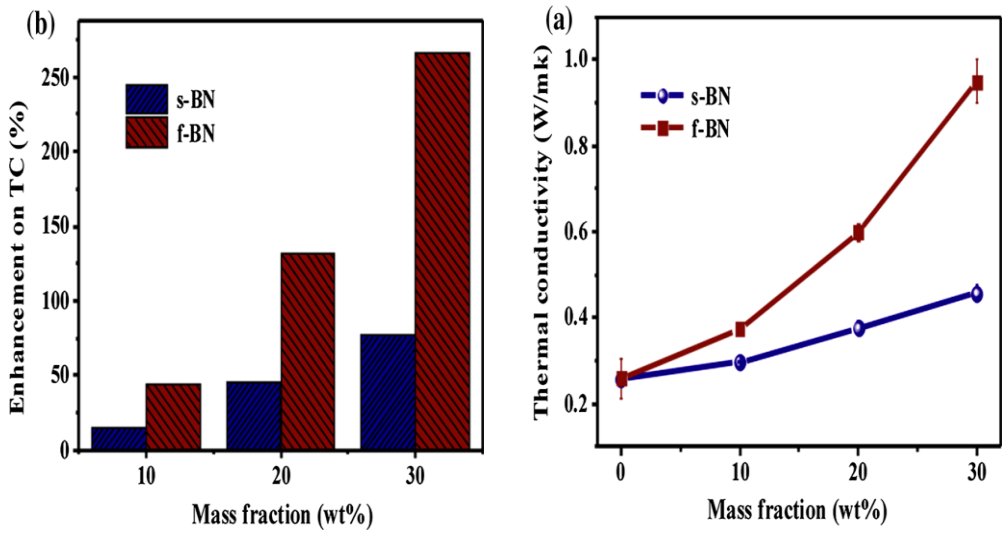

Fig. 13: Thermal conductivity and thermal conductivity enhancement of epoxy composites filled with s-BN and f-BN fillers at different filler content. Adapted from [121]**.**

1.2.4.3.1.6. Filler Treatment

Polymers being organic are mostly hydrophilic in nature. Thus the inorganic fillers, such as metals and ceramics, encounter some interfacial bonding resistances with the polymer matrix. Interfacial thermal resistance is one of the main limitations of thermal enhancement in polymer nanocomposites [29]. This problem can be mitigated by filler treatments; such as filler surface treatment, filler purification, or filler functionalization [25].

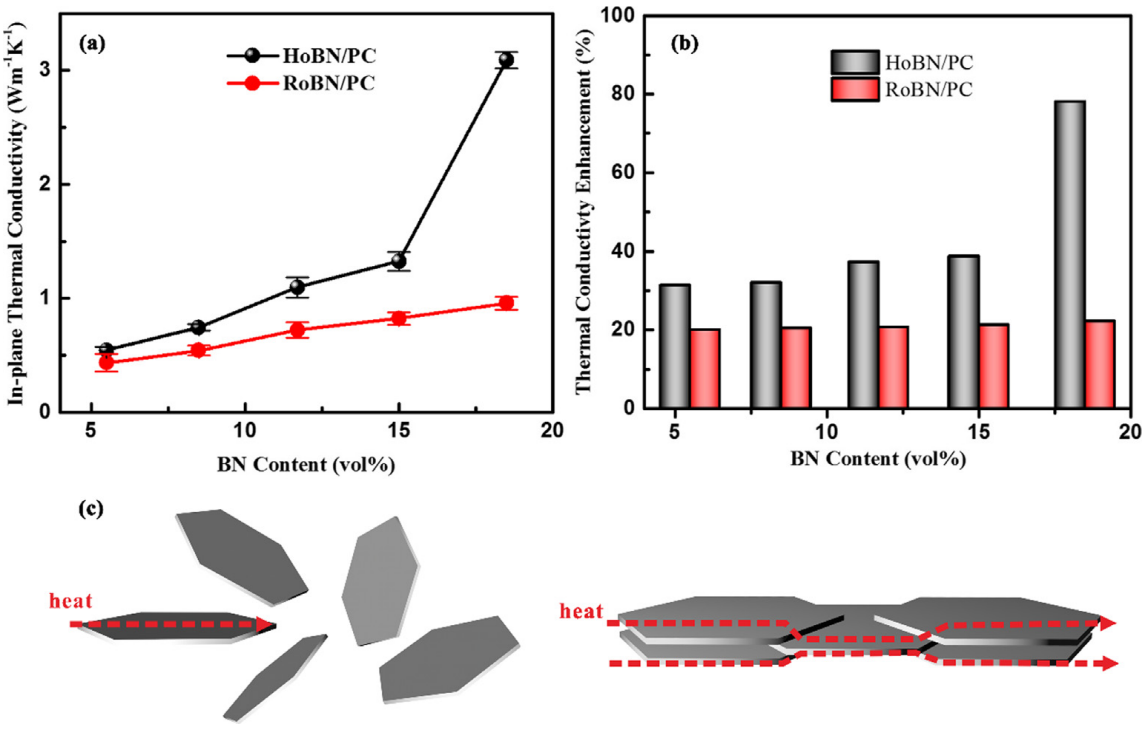

Fig. 14: Thermal conductivity (a) and Thermal conductivity enhancement (b) of BN/PC at different filler loading. (c) shows the heat flow in RoBN/PC left and HoBN/PC right composites. Adapted from [124].

By far, Organo-Silanes are the most effective and widely used surface modifier [29] [25]. Donnay *et al.* stated that high concentration of silane coupling agent has beneficial effect on the thermal conductivity of BN epoxy composites [125]. Also, Fu et al treated BN by silanes and diisocyanate, and then added them to epoxy polymers [117]. They indicated that the addition of surface modifier was useful for the thermal conductivity, by reducing the interfacial thermal resistance.

Beside organo-silanes, there are several chemicals and methods of reducing interfacial thermal resistance. Ahn *et al.* indicated that BN/poly (vinyl butyral) treated with amphiphilic agent such as $C_{14}H_6O_8$ and $C_{27}H_{27}N_3O_2$ showed better 'λ' enhancement

than that of untreated composites [122]. Jiang *et al.* grafted poly (glycidyl methacrylate) (PGM) on the surface of h-BN to form h-BN/PGM complex [107]. Afterwards, the h-BN/PGM was added to epoxy (EP) to form a composite with a high 'λ'. They stated that the thermal conductivity of the resultant composites was improved by 60%, 203%, and 505% up on the addition of 3, 9, and 15 vol. % of h-BN/PGM, respectively.

1.2.4.4. Mechanical Properties of h-BN/Polymer Composites

Besides having exceptionally high thermal conductivity, h-BNNSs possess peculiar mechanical properties. For instance, the calculated values of Young's modulus and breaking strength of h-BNNSs are 0.71–0.97 TPa and 120–165 GPa respectively, i.e. comparable to graphene [70]. The mechanical properties of few layered h-BN do not show clear dependence on the number of sheets, i.e. unlike graphene [126]. For instance, the Young's modulus values of 1 and 9 layered h-BN are 0.865 ± 0.073 and 0.856 ± 0.003 TPa, respectively [126]. Similar to h-BNNSs, multilayered h-BN shows very high mechanical properties. For example, the Young's modulus of multilayered h-BN is 1.16 ± 0.1 TPa [94] or 0.81-1.3 TPa [127]. For these exceptional mechanical properties, h-BN are frequently used in polymer composites reinforcements [10][11].

The incorporation of h-BN in polybutylene terephthalate lowered the elongation at break and improved the tensile strength to reach a maximum at 15 wt. % h-BN loading [128]. Similarly, the flexural strength and modulus of h-BN/epoxy composites rose from 25.7 MPa and 2.46 GPa in pure polymer to 47.6 MPa and 3.1 GPa at 37 vol. % h-BN content, respectively [45]. The storage modulus also shows similar dependence. For example, at 15 vol. % h-BN loading the storage modulus of epoxy increased from ~ 1.79

GPa to ~ 3.19 GPa [107]. Equivalently, upon the addition of 1.5 wt. % h-BN on 20 wt. % graphene/polystyrene (20GP) composites, the Young' Modulus increased from 4.7 to 6.3 GPa [129]. However, at a very high filler loading the mechanical properties of the composites, such as the tensile strength [128] and the impact strength [45], deteriorates, i.e. the composites become brittle. These deteriorations in the mechanical properties are attributed to the formation of filler agglomeration which can act as a source of mechanical failure [25].

1.2.5. Overview of Hexagonal Boron Nitride-Polyethylene Composites

Polyethylene (PE) is a polyolefin thermoplastic made by the polymerization of ethylene monomer [130][131]. PE possess very good properties such as chemical stability, toughness, moisture resistance, electrical insulation, and ease of fabrication [132][133][134]. PE has extremely large field of applications including in pipes, packaging, insulating electric cables, and automobiles, making it the most widely used plastic in the world [131][132][133].

PE is classified based on its degree of branching into high density PE (HDPE), linear low density PE (LLDPE), and low density PE (LDPE) [130][133]. The degree of branching affects the properties of PE, such as its density, crystallinity, and thermos-mechanical properties. For instance, HDPE contains less branches compared to LLDPE and LDPE, hence it has higher density, crystallinity, and thermal conductivity [130]. Table 2 summarizes the most common properties of LDPE, LLDPE, and HDPE.

Table 2: Common properties of LDPE, LLDPE, and HDPE

Property	LDPE	LLDPE	HDPE	Reference
Density (g/cm^3)	0.915-0.925	0.90-0.94	0.941-0.965	[130][133]
Crystallinity (%) from calorimetry	30-54	22-55	55-77	[130]
Melting point (°C)	98-115	100-125	125-132	[130]
Tensile strength (MPa)	10-20	25-45	13-51	[130][135][136][137]
Tensile modulus (GPa)	0.13-0.3	0.26-0.52	0.5-1.1	[130][135][136][137]
Flexural modulus	0.23-0.25	0.28-0.735	0.75-1.6	[135][136][137]
Thermal conductivity ($W\ m^{-1}\ K^{-1}$)	0.32-0.4	0.32	0.45-0.52	[43][138][139]

1.2.5.1. h-BN/PE Composites

Although the attributes of pristine PE polymers such as chemical inertness, electrical insulation, and ease of processing play great role in their applications [133], other properties such as mechanical and thermal properties requires improvements [140]. For instance, enhancing the thermo-mechanical properties of PE polymers is vital for their utilization in thermal management applications. Thus, inorganic fillers, such as h-BN and graphene, are frequently used to boost these properties.

Many researches have been done to study the effect of incorporating h-BN on the thermo-mechanical properties of PE composites [46][141][142][143]. For example, the thermal conductivity of HDPE was improved from 0.35 $W\ m^{-1}\ K^{-1}$ for pure HDPE to 2.08 $W\ m^{-1}\ K^{-1}$ at 50 wt. % h-BN concentration [144]. Similarly, the thermal conductivity of LDPE improved by 22 % at 5 wt. % h-BNNSs loading [145]. Also, the thermal conductivity of LLDPE showed clear dependence on h-BN content [146].

Shin *et al.* studied the effect of BN content and particle size on the thermal properties of HDPE composites [46]. They indicated that the thermal diffusivity increased with BN content. At the same BN loading, the thermal diffusivity increased with the increase in BN particle size, for instance the thermal diffusivity at 50 wt. % was 2.253, 2.548, and 2.653 mm^2/s for 3, 10, and 20 µm BN particle sizes, respectively. Zhang *et al.* investigated the effect of improving BN and HDPE interfacial interaction on the properties of the composites [143]. They treated the surface of h-BN with KF550 agent, in addition, they prepared h-BN/HDPE with the addition of polyethylene-g-maleic (PGM) anhydride. As expected, they found that the filler treatment and the addition PGM was very beneficial in improving the thermal conductivity. For more examples of h-BN/PE composites, refer to Table 3.

Table 3: Thermal Conductivity of h-BN/PE composites.

Filler	Matrix	Processing	K ($W\ m^{-1}K^{-1}$)	Ref.
h-BN (3-5 µm) 30 wt. %	HDPE	Multi-stage extrusion: (1) compounding in twin screw extruder running at 200 rpm and temperature of 80, 180, 180, and 170 ℃ and (2) stretching in a single screw extruder.	1.21	[63]
h-BN (2-5 µm) 50 wt. %	HDPE	Melt blending using Roller mixer with roller temperature of 153 ℃ front and 150 ℃ back.	2.08	[144]
h-BN (20 µm) 50 vol. %	HDPE	Melt blending at 200 ℃ and 30 rpm for 20 min.	~ 4.6	[46]
h-BN (4.1 µm) 50 wt. %	HDPE	Melt blending at 180 ℃ and 30 rpm for 8 min. The interfacial interaction was enhanced by adding PGM.	~ 2.6	[143]
h-BN (10 µm and 50 nm ratio 3:1) was treated with silane agent KH550. 40 wt. %	LDPE	Powder mixing and hot pressing at 170 ℃ for 30 min.	0.95	[143]
h-BN (6 µm) 27.63 vol. %	LDPE	LDPE was ground to powder of 250-500 µm average sizes. The compositewas prepared by powder mixing and pressed at room temperature for 1 min under 20 MPa, followed by hot pressing	~ 2.6	[147]
h-BN (60 µm) 33.3 vol. %	LLDPE	Melt blending in twin screw extruder at 150 ℃ for 10 min.	~ 2.8	[146]

2. RESEARCH OBJECTIVES

One of the most important applications of polymer composites is in thermal dissipation management of electronic devices. However, polymers suffer from poor thermal and mechanical properties. Thus, the properties of polymers are commonly enriched by the incorporation of fillers, such as metals and ceramics. Due to their similarity with graphite and 2D graphene, h-BN and h-BNNSs possess high mechanical, physical, and thermal properties [9][10][11], making them suitable for nanocomposites applications. Unlike graphene, the exfoliation of h-BN to h-BNNS is very difficult especially in a large scale. In addition, h-BNNS is not commercially available. Consequently, it is of high interest for researchers to devise a facile method for the production of h-BNNS in a large scale.

This work aims to synthesize thermally enhanced polyethylene (PE) polymer composites and nanocomposites based on h-BN and its exfoliated nanosheets (h-BNNS)

Tasks:

1. Exfoliation of h-BN
2. Fabrication of h-BN-PE composites with different h-BN loadings
3. Fabrication of h-BNNS-PE nanocomposites with different h-BNNS loadings
4. Characterization of h-BN and h-BNNS
5. Characterization of the fabricated composites and nanocomposites

Key Questions to Answer

- What is the impact of processing method on the composite and nanocomposite thermal conductivity, thermal properties, crystallinity and mechanical properties?
- What is the impact of the h-BN exfoliation on the processing and the properties of the nanocomposites?
- What is the impact of the h-BN and h-BNNS loading on processing and properties of the composites/nanocomposites?
- What is the impact of h-BN particle size on the processing and the properties of the composites/nanocomposites?

3. METHODOLOGY

As previously mentioned, composites depend on many factors as shown in Fig. 2. Here, the impact of h-BN particle size, polymer matrix, processing method, and h-BN exfoliation on the composite properties are studied, see Fig. 15.

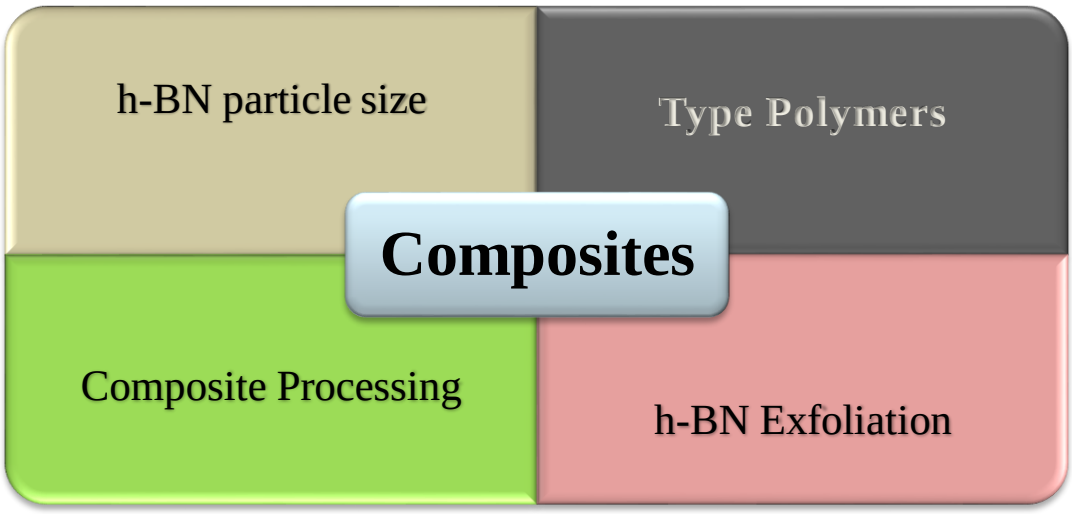

Fig. 15: Factors to be addressed in this thesis.

In general, in this thesis the process methodology can be divided into three main experimental steps: h-BN exfoliation and characterization, h-BN/PE composites fabrication, and h-BN/PE composites characterization as shown in Fig. 16. In the first step, h-BN powder is exfoliated to h-BNNS through ball milling method. The exfoliation is confirmed using different characterization techniques, such as XRD, SEM, AFM, TEM, EDS, and XPS. In the second step h-BN and h-BNNS/PE composites are fabricated by melt and dry blending methods. The composites is melt blended by twin screw extruder,

and dry mixed using a ball mill. In the final step, the composites is characterized for several desired properties, including thermal, physical, and mechanical properties.

Fig. 16: Generalized experimental steps

3.1. Materials

In this thesis, h-BN powder was provided by Asbury Carbon with 6 and 35 µm average particle size and 99.0% purity. LDPE pellets and LLDPE powder with densities and melting points of 0.923 g/ cm^3 and ~108 °C, 0.916 g/ cm^3 and ~122 °C, respectively, were kindly supplied by QAPCO. HDPE pellets with density and melting point of 0.938 g/ cm^3 and ~134 °C, were kindly supplied by Q-chem. IPA (99% purity) was purchased from Research Lab, India. Important h-BN and PE polymers properties are given in Table 4 and Table 5 respectively.

Table 4: Important h-BN properties

Property	hBN6	hBN35
ρ [kg/m^3]	2280	2280
$\lambda_{in\text{-}plane}$ [w $m^{-1}K^{-1}$]	300	300
$\lambda_{through\text{-}plane}$ [w $m^{-1}K^{-1}$]	3	3
L [µm]	6	35
t [µm]	0.5	2
A [m^2/g]	15	1.4

Table 5: PE polymers properties.

Properties	LDPE	LLDPE	HDPE
Grade	Lotrene FD0274	Lotrene Q2018	Lotrene Q3802
Density (g/cm^3)	0.923	0.916	0.938
Melt Flow index (190 ℃/ 2.16 kg)	2.4	2	0.2
Melting Temperature (℃)	108	122	134
Tensile Strength MD/TD (MPa)	11/11	11/11	19
Secant Modulus @ 1 % MD/TD (MPa)		215/245	
Elongation at break MD/TD (%)	300/600	850/900	>600

3.2. Experimental Work

3.2.1. h-BN Exfoliation

Several techniques have been devised to synthesis h-BNNS, including mechanical, liquid, and thermal exfoliation techniques. Results from liquid and thermal exfoliation methods are given in appendix A. In this work, ball milling method was used for h-BN exfoliation. Ball milling is one of the easiest and efficient methods for h-BN exfoliation [148][149]. However, ball milling method is known to create defects and reduce the particle size catastrophically [150]. Nevertheless, these problems can be mitigated by controlling: ball size, ball to powder ratio, milling frequency, and milling time. Another solution is wet ball milling, in which h-BN is milled in a solution [148][149][74]. Here, the effect of milling time on the h-BNNS yield was investigated. In addition, the impact of adding LLDPE to h-BN during the ball milling treatment on the h-BNNS and their

nanocomposites was investigated. Throughout the study the ball to powder ratio and the milling frequency are kept constant

3.2.1.1. Dry Mixing of Pure h-BN

h-BNNS was synthesized using Retsch Mill CryoMill, as shown in Fig. 17 (a). In each run, 3 to 4 g of bulk h-BN and 8 mm diameter steel balls (~ 2 g) were loaded into the steel vial, as shown in Fig. 17 (b), at a ball to powder ratio of 10:1 and at a milling frequency of 30 Hz. The milling time was changed depending on the purpose as follows:

- To study the effect of milling time on the h-BNNS yield, h-BN was milled for 0.5, 1, 1.5, 3, and 4.5 h
- For composites synthesis, h-BN was milled for 1.5 h

3.2.1.2. Dry Mixing of 80%h-BN

To alleviate the ball milling action LLDPE was added to the h-BN powder at a ratio of 1:4. In each run, 4 g containing 80 wt. % h-BN and 20 wt. % LLDPE (80%h-BN) and 8 mm diameter steel balls (~ 2 g) were loaded into the steel vial, at a ball to powder ratio of 10:1 and at a milling frequency of 30 Hz. The mixture was milled for 0.75 and 1.5 h.

To study the effect of milling time on the h-BNNS yield, particle size, and particle thickness, 6 µm h-BN powder (h-BN6) was milled for 0.5, 1, 1.5, 3, and 4.5 hours (h). The resultant was dispersed in isopropanol (IPA) at a concentration of 2 mg/ml. h-BN/IPA mixture was sonicated in a bath sonicator (Branson 2510) for 3 hours to disintegrate the h-BN agglomerates created by the ball milling action and to stabilize the suspension.

To calculate h-BNNS yield, the h-BN suspension was centrifuged using Sigma 3-18KS, 12159 H rotor, at 1500 rpm for 10 minutes. The supernatant was separated, dried, and used to calculate the h-BNNSs yield.

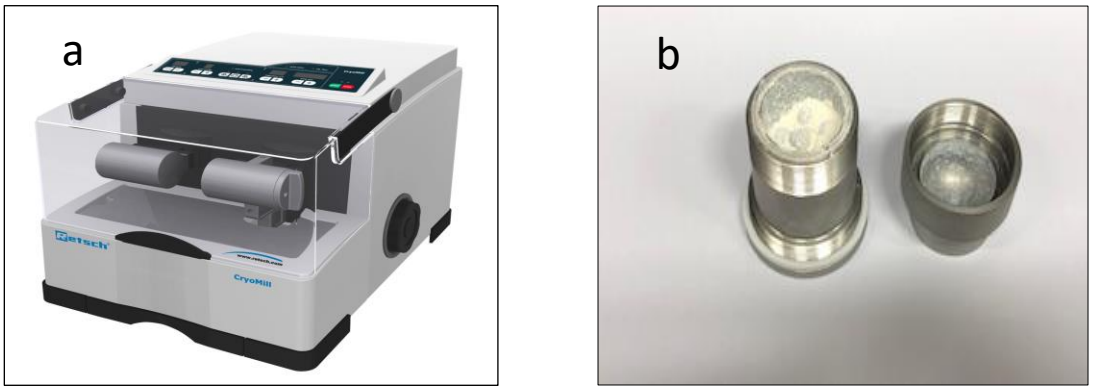

Fig. 17: Ball milling setup. (a) Ball mill and (b) Steel vial loaded with h-BN powder.

3.2.2. Composites Synthesis

As mentioned previously, composites fabrication methods have profound impact on their properties. Therefore, the choice of fabrication method is very vital to achieve their desired properties. Commonly, polymer nanocomposites are prepared by in situ polymerization, melt intercalation, sol gel, and direct powder mixing methods [102]. Of which, dry mixing and melt blending are experimentally simpler and environmentally friendly, due to the absence of solvents or reagents. Fig. 18 illustrates the general methodology followed in preparing the composites.

In this work, the effect of h-BN content, pure h-BN particle sizes, and particle thickness on the composite properties were investigated. In addition, the effect of

processing, composite sheet thickness, and the type of polymer matrix on the composite properties were also investigated. The impact of polymer matrix and h-BN loading was carried by using LDPE, LLDPE and HDPE as a matrix and h-BN content was varied from 0-60 wt. %. The effect of particle size was investigated by incorporating two particle sizes: h-BN6 (6 µm) and h-BN35 (35 µm). The influence of h-BN particle thickness was addressed by incorporating bulk and exfoliated h-BN. Finally, to investigate the the effect of processing and sheet thickness, the composites were prepared by dry mixing and melt blending methods. Afterwards the composites were pressed into 0.5-1 mm and 1-2 mm thick sheets.

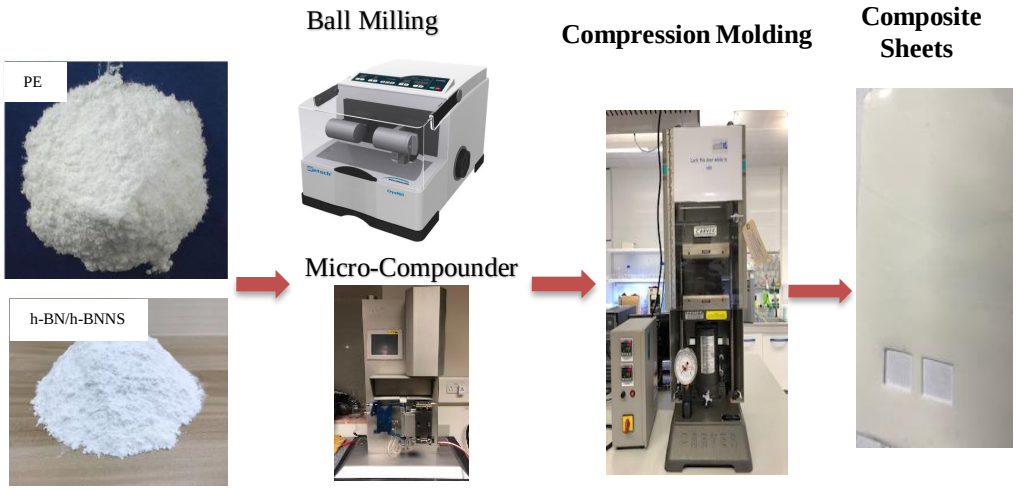

Fig. 18: Composites preparation process.

3.2.2.1. Dry Mixing

h-BN/LLDPE composites and h-BNNSs/LLDPE nanocomposites of several filler loading were prepared by ball milling method. The composites were fabricated using

Retsch Mill CryoMill. Each batch containing 4 g of the filler and LLDPE powders along with 8 mm diameter steel balls (~ 2g) were loaded into the steel vial at ball to powder ratio of 10:1. Then, the mixture was milled at 30 Hz for 45 min.

3.2.2.2. Melt Blending

h-BN/PE composites and h-BNNS/PE nanocomposites were prepared by Xplore Twin Screw 15 ml Micro-Compounder, see Fig. 19. In each batch, 5-9 g of the composites (h-BN powder and PE), were premixed and fed to the extruder slowly to prevent h-BN powder scattering. The process conditions were optimized initially, and hence all experiments were conducted at the optimum operating conditions. These conditions include uniform temperature of 210°C, 100 rpm rotation rate, and 12 min residence time.

Fig. 19: Twin Screw Extruder (Micro-Compounder).

3.2.2.3. Compression Molding

Compression molding was accomplished using Craver Bench Top Heated Manual Press (Model 4386), as shown in Fig. 20. The composites were pressed into ~ 0.5 – 2 mm sheets at a temperature of 180°C and a pressure of ~ 10 bar for 5 min. The composites were pressed into sheets for characterization purposes.

Fig. 20: Craver Bench Top Heated Manual Press.

3.3. Characterization

Characterization is an important part of material science and engineering. Material characterization help in providing information such as mechanical, thermal, chemical, and morphological properties; which play a vital role in process design [151].

In this work, various characterization techniques were utilized, playing a crucial role in achieving our ultimate objective. The characterization techniques were divided into four groups; thermal properties, surface chemistry, morphology and crystal structure, and mechanical properties characterizations.

3.3.1. Thermal Properties

3.3.1.1. Thermogravimetric Analysis (TGA)

TGA is a technique used to measure the weight change of materials as a function of time or temperature [134] [133]. Usually, in this method the temperature is changed at a constant rate and the change in the sample mass over time is measured. TGA can be conducted under several environments, such as nitrogen, air, helium, or even vacuum. This technique is a very useful method to determine the thermal and chemical (oxidation) stability with temperature [152]. In addition, TGA is commonly used to find the composition of materials. For instance, the filler contents of composites are usually determined by heating the composites to a temperature at which the polymer decomposes, then from the reminder the filler content is calculated.

In this study, TGA was performed using Discovery TGA (TA) in a temperature range of 25 ℃ to 700 ℃, at a heating rate of 10℃/min, and under nitrogen environment.

3.3.1.2. Differential Scanning Calorimeter (DSC)

DSC is a thermal technique that detects temperature and heat transfer of materials, associated with transitions or phase change, as a function of time and temperature [153]. DSC measures the amount of heat absorbed or released by a material as a function of temperature and time. DSC provides several thermal properties such as glass transition

temperature, crystalline phase transition temperatures, melting point, specific heat capacity, heat of fusion, and heat of vaporization [153]. For PE composites, DSC measurements are usually conducted under nitrogen environment, heating and cooling at temperature range of 30 ℃ to 200 ℃, and at a heating rate of 10 ℃/min [133].

In this thesis, DSC measurements were done using Q2000 DSC (TA). All measurements were performed under nitrogen environment at a heating and cooling rate of 10 ℃/min. In each run, 5 mg sample was heated from 25 ℃ to 200 ℃ and then cooled from 200 ℃ to 25 ℃ at a heating rate of 10 ℃/min and 3 ℃/min under nitrogen atmosphere.

3.3.1.3. Thermal Conductivity Measurement

There are two main techniques used to measure the thermal conductivity of materials: steady state and transient state. From the name in steady state the measurement is performed in an isothermal condition, while in transient the measurement is performed during the process of heating [154].

In this study, LINSEIS LFA 500 Laser Flash Diffusivity instrument was used to determine the thermal diffusivity and the thermal conductivity of the composites, see Fig. 21 and Fig. 22. In laser flash diffusivity the front of the material is subject to heating and the temperature change at the rare of the sample is observed by infrared scanner as a function of time. To calculate the thermal diffusivity and thermal conductivity, sample information such as thickness, surface area, density, and specific heat capacity are required. The machine determines the half time ($t_{1/2}$), which is the time required by the sample to reach half the maximum temperature. The thermal diffusivity (α) is calculated

from the sample thickness (l) and half time ($t_{1/2}$), as shown in equation 3.1. Subsequently, the thermal conductivity (K) is calculated from the thermal diffusivity (α), the specific heat capacity (C_P), and the density(ρ) of the material, as shown in equation 3.2.

$$\alpha = 0.13879 \frac{L^2}{t_{\frac{1}{2}}} \quad 3.1$$

$$K = \alpha\, C_P\, \rho \quad 3.2$$

LFA 500 is equipped with sample holders of different sizes and shapes. In this work, square specimen holder of 10 cm by 10 cm dimensions was used. Therefore, the samples were cut by 10 cm by 10 cm square die and the surface of the samples were smoothed by sand papers to keep their thickness in the range of 0.1 mm-2 mm. Afterward, the specimens were coated with graphite spray to aid their ability to absorb and emit radiation. The measurement was conducted at room temperature and repeated several times for statistical purposes.

Fig. 21: LINSEIS Laser Flash Diffusivity instrument used for thermal conductivity measurements.

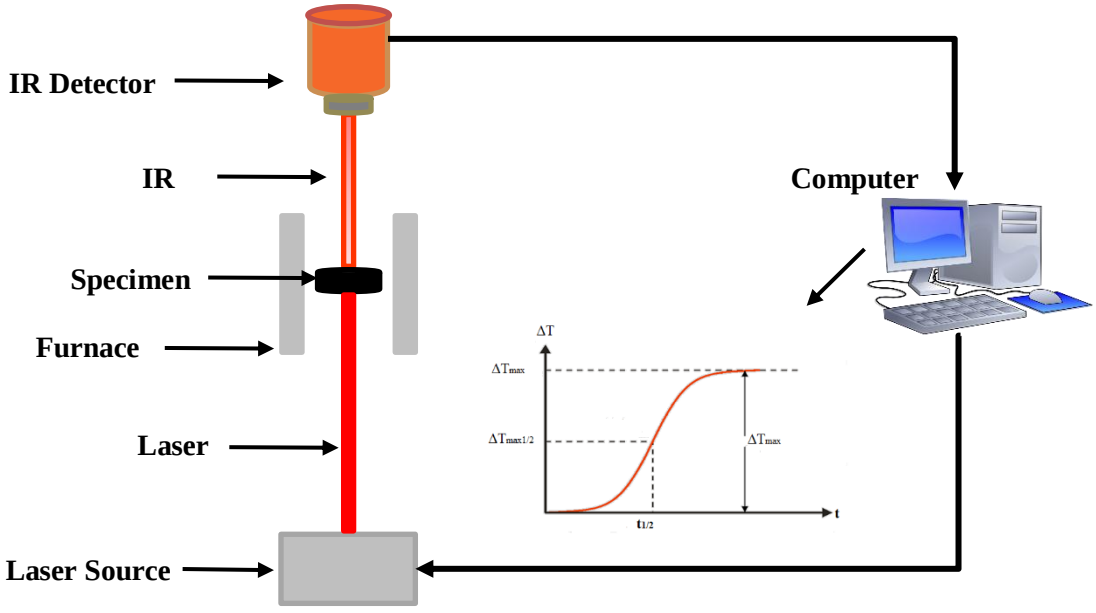

Fig. 22: Schematic Diagram of Laser Flash Thermal Diffusivity.

3.3.2. Surface Chemistry

3.3.2.1. X-ray Photoelectron Spectroscopy (XPS)

XPS is a very strong surface analysis technique that can provide elemental and chemical state data. XPS can analysis is limited to the sample surface due to its limited penetration to about 2-5 nm depth. In XPS, the sample is irradiated with x-rays which lead to sample excitation as a result the sample emits photoelectrons. The binding energy which is related to the kinetic energy of the emitted electrons, is a unique characteristic of each atom, is used to construct spectrum [155]. All atoms in the sample are assigned to each peak in the spectrum. As a result, information such as atomic concentration and chemical bonding can be acquired from XPS data.

In this work, XPS was utilized to analyze h-BN before and after the ball milling treatment.

3.3.2.2. Energy-Dispersive X-ray spectroscopy (EDS)

EDS is a technique used to determine and quantify elemental compositions of a material. EDS is assembled in conjunction with SEM, in which the electron beams from the SEM bombard the sample which excites the samples causing it to release x-rays. The x-rays are detected by an energy dispersive detector of the EDS. The detector measures the intensity (quantity) and energy of the emitted x-rays constructing spectrum. Each peak in the spectrum is ascribed to a specific element in the sample [156]. Beside elemental quantification, EDS is a very strong technique for elemental mapping especially that it can analyze materials in a micrometer scale.

In this study, EDS was done using AMETEK EDAX integrated in QUANTA 400 SEM. EDS was used to characterize h-BN before and after the ball milling treatment.

3.3.3. Morphology and Crystal Structure

3.3.3.1. X-ray Diffraction (XRD)

X-ray diffraction is a technique used to determine the crystal structure of materials. XRD provides information such as the average atomic spacing, crystal structure, phases, sample purity, average grain size, and defects [157]. In XRD the samples are irradiated with x-rays at different angles and the diffraction or scattering of these rays caused by the different lattice plane are used to produce different peaks. The interaction of the sample and the incident rays form constructive interference if they satisfy Bragg's Law:

$$n\gamma = 2dsin(\theta) \quad 3.3$$

where 'γ' is the wave length of the incident ray, 'd' is the inter-planar spacing (d-spacing), and 'θ' is the diffraction angle or Bragg's angle. All parameters in eqn. 3.3 are known except the d-spacing, thus it can be easily calculated.

XRD data can also be used to approximate the crystallite size (C_s) using Scherrer equation as follows [158][159]:

$$C_s = \frac{f\,\gamma}{\beta\, Cos\,(\theta)} \quad 3.4$$

where 'f' is the shape factor usually taken as 0.89 or 0.94, 'γ' is the wave length, 'β', also written as FWHM, is the full width as maximum height, and 'θ' is the Bragg's angle.

In this work, XRD was done by Ultima IV X-RAY DIFFRACTOMETER. CuK (alpha) (0.1542 nm) radiation at 40 kV and 20 mA was used to analyze h-BN, h-BNNSs, and their

composites. The process conditions were: 0.02^{O} step size, 1 s dwell time, and $10\text{-}60^{O}$ scan range.

3.3.3.2. Scanning Electron Microscopy (SEM)

Scanning electron microscope scans the sample surface with strong focused electron beam to create high resolution images of up to ~ 1 nm. As a sample is bombarded by the electron beams three main signals are created: electrons back-scattering, the sample emitting secondary electron, and x-ray being emitted. X-ray can be used for elemental analysis as aforementioned in EDS. While back-scattered and secondary electrons are used for morphological analysis. SEM provides surface information such as texture, defects, particle size, and particle shape [156][160][161].

Here, FEI Nova NanoSEM 450 was used to analyze the morphology of h-BN, h-BNNSs, and their composites. Because of the insulative nature of h-BN and their composites, the specimens in this work were coated with gold prior to the SEM analysis. The analyses were performed at 5-30 KV, high vacuum, and magnification of 10000 to 400000.

3.3.3.3. Transmission Electron Microscope (TEM)

TEM is another electron microscsopy techniques where electrons are transmitted through the sample creating high resolution images. Unlike SEM, TEM give information beyond the surface of the sample, such as crystal structure, chemical composition of phases, defects, orientation, and even mechanical properties. In addition, the electron beams in TEM is above 100 KV enabling it to give high resolution images in a molecular

level [156][161][162][163]. In TEM, the sample preparation is very vital; typically the sample thickness is in the range of 100-200 nm [156].

In this study, FEI Talos F200X TEM was used to analyze the morphology of h-BNNSs. Images with resolution ranging from 5 nm to 200 nm were captured.

3.3.3.4. Atomic Force Microscopy (AFM)

AFM is a high-resolution surface characterization technique that use a tip to study the surface topography and the properties of materials at atomic level. AFM works by scanning the sample by a tip attached to a spring cantilever. As the tip move close to the sample the atoms of the sample and the tip interact by an attractive and repulsive force. The deflection of the tip is detected by the laser analyzing the surface topographies of the material. AFM provides information on surface topography, including sample roughness, thickness, and height giving 3D images. In addition, AFM can also provide atomic level mechanical, electrical, magnetic and even chemical properties [156][164].

In this work, BRUKER DIMENSION icon was used to perform AFM analysis on h-BN before and after BM. The samples were dispersed in IPA with the help of bath sonicator. Afterwards, one drop of the suspension was placed in a mica sample holder. Finally, the analysis was conducted under a peak force QNM in air mode, at 0.3-0.5 Hz scan rate, and 5-20 μm scan area.

3.3.4. Mechanical Properties

Knowing the mechanical properties of a material is very essential for the engineering design and material fabrication process. For instance, polymers are very flexible making their processing relatively easier. The incorporation of h-BN in the PE

matrix is known to enhance their mechanical properties [63][165]. However, at high h-BN loading the mechanical properties of PE composites deteriorate. Moreover, the composites become very viscous leading to difficulty in processing. Therefore, studying the mechanical properties is indispensable in nanocomposites.

Generally, the mechanical properties of a material are determined by subjecting the material to a force and the change in the material behavior is translated into specific properties. Mechanical properties of PE is usually characterized by tensile, flexural, impact, and hardness tests. Tensile test is the most common mechanical test, in which a material of known dimensions is subjected to an axial load pulling the specimen at one end. The change in the material dimension is recorded as a function of the load; which is afterward used to obtain stress-strain curve. The stress-strain curves provide information such as Young's modulus, yield stress, elongation at break, and ultimate tensile strength. Depending on the measurement conditions such as temperature, load, and applied strain, PE composites can be glassy, brittle, or elastic [133].

In this work, tensile test was performed using MTS Insight Electromechanical testing system (1 kN). The polymer samples were prepared using a dumbbell-shaped ASTM D638-5 die.

3.3.5. Wettability

Wettability is a surface property of a material that determines the wetting ability of a liquid in contact with a solid surface. Wettability is governed by the intermolecular interactions, cohesive and adhesive forces, between a fluid and a solid. When two fluid phases, such as water and air, are in contact with a solid surface; the wetting ability of one

of the phases is characterized by the contact angle (CA) formed between that phase and the solid phase. A wetting fluid will spread and form a low CA (< 90º) indicating good wettability. In contrast, a non-wetting fluid will contract and minimize the contact with the solid surface and form a high CA (>90º) [166].

Many researches has shown that the wettability a heat transfer surface has tremendous impact on the heat transfer performance [167][168][169]. The wettability of PE polymers is very poor due their nonpolar hydrophobic surface. Nonetheless, the wettability of these polymers can be enhanced by several treatments, including plasma treatment, chemical etching, corona discharge, mechanical abrasion, primers, and UV irradiation [170].

In this thesis, the CA measurements were used to evaluate the wettability of the h-BN/PE composites. The CA measurements were conducted using Kruse drop shape analyzer DSA25. The Sample preparations included cutting the composite into a small stripe with a flat surface. A 2 µl DI water droplet was placed on the top of the composite stripe and the contact angle of the water droplet was measured. The measurement was repeated three times or more for statistical purposes.

4. RESULTS AND DISCUSSION

4.1. Bulk h-BN

h-BN is composed of equal number of boron and nitrogen elements. Table 6 displays the atomic surface composition of bulk h-BN6 and h-BN35 obtained from XPS. The data are in good agreement with the h-BN purity (~ 99 %) provided by the manufacturer. The XRD patterns (Fig. 23) of h-BN6 and h-BN35 confirmed presence all the typical peaks of h-BN located at at 2θ of 26.66º, 41.7º, 43.9º, 50.2º, and 55.4º corresponding to (002), (100), (101), (102), and (004) planes, respectively [75][171][172]. Both h-BN6 and h-BN35 showed very high crystallinity demonstrated by the very sharp peaks, which is a very common feature of h-BN. The XRD pattern of h-BN35 showed relatively sharper peaks which might be attributed to their larger crystallite, i.e. number of layers (stacking).

Fig. 24 shows the SEM images of h-BN6 and h-BN35. The particles of both h-BN6 and h-BN35 appear as agglomerated multilayered sheets with range of particle sizes. The average h-BN particle sizes ranged between 1 to 6 µm and that of h-BN35 ranged from 10 µm to 50 µm. These values are in also good agreement with the data provided by the manufacturer, which are 6 µm for h-BN6 and 35 µm for h-BN35.

Table 6: Surface atomic composition of bulk h-BN6 and h-BN35.

Sample	B 1s (%)	N 1s (%)	O 1s (%)
Bulk h-BN6	53.5	43.9	2.6
Bulk h-BN35	46.7	50.9	2.4

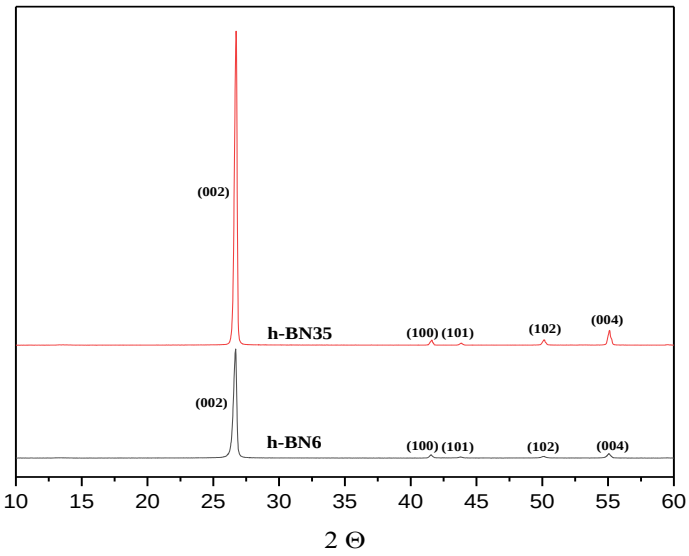

Fig. 23: XRD spectra of bulk h-BN6 and h-BN35.

4.2. h-BN Exfoliation

To investigate the impacts of BM treatment on h-BN features, h-BN of two particle sizes, h-BN6 and h-BN35, were used as a raw material. Most of the exfoliation experiments were performed on h-BN6. After the BM treatment, h-BN6 was analyzed using various characterization methods, including yield and stability, XRD, AFM, SEM, TEM, EDS, and XPS. Thereafter, the effect of exfoliation on the two h-BN particle sizes was studied as well. Finally, ways of improving the BM treatment was examined.

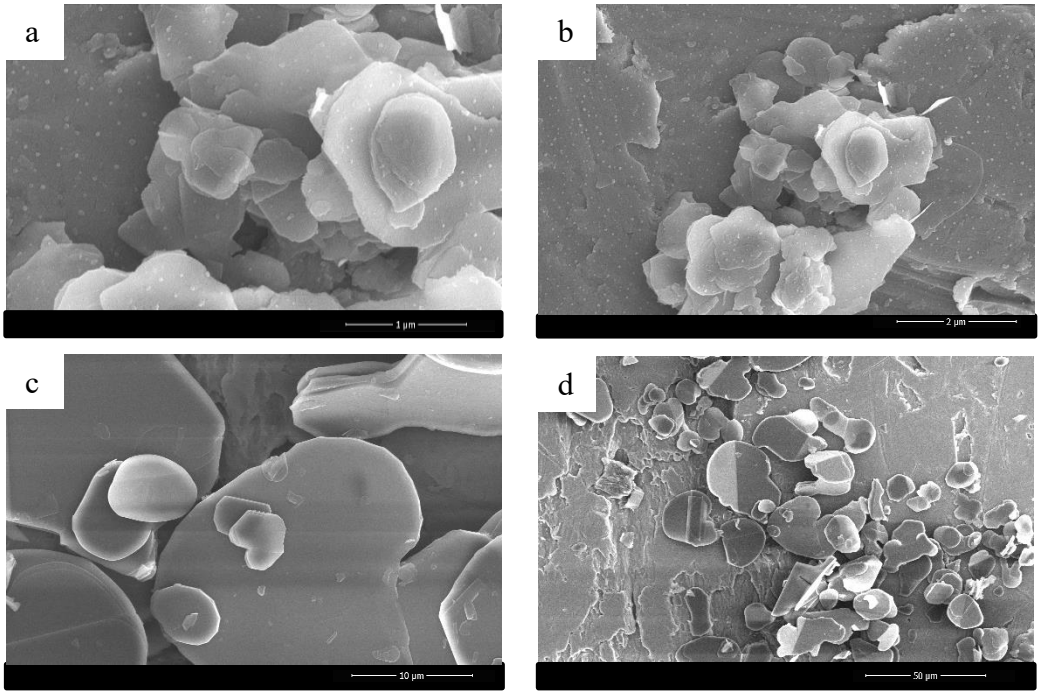

Fig. 24: SEM images of bulk h-BN; h-BN6 ((a) and (b)) and h-BN35 ((c) and (d)).

4.2.1. Yield and Stability of h-BN6 after the BM Treatment

Yield and stability of h-BNNS were used to determine the optimum BM time. Fig. 25 displays h-BNNSs yield as a function of BM time. The yield of h-BNNSs was surprisingly high, ranging from 38 % at 0.5 h to 61 % at 4.5 h. In the first 4 milling times, 0.5, 1, 1.5 and 3 h, the yield showed significant improvements ranging from 38 % at 0.5 h to 58 % at 3 h; suggesting very strong dependence on milling time. In contrast, no clear improvement was observed when the milling time was increased further to 4.5 h. For example, the yield only increased by 3 factors to reach 61 %. It seems that at lower BM time the exfoliation effect is significant producing light h-BN particles. However, at higher milling time, i.e. 4.5 h, the exfoliated product starts to agglomerate resulting in heavy h-

BN particles. Namba et al. stated that at a high BM rotation speeds h-BN formed agglomeration [171], which suggest similar results at a high milling time as in this study. Obviously, the lighter the particles the higher the yield. Therefore, based on the yield results the optimum BM time is in the range of 1.5 – 3 h. Nevertheless, the high h-BNNS yield even at 0.5 h milling time indicates a very high efficiency of this method. The high h-BNNS yield in this work is comparable to literature values of similar BM methods [74][149][173], and it is much higher than liquid exfoliation method [75].

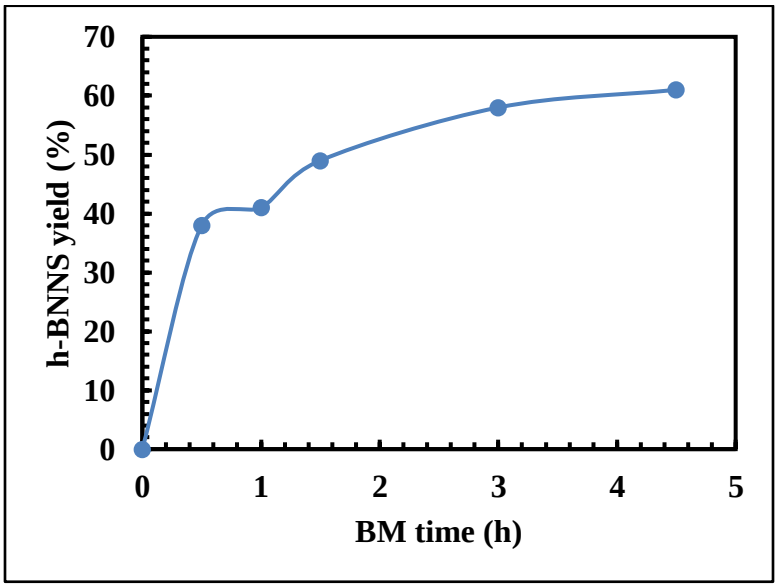

Fig. 25: h-BNNS yield, synthesized from h-BN6, as a function of BM time.

The stabilities of h-BN ball milled at a various milling time were investigated by dispersing them in IPA, as shown in Fig. 26 (a). After 2 weeks, these suspensions exhibited a milky white color, indicating very high stability. Moreover, h-BN 1.5 h and h-BN 3 h were dispersed in water with the assistance of a mild bath sonication (3 h) and compared

with aqueous suspension of h-BN prepared by vigorous bath sonication (24 h), i.e. liquid exfoliation, as shown in Fig. 26 (b). The aqueous suspensions of h-BN 1.5 h and h-BN 3 h demonstrated a milky white color with a high stability of more than 1 week. However, the liquid exfoliation product displayed a slightly transparent suspension indicating limited exfoliation.

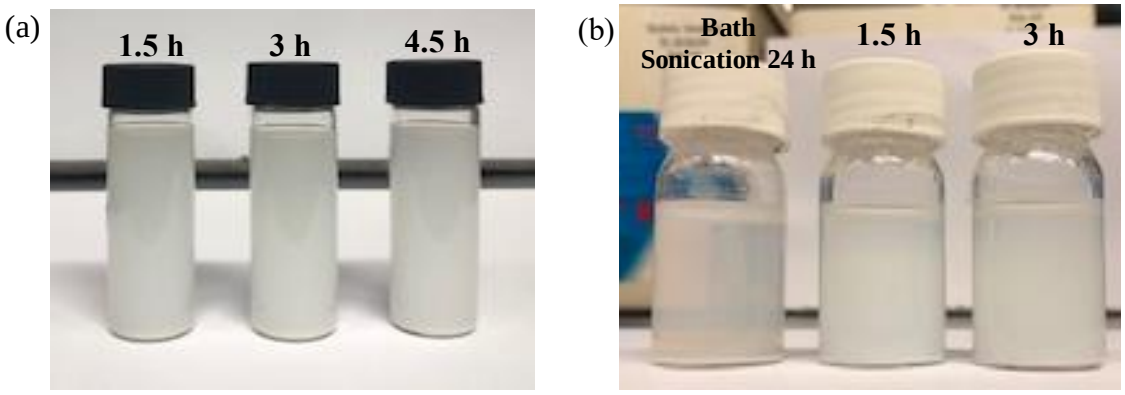

Fig. 26: Stability of h-BNNS, synthesized from h-BN6, prepared by BM and liquid exfoliation. (a) Compare the stability of h-BNNS in IPA prepared by various milling time (after 2 weeks) and (b) Compare the stability of h-BNNS in water prepared by 24 h of bath sonication with that prepared by BM (after 1 week).

Driven by the high h-BNNS yield and excellent stability. The BM products were further studied using XRD, SEM, TEM, XPS, AFM and EDS. It is worth noted that all analyses were conducted right after the BM treatments without additional separation step, i.e. separation of the exfoliated h-BN from the bulk h-BN.

4.2.2. Morphology and Crystal Structure of h-BN6 after the BM Treatment

The XRD patterns of bulk h-BN (0 h), as well as h-BN ball milled for several milling time are shown in Fig. 27. Bulk h-BN showed peaks at 2 θ values of 26.66º, 41.7º, 43.9º, 50.2º, and 55.4º, which corresponds to the (002), (100), (101), (102), and (004) planes respectively [75][171][172]. These peaks diminished significantly or almost disappeared with increasing milling time. Clear reduction in the (002) peaks was observed when the milling time was increased from 0.5 h to 1.5 h. However, no significant reduction was observed above 1.5 h milling time, i.e. at 3 h and 4.5 h, suggesting that most h-BNNSs were formed at or below 1.5 h. The XRD results clearly agrees with the yield and stability results discussed earlier.

In addition, the (002) peaks broadened and shifted to the left as the milling time progressed. As compared to the bulk h-BN, the ball milled h-BN exhibited higher d-spacing and FWHM, which is a sign of exfoliation. For example, the d-spacing and FWHM increased from 3.3406 and 0.2741 of bulk h-BN (0 h) to 3.3891 and 3.5262 of h-BN 4.5 h, respectively. Moreover, the average crystallite sizes of h-BN 0 h and h-BN 4.5 h, calculated by Scherrer's equation (eqn. 4.3), were found to be approximately 29 nm and 2.3 nm respectively. Furthermore, the number of nanosheets (layers) was approximated by dividing the average crystallite size by the d-spacing. The average number of layers of bulk h-BN and h-BN milled for 4.5 h were approximately 90 and 7 layers respectively. The summary of the XRD analyses are given in Table 7.

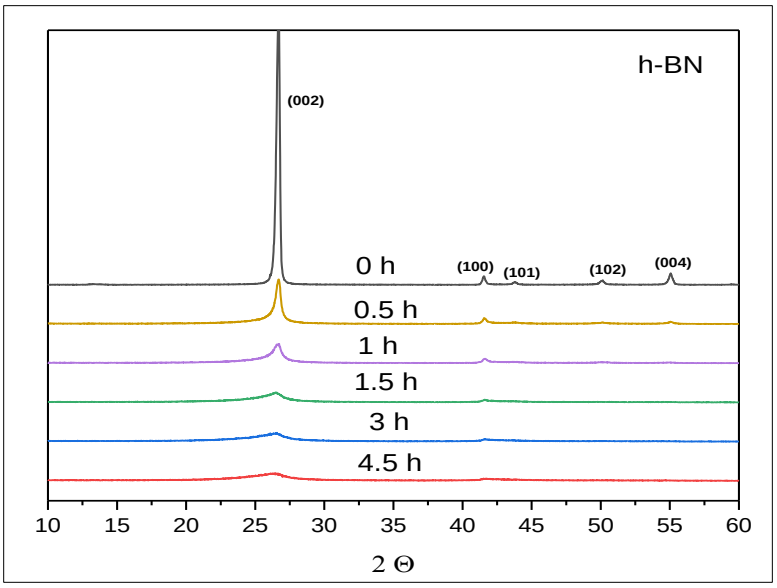

Fig. 27: XRD patterns of h-BN before and after BM for various durations.

Table 7: Position of (002) peak, d-spacing, and crystallite size of bulk h-BN, and h-BN milled for various milling time.

Milling Time (h)	2 θ (°)	d-spacing (nm)	FWHM (°)	Crystallite size (nm)	Layers
0	26.66	0.334	0.274	29.8	90
0.5	26.66	0.334	0.487	16.7	50
1	26.62	0.335	0.928	8.8	27
1.5	26.47	0.337	2.19	3.7	11
3	26.45	0.338	2.91	2.8	9
4.5	26.27	0.339	3.53	2.3	7

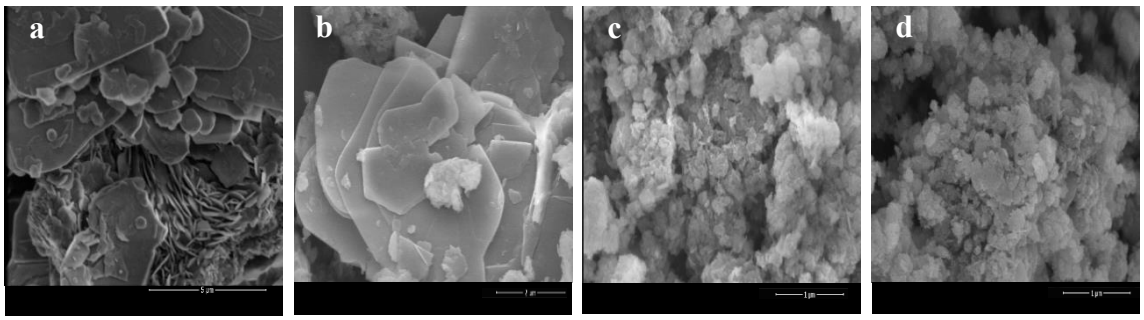

Fig. 28: SEM images of (a) Bulk h-BN6 and h-BN6 milled for (b) 0.5 hours, (c) 1.5 hours, and (d) 3 hours.

Fig. 28 (a-d)) shows SEM images of h-BN before and after BM treatment. Pristine h-BN presented as an agglomerated sheets of different particle sizes with an average of ~ 4-6 µm. Clearly, the average particle size dropped significantly with the increase in milling time. The average particle size of h-BN 0.5 h was similar to the pristine h-BN, however at 1.5 and 3 h the average particle size dropped drastically to below 500 nm. The reduction in the average particle size is usually accompanied by the reduction in the particle thickness, which is an indication of h-BN exfoliation. As in the XRD, yield, and stability results, the average particle size demonstrated no variation between h-BN 1.5 h and h-BN 3 h, suggesting sufficient exfoliation at 1.5 h.

The TEM images displayed in Fig. 29 (a-c) confirmed the presence of single and few-layered h-BN nanosheets. In Fig. 29 (a), an agglomerated h-BN nanosheets are shown, in addition, a single transparent sheet is shown at the bottom left corner. Fig. 29 (b and c) displays h-BNNSs of various thickness, ranging from less than 5 nm to 10 nm, validating the average crystallite size values found in the XRD analyses.

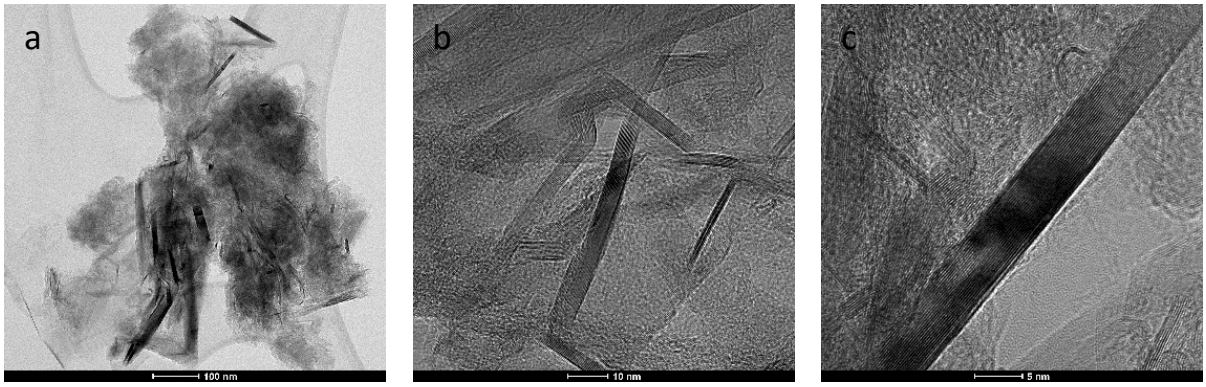

Fig. 29: TEM images of h-BN6 milled for 1.5 h.

4.2.3. Surface Chemistry of h-BN6 After the BM Treatment

Fig. 30 displays the XPS spectra of h-BN6 before and after the BM treatment. Bulk h-BN6 exhibited a clear peak at 190.4 eV related to the B-N group, see Fig. 29 (a). In addition, the bulk h-BN had a weak peak at 191.1 eV which was assigned to the B-O group, similar peak at 193.1 eV was found by Namba et al [171], which they assigned to an oxidized boron. After the BM treatment the peak related to the B-O group intensified and partially shifted to 191.8 eV. The presence of a weak B-O group peak in the bulk h-BN spectrum is caused by the small atomic concentration of oxygen (~2.58 %). The atomic concentration of oxygen increased to 10.23 % after the BM treatment, justifying the B-O group peak intensification. However, the actual oxygen group is not determined, for example, Namba's group assigned the oxygen group to an OH group. Nevertheless, the existence of chemical reaction was manifested during the BM treatment. For instance, the color of h-BN changed from white initially to beige after the ball milling treatment,

and then to off white after few seconds of atmospheric exposure, indicating a chemical change, as shown in Fig 31.

Since no vacuum was utilized during the BM experiment, oxygen was present during the BM treatment. Therefore, the first discoloration, beige color, might be caused by the oxidation and the second discoloration, off white, might be caused by the absorption of moisture. N 1s XPS spectra, shown in Fig. 30 (b), had a peak at 398 eV, which broadened and weakened after the ball milling treatment. In contrast, O 1s XPS spectra, displayed in Fig. 30 (c), had a peak at 532.6 eV, which intensified after the ball milling treatment. The changes in the N 1s and O 1s spectra might be caused by the increase in the atomic concentration of oxygen, which was accompanied by the reduction in the atomic concentration of nitrogen. Table 8 summarizes the surface compositions (atomic concentration) of h-BN6 before and after the ball milling treatment.

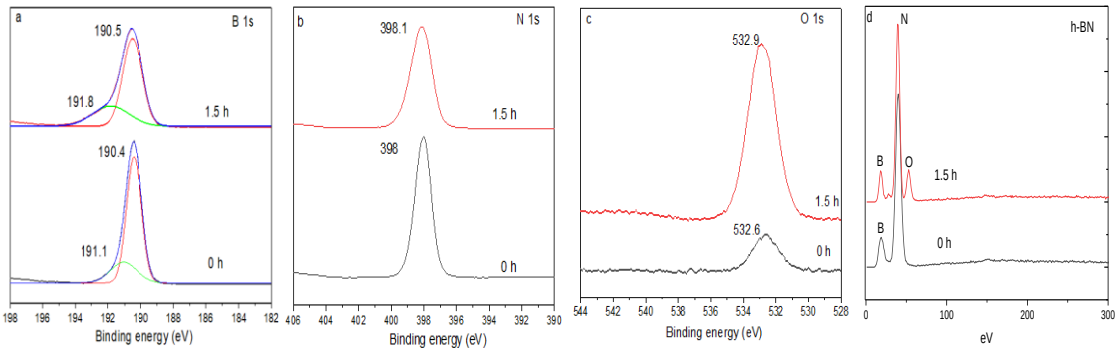

Fig. 30: XPS and EDX spectra of bulk h-BN6 and ball milled h-BN6 for 1.5 h. XPS spectra: (a) B 1s, (b) N 1s, and (c) O 1s. (d) EDX spectra.

Fig. 31: h-BN6 color change after the BM treatment.

Fig. 30 (d) shows EDX spectra of h-BN6 before and after the ball milling treatment. As expected, bulk h-BN (0 h) had two peaks attributed to boron and nitrogen. As in the XPS, a new peak ascribed to oxygen appeared after the ball milling treatment.

Table 8: The surface compositions, atomic concentration (%), of h-BN6 before and after the BM treatment

Sample	**B 1s (%)**	**N 1s (%)**	**O 1s (%)**
Bulk h-BN6	53.5	43.9	2.6
Ball milled h-BN6	50.3	39.1	10.5

4.2.4. The Effect of the BM Treatment on the Particle Sizes of h-BN6 and h-BN35

From the above results, the optimum BM time was chosen to be 1.5 h. Thereafter, the effect of BM (1.5 h) on two h-BN particle sizes, h-BN6 and h-BN35, was explored. Fig. 32 shows the XRD patterns of h-BN6 and h-BN35 after the BM treatment. The XRD patterns of h-BN6 and h-BN35 displayed a similar trend. For instance, both h-BN6 and h-BN35 exhibited (002) and (100) peaks and lost the other peaks. Nonetheless, their average crystallite size, FWHM, and d-spacing, showed slight differences. For instance, the

crystallite sizes of h-BN6 and h-BN35 after the BM treatment were ~3.7 nm and ~ 6.4 nm. This was expected since the pristine h-BN35 is much bigger than h-BN6. Nevertheless, their crystallite sizes reduced drastically which is an indication of exfoliation. The exfoliation of both h-BN6 and h-BN35 was also supported by their remarkable stability in IPA, more than one month, as shown in Fig. 33.

The SEM images, shown in Fig. 34 (a-d), illustrates the effect of ball milling treatment on the particle sizes of h-BN6 and h-BN35. Substantial lowering on the average particle sizes was noticed in both h-BN6 and h-BN35, as shown in Fig 34 (b and d). In particular, the average particle size of h-BN6 and h-BN35 dropped from 6 µm and 35 µm in the pure h-BN to below ~ 500 nm and ~ 1 µm after the BM treatment, respectively.

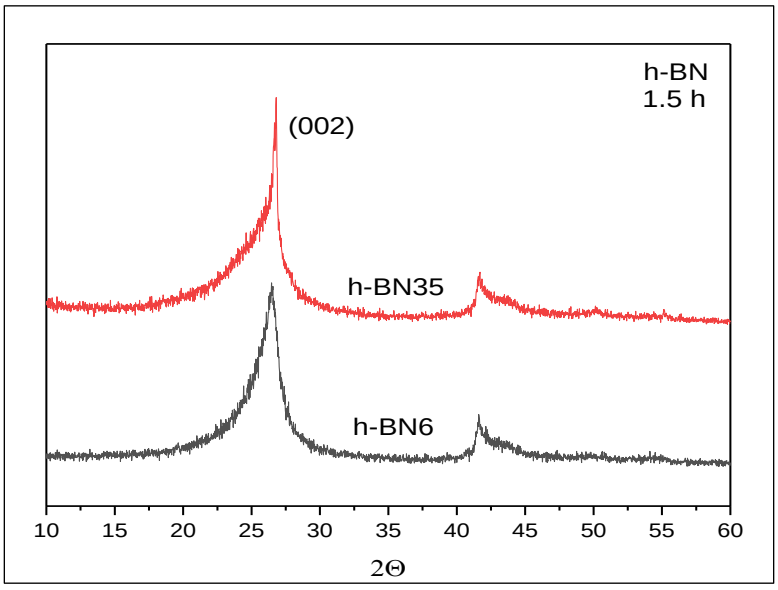

Fig. 32: XRD pattern of h-BN6 and h-BN35 after 1.5 h of BM treatment.

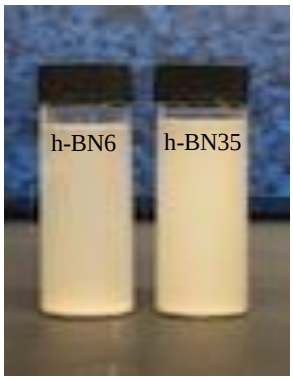

Fig. 33: Stability of h-BN6 and h-BN 35 after 1.5 h of BM treatment in IPA (1 month).

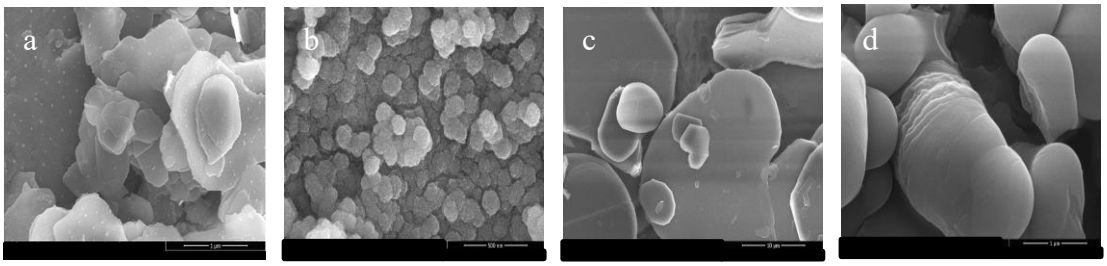

Fig. 34: SEM images of bulk h-BN (a) 6 µm and (c) 35 µm and h-BN milled for 1.5 h (b) 6 µm and (d) 35 µm.

4.2.5. Drawbacks of BM Exfoliation and Proposed Mitigation

4.2.5.1. Drawbacks of the BM Treatment

As discussed above, the milling action has catastrophic impacts on the particle size. The substantial drop on the average particle size rises some concern on their subsequent application, i.e. in thermally conductive nanocomposites. As aforementioned previously, bigger particles tend to form network easily inside the polymer matrix, hence they are more suitable for the thermal conductivity enhancement.

Beside particle size, the BM treatment might lead to filler defects and amorphization [150]. For example, the milling action could lead to a positive shear force that pill the h-BN layers or could lead to bends and defects, as illustrated in Fig. 35 (a-d). For example, Fig. 35 (a) shows the splitting of h-BN layers, which prompts exfoliation, whereas Fig. 35 (b) shows the bending of h-BN layers. Obviously, bending is undesired because it acts as source of defects, which as previously discussed are the main causes of phonon scattering. As stated earlier, phonon scattering deteriorates the thermal conductivity. Thus, it is highly desired to minimize the impacts of the BM treatment; substantial reduction on particle size, defects formation, and filler amorphization.

4.2.5.2. Mitigation

The side effects of the BM treatments are usually tackled by reducing the milling time, using small balls (light-weight), lowering the ball to powder ratio, lowering the milling frequency, or by adding materials, such as solvents or polymers, to alleviate the shear force [74] [171][174][149].

Here, the problems of defects formation and amorphization are mitigated by the incorporation of LLDPE powder along with h-BN35 during the BM treatment. For example, a mixture of h-BN35 and LLDPE containing 80 wt. % h-BN35 (80%h-BN35) was ball milled for 45 min, 90 min, and 120 min, and their products were analyzed by XRD, SEM, and XPS.

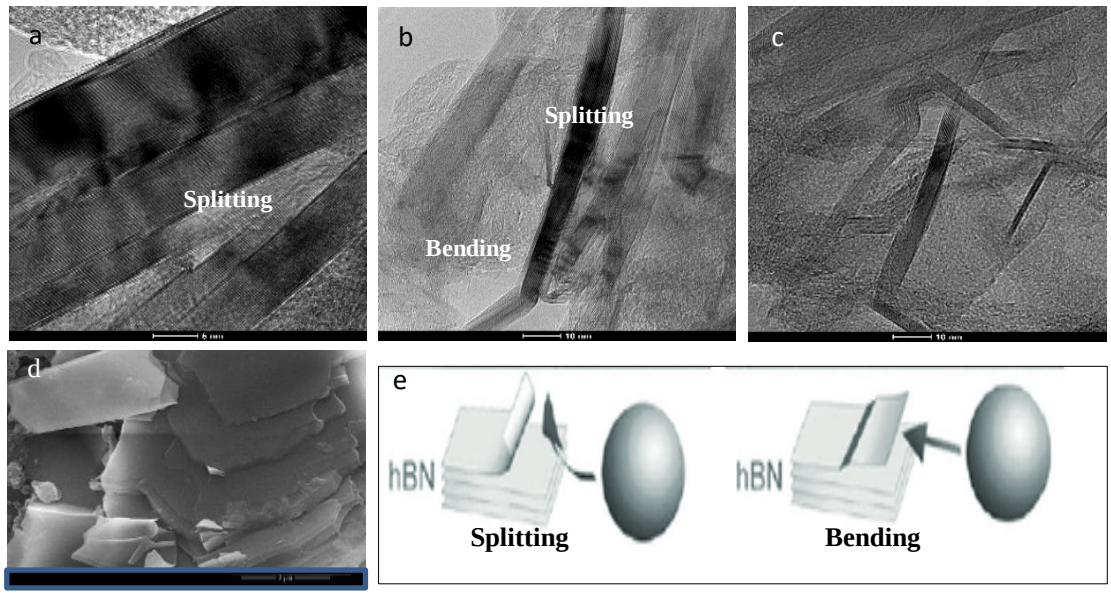

Fig. 35: TEM images, SEM image, and Schematic diagram of h-BN illustrating the effect of the BM action. TEM images (a) Splitting of h-BN layers, (b) Splitting and bending of h-BN layers, and (c) Separating of h-BN layers. (d) SEM image illustrate splitting of h-BN layers. (e) Schematic diagram illustrating the effect of BM action; splitting and bending. Fig 35 (e) was modified from [70]**.**

Fig. 36 shows the XRD patterns of h-BN35 and 80%h-BN35 after 90 min of BM treatment. The XRD spectrum of h-BN35 shows two asymmetrically broadened peaks corresponding to the (002) and the (100) planes. Peak asymmetry is frequently seen in BM treatment and it is ascribed to the defects formation and amorphization [150][175][176]. In contrast, the XRD pattern of 80%h-BN35 shows clearly symmetrical (002) peak. However, the left side of peak (002) seems to be swelled, which is caused by the presence of two neighboring peaks at 2θ values of 21.56º and 23.7º corresponding to the crystalline and amorphous phases of LLDPE respectively [177][178]. In addition, the (101) peak almost disappeared in 80%h-BN35 while it is present in h-BN35, whereas the (004) peak

is present in 80%h-BN35 and it is absent in h-BN35. Li et al [179], reported high quality h-BNNS synthesis using BM method. The XRD pattern of their h-BNNS showed the disappearance of all other peaks but (002) and (004) peaks after 2 h of BM curing. They stated that their h-BNNS preferred an orientation or alignment parallel to the (002) basal plane.

Fig. 37 shows the XRD spectra of BMd-80%h-BN35 at various milling time. Bulk h-BN35 showed peaks at 2 θ values of 26.72º, 41.5º, 43.8º, 50.1º, and 55.1º, which corresponds to the (002), (100), (101), (102), and (004) planes respectively [75][171][172]. The XRD spectra of 80%h-BN35 showed clear reduction in the (100), (101), and (102) peaks as the milling time was raised. In addition, the (002) peak demonstrated slight weakening functionality with milling time. As stated above, this might be caused by the preferential orientation of the milled 80%h-BN35. Besides, the (002) peak of the milled 80%h-BN35 broadened and shifted to the left, implying exfoliation. For example, the d-spacing and FWHM increased from 0.33335 nm and 0.2382º of the un-milled h-BN35 (0 h) to 0.3371nm and 0.3261º of the milled (0.75 h) 80%h-BN35, respectively. The summary of the XRD analyses are given in Table 9.

Table 9: Position of (002) peak, d-spacing, and crystallite size of bulk h-BN35, and 80%h-BN35 milled for various milling time.

Milling Time (h)	2 θ (°)	d-spacing (nm)	FWHM (°)	Crystallite size (nm)	Number of Layers
0	26.72	0.333	0.238	34.3	103
0.45	26.69	0.337	0.326	25.0	74
1.5	26.69	0.337	0.400	20.4	61
2	26.72	0.333	0.398	20.5	62

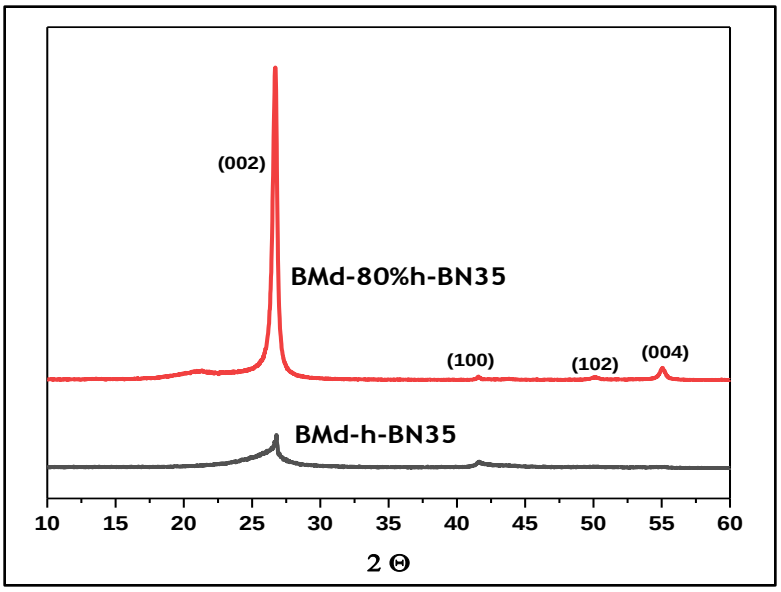

Fig. 36: XRD patterns of h-BN35 and h-BN35/LLDPE mixture ball milled for 1.5 h.

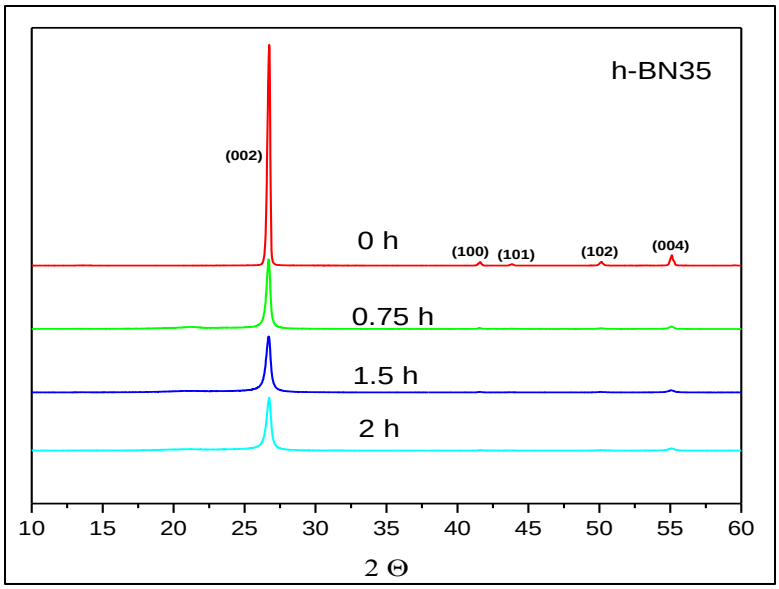

Fig. 37: XRD patterns of h-BN35 and 80%h-BN35/LLDPE at several milling time.

4.3. h-BN/PE Composites

Aforementioned in chapter 3, the ultimate goal of this work is to synthesis PE composites with enhanced thermal, mechanical, and physical properties. The thermal and mechanical properties of polymers, PE in this case, are frequently enhanced by the incorporation of fillers. In general, the properties of the resultant composites depend on many variables, such as filler type and features, polymer type and features, filler and polymer composites preparation methods. Here, the effect of composite processing method, type of polymers, and filler features on the physical, thermal, and mechanical properties of PE composite were examined.

4.3.1. Morphology and Crystal Structure of h-BN/PE Composites

Fig. 38 shows the XRD spectra of h-BN/LLDPE composites. The magnified XRD spectrum of pure LLDPE shows two peaks at a 2θ values of 21.56° and 23.94° which correspond to the (110) and (221) planes, respectively [180]. Beside the above LLDPE peaks, the XRD spectra of h-BN6/LLDPE and h-BN35/LLDPE shows two clear h-BN peaks at a 2θ values of 26.7° and 55.1º which correspond to the (002) and (004) planes. The presence of (002) and (004) peaks and the absence of (100), (101), and (102) peaks in the h-BN/LLDPE composites are usually associated with the h-BN orientation inside the polymer matrix, in this case horizontal orientation [181]. Similar results were found for h-BN/LDPE composites, and the results are included in Appendix B, Fig. B. 1.

Fig. 39 shows the SEM images of pure LLDPE and h-BN35/LLDPE composites. The cross-sectional surface of pure LLDPE is shown as a smooth surface, see Fig. 39 (a). Fig. 39 (b) and Fig. 39 (c) display the SEM images of h-BN35/LLDPE composites, in

which the h-BN particles were arranged horizontally and vertically, respectively. Obviously, h-BN orientation plays vital role on the thermal conductivity enhancement. For instance, the in-plane and through-plane 'λ' of h-BN are 300 and 3 W m^{-1} K^{-1}, respectively. In the horizontal arrangement, h-BN is oriented in the through plane direction, thus the 'λ' value is 3 W m^{-1} K^{-1}. While, in the vertical arrangement, h-BN is oriented in the in-plane direction, and hence the 'λ' value is 300 W m^{-1} K^{-1}. Clearly, vertical arrangement is favored for better thermal conductivity improvement.

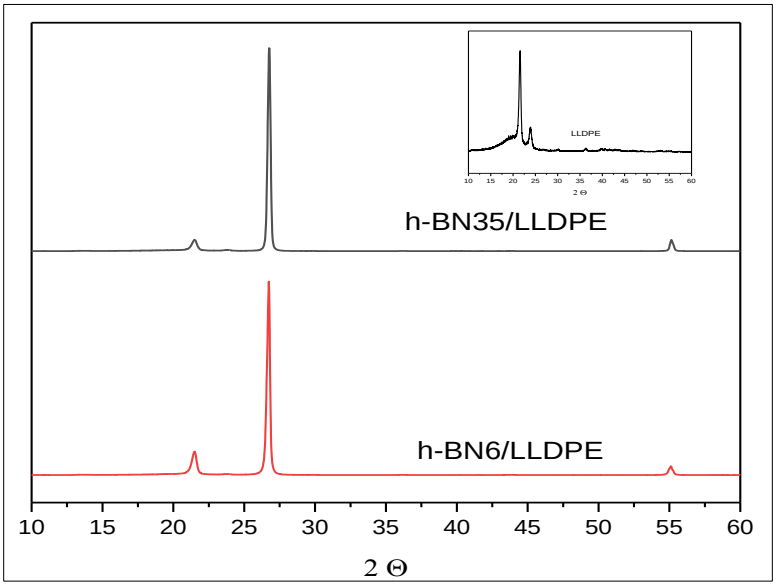

Fig. 38: XRD spectra of h-BN6/LLDPE and h-BN35/LLDPE composites.

Fig. 40 and Fig. 41 shows the SEM images h-BN35/LDPE and h-BN6/LDPE composites at various h-BN loading, respectively. As expected, at low h-BN loading more h-BN LDPE interfaces are available. These interfaces diminish at high h-BN loading, at

which h-BN particles tend to form networks. In h-BN35/LDPE composites less h-BN-LDPE interfaces were available as compared to h-BN6/LDPE, and that is due to their relatively bigger particle size.

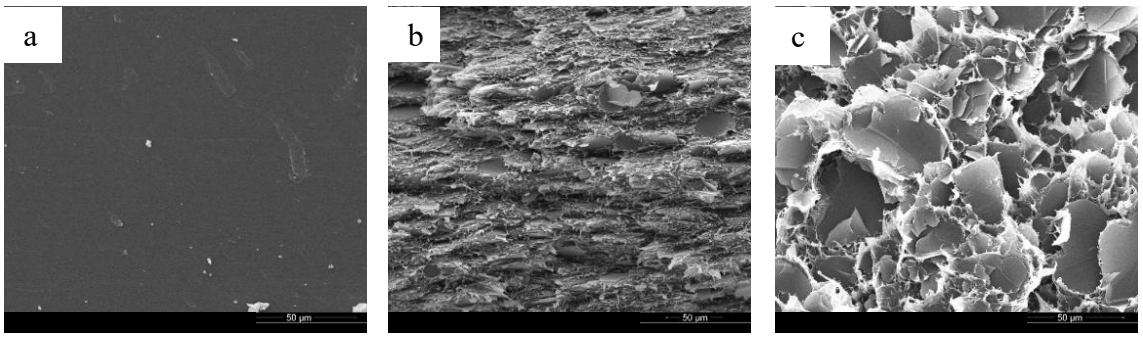

Fig. 39: SEM images of a cross-sectional surface of (a) pure LLDPE and (b and c) 22.5 vol. % h-BN35/LLDPE composites. (b) Horizontally arranged h-BN35 and (c) Vertically arranged h-BN35.

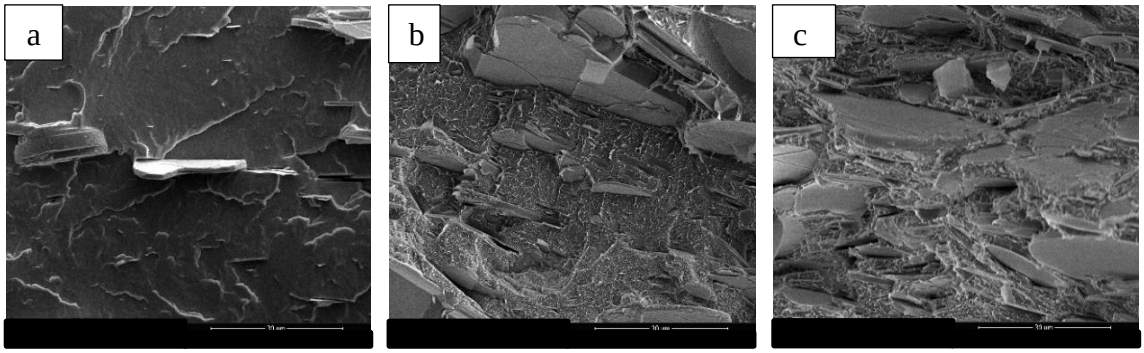

Fig. 40: SEM images of h-BN35/LDPE composites at different h-BN loading prepared by MB method. (a) 4.6 vol. %, (b) 22.5 vol. %, and (c) 39.6 vol. %.

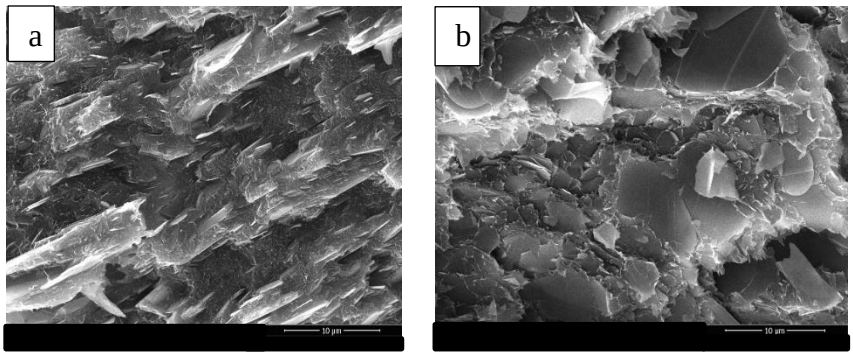

Fig. 41: SEM images of h-BN6/LDPE composites at different h-BN loading prepared by MB method. (a) 22.5 vol. %, and (b) 39.6 vol. % h-BN6/LDPE.

4.3.2. Thermal Conductivity

Generally, the thermal conductivity of h-BN/PE composites increase with h-BN loading because the intrinsic thermal conductivity of h-BN is much higher than that of PE polymers. At lower h-BN loading, i.e. below 22.5 vol. %, the thermal conductivity enhancement is insignificant. However, at above 22.5 vol. % h-BN loading, there is a sudden jump in the thermal conductivity. That is because at a very high loading thermal networks and bridges are produced leading to low thermal interface resistance. This was demonstrated in Fig. 40 and Fig. 41, where the h-BN networks are very obvious at 39.6 vol. % h-BN loading. Beside, h-BN/PE composites are influenced by many other factors such as processing method, composite sheet thickness, PE polymer type, h-BN particle size, h-BN exfoliation, filler alignment, and specimen thickness. In the following section these factors are thoroughly studied.

4.3.2.1. Factors that Affect the Thermal Conductivity h-BN/PE Composites

4.3.2.1.1. Effect of Composite Processing

To study the effect of processing method, the composite were prepared using MB and BM methods. Moreover, the composites were pressed into thin and thick sheets with sheet thicknesses of 0.5 mm and 2 mm, respectively.

Fig. 42 displays the thermal conductivity of h-BN35/LLDPE composites at different h-BN loading prepared by MB and BM methods. At all h-BN content, BM method demonstrated improved thermal conductivity compared to MB method. At low h-BN loading, BM method manifested obvious improvement in 'λ' to reach 1.15 W m^{-1} K^{-1} at 22.5 vol. % compared to 0.8 W m^{-1} K^{-1} of MB method. However, at high h-BN loading there was no significant difference in 'λ'. In the MB method, h-BN was uniformly distributed in the polymer matrix forming more LLDPE-h-BN interfaces. Conversely, in the BM method h-BN is unevenly distributed in the polymer matrix forming agglomerates and networks, as shown in Fig. B. 2. These agglomerates and networks provide bridges for heat transfers, and hence improves 'λ'. Kim *et al*. [182], reported a relatively better thermal of h-BN/polyphenylene sulfide composites prepared by a powder mixing method as compared to those prepared by a MB method. In addition to agglomerate formation, BM method might initiate h-BN exfoliation, and thereby improving the thermal conductivity.

Fig. 43 shows the thermal conductivity of h-BN35/LLDPE composites with sheet thicknesses of 0.5 mm and 2 mm. Clearly, the 2 mm sheets exhibited better thermal conductivity than the 0.5 mm sheets. For example, at ~ 40 vol. % the thermal

conductivities of 0.5 mm and 2 mm sheets were 1.07 W m^{-1} K^{-1} and 1.8 W m^{-1} K^{-1}, respectively. As provided in Table 4, the thermal conductivity of h-BN is highly dependent on the h-BN orientation, i.e. anisotropic, and hence their composites are anisotropic as well. Due to the geometry of h-BN sheets, h-BN particles tend to arrange themselves during the compression molding. In the thin sheets, h-BN particles are forced to align in the horizontal direction, as illustrated in Fig. B. 3 (a) and (b), a direction where the thermal conductivity of h-BN is 3 W m^{-1} K^{-1}, leading to a lower thermal conductivity. However, in the 2 mm sheets h-BN particles tend to take a random orientation, as shown in Fig. B. 3 (c) and (d), leading to a relatively better thermal conductivity.

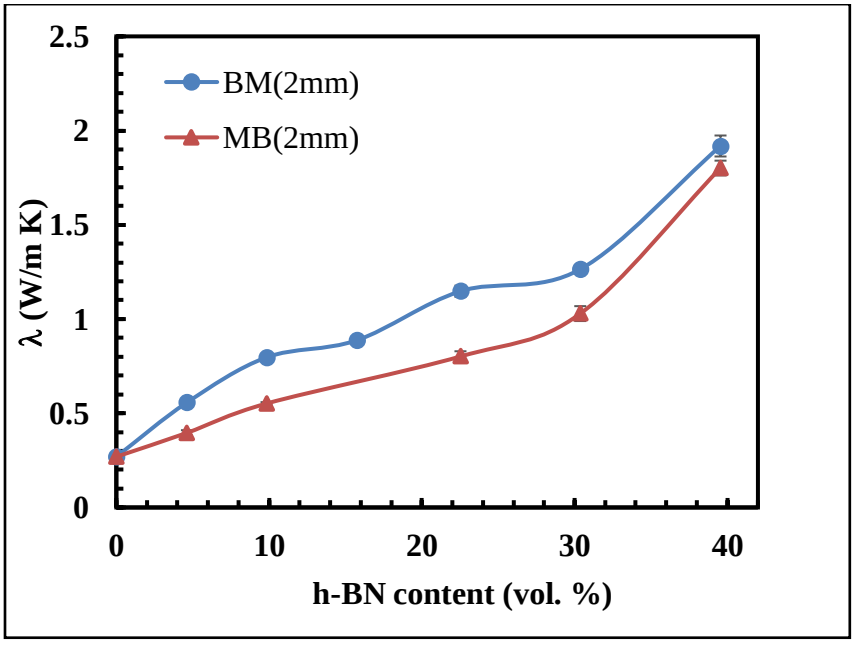

Fig. 42: The thermal conductivity of h-BN35/LLDPE composites prepared by BM and MB methods.

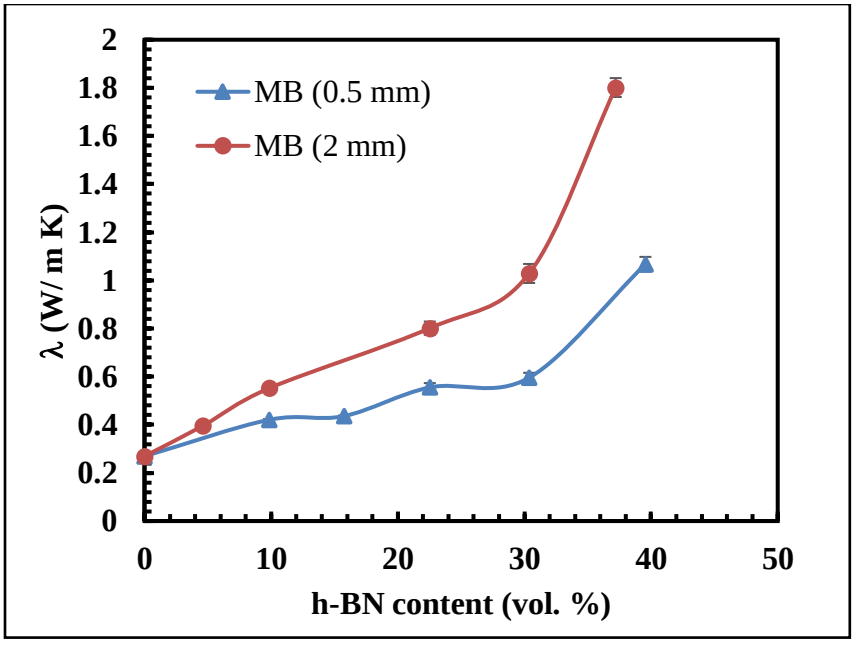

Fig. 43: The thermal conductivity of BN35/LLDPE composites with sheet thicknesses of 0.5 and 2 mm.

4.3.2.1.2. Effect of Polymer Type and h-BN Particle Size

To study the effect of the polymer matrices, three different polymers were used; HDPE, LLDPE, and LDPE. HDPE and LDPE were available in pellets forms only. Therefore, their composites were prepared using melt blending method. However, LLDPE was available in a powder form, thus it was fabricated using both MB and BM methods. Moreover, the effect of h-BN particle sizes was also investigated by preparing h-BN6 and h-BN35/PE composites.

Fig. 44 shows the thermal conductivity of h-BN35/LDPE, h-BN35/LLDPE, and h-BN35/HDPE. At low h-BN loading, LDPE and LLDPE showed similar thermal conductivity trends. However, at high h-BN loading LLDPE showed slightly higher

thermal conductivity improvement. Conversely, at all h-BN loading, HDPE composites displayed higher thermal conductivity improvements compared to the LDPE and LLDPE composites. For example, the thermal conductivities of LDPE, LLDPE, and HDPE increased from 0.256, 0.269, and 0.384 W m^{-1} K^{-1} in the pure polymer to 1.40, 1.80, and 2.72 W m^{-1} K^{-1} at ~ 40 vol. % h-BN content, respectively. Theoretically speaking, HDPE have higher intrinsic 'λ', higher density, higher crystallinity, and less branches compared to LDPE and LLDPE. The high crystallinity and less branches of HDPE help in reducing phonon scattering. In addition, the highest density and viscosity of HDPE seem to help in h-BN particle orientation, especially during the compression molding step, leading to a better thermal conductivity enrichment.

Fig. 45 shows the effect of incorporating h-BN6 and h-BN35 on the thermal conductivity of LLDPE and HDPE. In both LLDPE and HDPE polymers, the effect of h-BN particle size was prominent only at high h-BN loading. For instance, the thermal conductivities of h-BN6/HDPE and h-BN35/HDPE at 4.6 vol. % were 0.493 and 0.476 W m^{-1} K^{-1} and at 39.6 vol. % were 1.12 and 1.43 W m^{-1} K^{-1}, respectively. Similar results were found in h-BN/LLDPE composites. For example, (Fig. 46) h-BN35/LLDPE composites exhibited higher thermal conductivities than h-BN6/LLDPE composites. In general, big particle sizes tend to form networks relatively easier, and hence reducing the thermal interface resistance [29]. Fig. 40 and Fig. 41 shows the SEM images of h-BN35/PE and h-BN6/PE composites at different loading. At 22.5 vol. % h-BN/PE, PE h-BN35/PE composites had less filler to polymer interfaces than h-BN6/PE composites, leading to a lower thermal interfacial resistance, and hence better thermal conductivity.

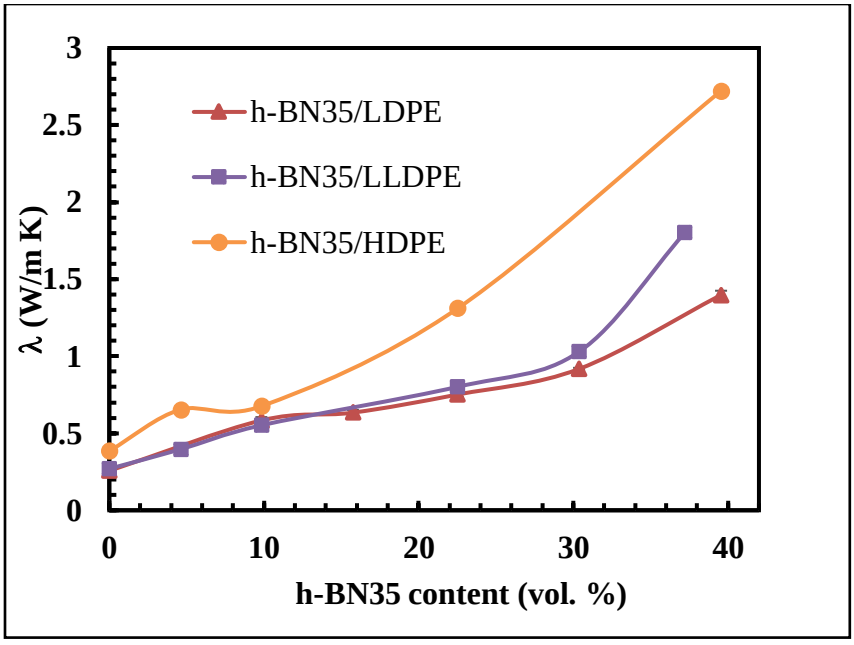

Fig. 44: The thermal conductivity of h-BN35/LDPE, h-BN35/LLDPE, and HDPE. The composites were prepared by MB (2 mm).

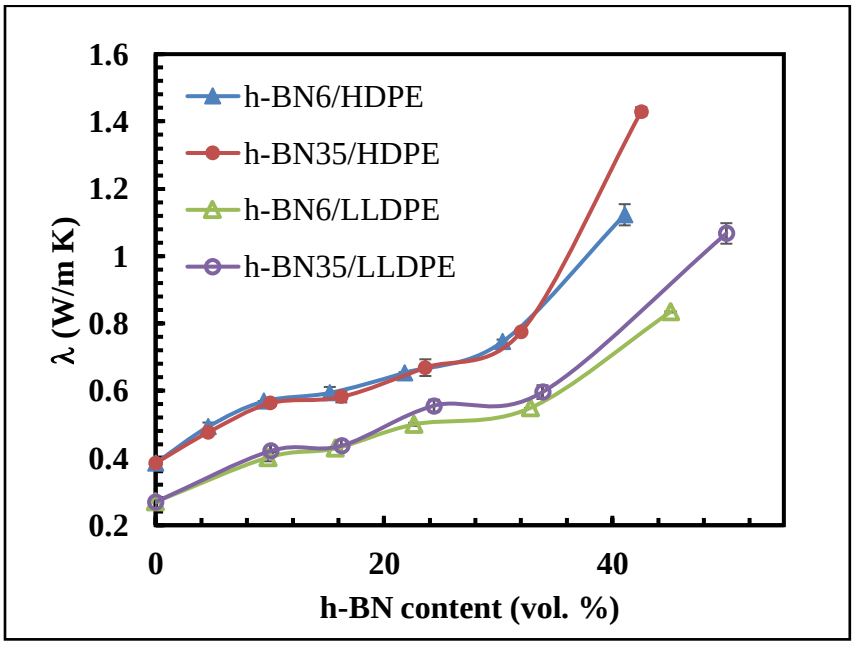

Fig. 45: The thermal conductivity of HDPE and LLDPE polymers filled with h-BN6 and h-BN35 at different h-BN loading. The composite were prepared by MB (0.5 mm).

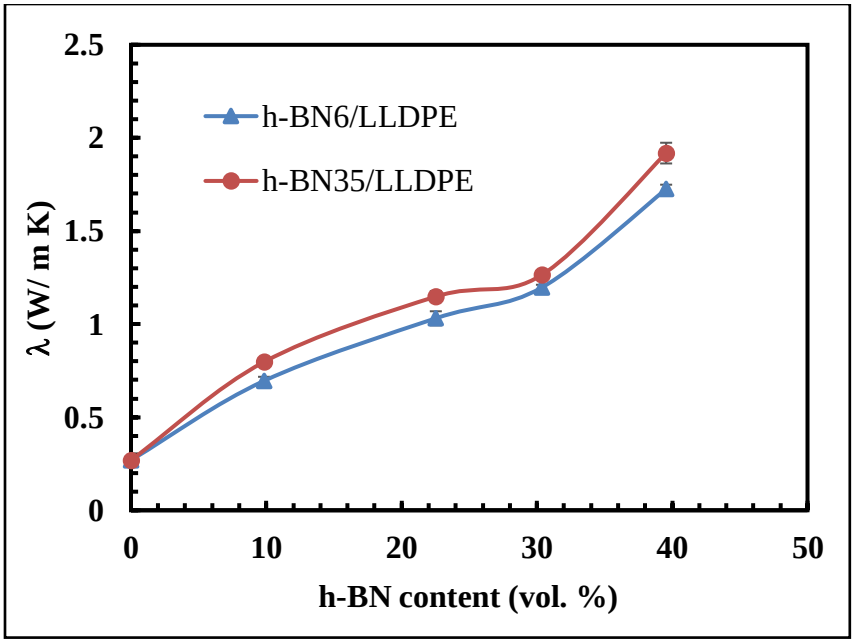

Fig. 46: The thermal conductivity of h-BN6/LLDPE and h-BN35/LLDPE composites prepared by BM method. Note the composites sheet thickness is 2 mm.

4.3.2.1.3. Effect of Exfoliation and Defect Mitigation

To study the effect of filler features, h-BN of two particle sizes were utilized. In addition, the effect of exfoliation was investigated by treating h-BN using a BM technique. In addition, the effect of adding LLDPE to the h-BN, in a ratio of h-BN to LLDPE of 4:1, during the BM treatment was also investigated, e.g. to prevent defect formation and lateral size reduction. Finally, the effect of BM time was also examined. Due to difficulty in processing BMd-h-BN35/LLDPE composites, the h-BN loading was limited to below 30.4 vol. %.

Fig. 47 shows the thermal conductivity of h-BN35/LLDPE and BMd-h-BN35/LLDPE composites for 0.5 mm and 2 mm-sheets. As was found earlier, the 2 mm-

sheets performed better than the 0.5 mm-sheets. In the 0.5 mm-sheets, BMd-h-BN35/LLDPE demonstrated improved thermal conductivity compared to h-BN35/LLDPE. Meanwhile, in the 2 mm-sheets the BMd-h-BN35/LLDPE showed better thermal conductivity than h-BN35/LLDPE only at intermediate h-BN loading, e.g. at 9.8 and 15.7 vol. % h-BN concentrations. In contrast, at high h-BN loading h-BN35/LLDPE demonstrated higher thermal conductivity. From Fig. B. 4, the SEM images of BMd-h-BN35 showed h-BN as agglomerates with spherical or oval shape. It seems that the circular agglomeration makes them unsusceptible to a forced orientation during the compression molding step. Thus, in the 0.5 mm-sheets, the thermal conductivity of the BMd-h-BN35/LLDPE composites were relatively higher than that of bulk h-BN35/LLDPE. While in the 2 mm-sheets, the effect of compression molding is slightly alleviated in the h-BN35/LLDPE, enhancing their 'λ'. Still at low h-BN concentration, h-BN35/LLDPE demonstrated relatively lower thermal conductivity compared to the BMd-h-BN35/LLDPE composites. It seems that the h-BN agglomeration in the BMd-h-BN35/LLDPE helps in building networks with relative ease, intensifying their 'λ'. However, at high loading h-BN35/LLDPE already formed h-BN networks, so their 'λ' was expected to increase. The higher 'λ' of the h-BN35/LLDPE compared to that of BMd-h-BN35/LLDPE was attributed the purity and crystallinity of the bulk h-BN. For instance, the oxygen functionalization and amorphization, which are known to cause phonon scattering [35][183][184], of the BMd-h-BN were expected to lower the thermal conductivity.

Despite the slightly improved 'λ' of the BMd-h-BN35/LLDPE composites. Their SEM images displayed agglomerates, which are not desirable especially from the mechanical properties' perspective. To mitigate this problem as well as the h-BN crystal defects and h-BN oxidation caused by the BM process; LLDPE was mixed with h-BN during the BM process.

Fig. 48 shows the thermal conductivity of the BMd-h-BN35/LLDPE and the BMd-80%h-BN35/LLDPE composites. Noticeably, the BMd-80%h-BN35/LLDPE displayed improved 'λ' relative to the BMd-h-BN35/LLDPE. For example, at 30 vol. % the thermal conductivity of the BMd-80%h-BN35/LLDPE was 1.46 W m^{-1} K^{-1}, which was about 74 % higher than that of the BMd-h-BN35/LLDPE. Fig. B. 5 ((a) and (b)) shows the SEM images of the BMd-h-BN35/LLDPE and the BMd-80%h-BN35/LLDPE composites. The h-BN particles of the former are shown as agglomerates, while the h-BN particles of the latter are shown as sheets uniformly distributed and vertically oriented. Beside their better alignment, less defects, and good dispersion inside their composites, BMd80%h-BN35 have low oxygen groups justifying the high 'λ' of their composites.

Fig. 49 shows the thermal conductivity of 80%h-BN35/LLDPE composites, where the h-BN is milled for 0, 45, and 90 min. Please note that '0 min' represents bulk h-BN35/LLDPE composites. Apparently, the thermal conductivity shows functionality with BM time. For instance, the thermal conductivity of the bulk (0 min) h-BN composites was lower than 45 min composites, which was in turn lower than that of 90 min composites. Fig. B. 6 shows the SEM images of the 0, 45, and 90 min composites. Clearly, there was reduction in particle sizes with the increase in milling time. In addition, 45 min and 90

min composites showed relatively higher number of h-BN particles due to this reduction. In addition, the h-BN particles in these composites were uniformly distributed, i.e. better dispersion. The better dispersion of h-BN particles in 45 min and 90 min composites might be caused by the increase in the aspect ratio of the h-BN particles due to exfoliation.

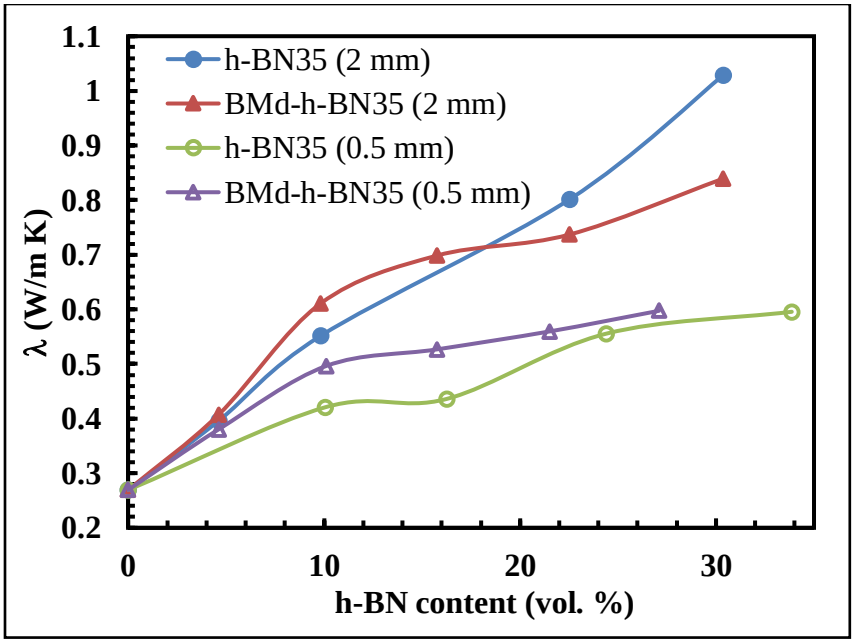

Fig. 47: The thermal conductivity of h-BN35/LLDPE and (BMd-h-BN35)/LLDPE composites of 0.5 and 2 mm sheet thicknesses. Please note that h-BN35 was BMd for 90 min.

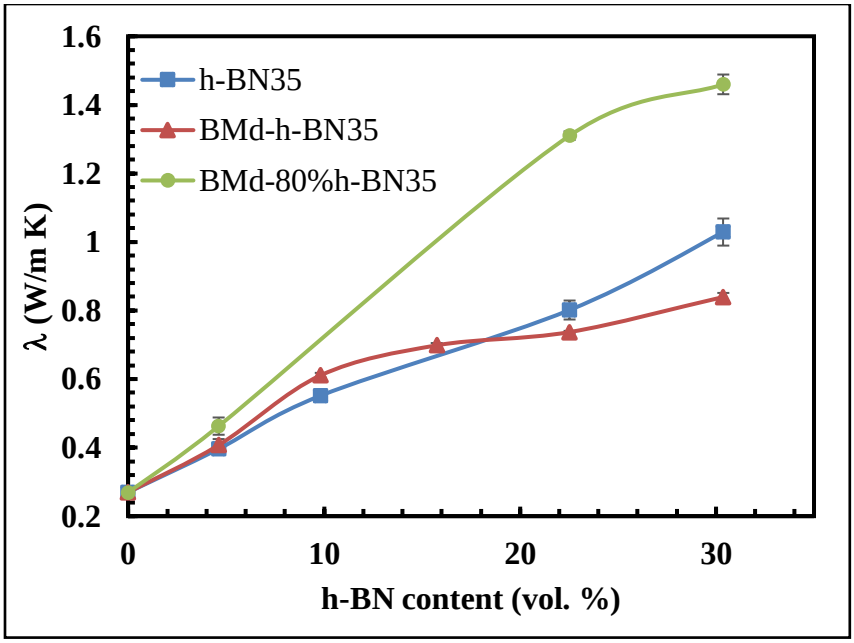

Fig. 48: The thermal conductivity of BMd-h-BN35/LLDPE and BMd-80%h-BN35/LLDPE prepared by MB method. Please note that h-BN35 was BMd for 90 min.

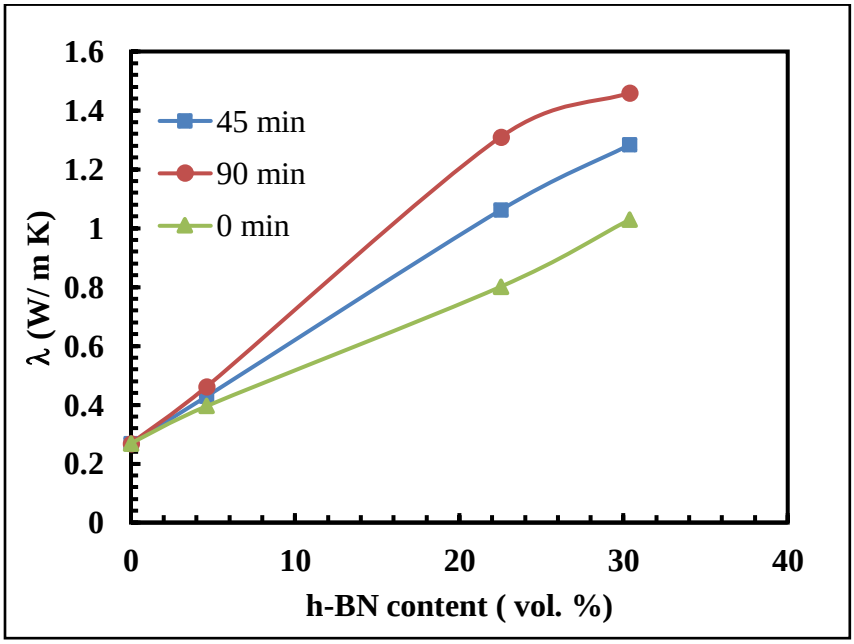

Fig. 49: The thermal conductivity of h-BN35/LLDPE and (BMd-80%h-BN35) prepared by MB method.

4.3.2.1.4. Effect of h-BN Alignment

To study the effect of h-BN alignment, the thermal conductivities of a highly aligned h-BN35/LLDPE composites were determined. The h-BN alignment was accomplished through three steps. Firstly, h-BN35/LLDPE composites were pressed into a very thin sheets forcing the h-BN particles to align horizontally. Secondly, the thin sheets were stacked upon each other forming a thick sheet with a 10 mm thickness. Finally, the 10 mm sheet was cut and rotated 90º, to get vertical alignment. Fig. 50 shows schematic of these steps.

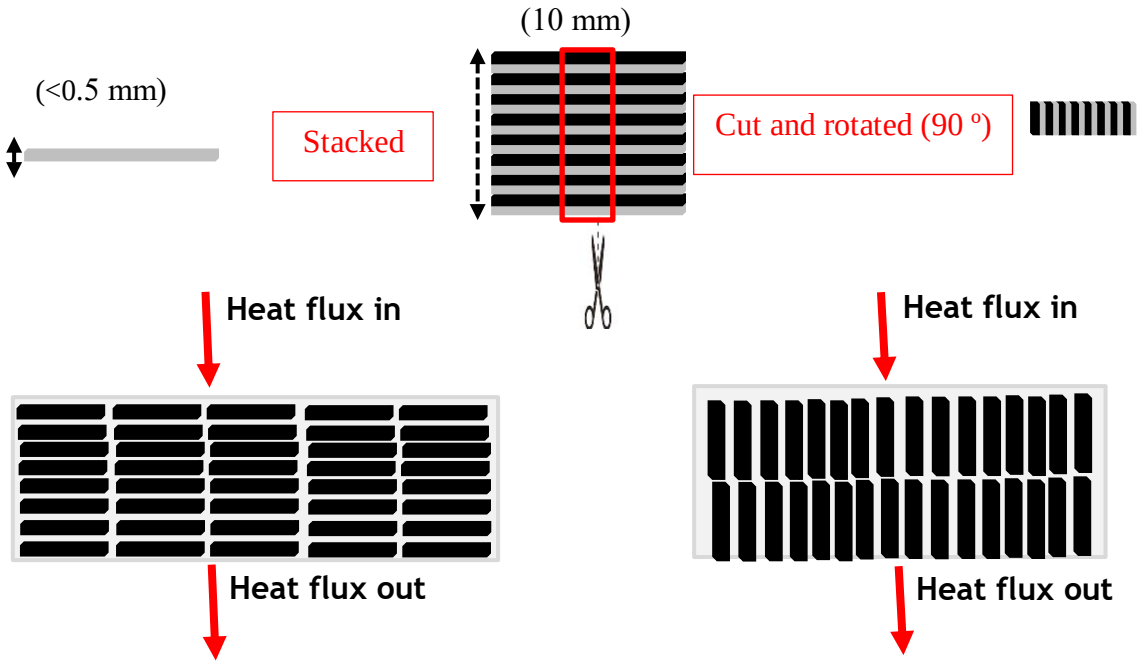

Fig. 50: Schematic of h-BN alignment steps in h-BN35/LLDPE composites to analyze the cross-section thermal conductivity.

Fig. 51 shows the cross-section and through plane thermal conductivities of h-BN35/LLDPE composites. The cross-section thermal conductivity exhibited remarkably higher thermal conductivity compared to the through-plane. For instance, the thermal conductivity of the cross-section showed approximately 300 and 600 improvement over the through-plane at 9.8 vol. % and 22.5 vol. % h-BN loadings, respectively. Obviously, this remarkable improvement in the thermal conductivity was cause by the highly aligned h-BN particles in these composites, as shown in Fig. 39 (c). Similar results was reported by Yang's group [181], in which they aligned h-BN in a similar fashion.

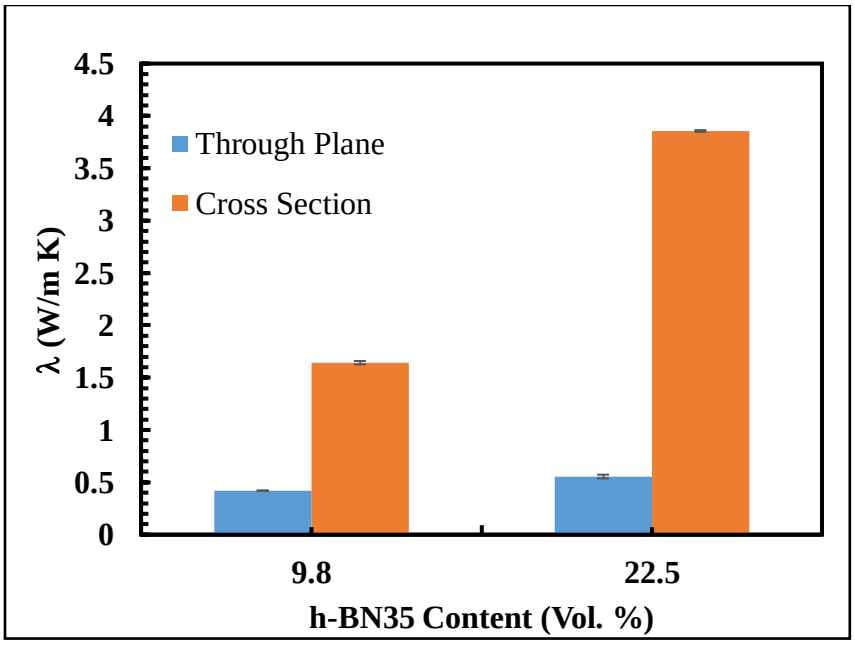

Fig. 51: The through-plane and cross-plane thermal conductivity of h-BN35/LLDPE composites.

4.3.2.1.5. Effect of Removing the Top and Bottom Specimen Layers (Skins)

Finally, the effect of removing the top and bottom layers on the thermal conductivity of h-BN35/PE composites was examined. To do so, starting from h-BN35/PE specimen of 2 mm thickness the top and bottom layers was removed by simple grinding to a desired specimen thickness For example, the specimen thickness was reduced from ~ 2 mm to ~ 0.5 mm at an interval of 0.5 mm, and the thermal conductivity at different specimen thickness was determined, as illustrated in Fig. 52.

(2 mm) (1-1.5 mm) (0.5 mm)

Fig. 52: Schematic diagram of specimen at various thickness. This was done by removing the top and bottom layers (skins)

Fig. 53 Fig. 53 shows the thermal conductivities of 39.6 vol. % h-BN35/LLDPE, 39.6 vol. % h-BN35/HDPE, and 22.5 vol. % cross-section h-BN35/LLDPE composites at different removed layer thickness. Cross-section h-BN35/LLDPE specimen was used as a control to find out the main cause of the change in thermal conductivity, i.e. alignment or sheet thickness. As shown, cross-section specimen showed insignificant change in the thermal conductivity when the thickness was reduced from 2 mm to 0.5 mm. Therefore, this result ruled out the effect of specimen thickness. In contrast, h-BN35/LLDPE and h-BN35/HDPE composites showed significant improvement in the thermal conductivity when the thickness was decreased. For example, when the thickness was reduced from ~

2 mm to ~ 0.5 mm the thermal conductivities of h-BN35/LLDPE and h-BN35/HDPE composites were increased by 60 % and 30 %, respectively. From the cross-section result it was deduced that the cause was not originated from the specimen thickness, leaving the effect of alignment. Fig. B. 7, shows the SEM images of 30.4 vol. % h-BN35/LLDPE composite, 2 mm thick, at different locations. Fig. B. 7 ((a) and (c)) show the edge and the middle of the specimen, respectively. In the edge, the h-BN particles were aligned horizontally, whereas in the middle they were aligned vertically. Fig. B. 7 (b) shows an intermediate location, the h-BN particles in this part were aligned with an angle, i.e. greater than '0º' and lower than '90º'. These clearly support that the change in the thermal conductivity with thickness was caused by the change in h-BN alignment. For instance, when the specimen was polished the areas where the h-BN particles were aligned horizontally were removed approaching the part where the h-BN particles were aligned vertically (center).

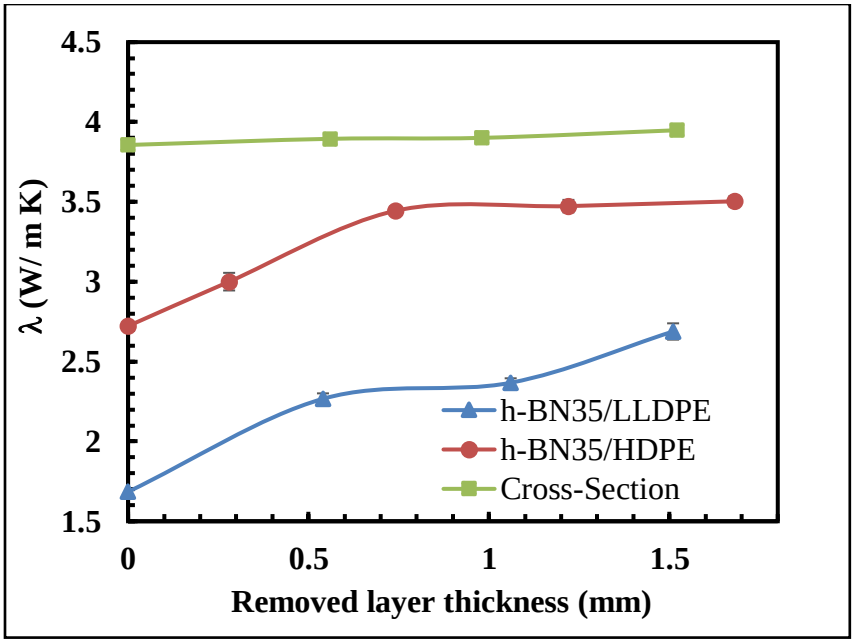

Fig. 53: The thermal conductivity of 39.6 vol. % h-BN35/LLDPE. 39.6 vol. % h-BN35/HDPE, and Cross-Section (22.5 vol. % h-BN35/LLDPE) at different removed layer thickness.

4.3.2.2. Comparing Experimental and Modeling Thermal Conductivities

Models are commonly utilized to describe the thermal conductivity of composites. Models help in experimental design by predicting the thermal conductivity for various set of experimental conditions. Here, Maxwell, Rayleigh, Bruggeman, Lewis-Nielsen, Agari models were used to fit the experimental data. Please refer to section 1.2.3 for their equations. In Lewis-Nielsen model, the values of 'A' and 'V_f^*' were 4.07 and 0.51 for the composites that were prepared by MB method (MB-composites) and 7.34 and 0.7 for those prepared by BM method (BM-composites), respectively. These values were comparable with literature values, such as tabulated data or values used in modeling the thermal

conductivity of h-BN/PE composites [60][56][46]. In Agari model, the values of 'C_m' and 'C_f' were found by fitting the model with the experimental thermal conductivity. The values of 'C_m' and 'C_f' are summarized in Table 10.

Fig. 54 and Fig. 55 show the thermal conductivity of h-BN35/LLDPE composites obtained from experimental data and calculated using various models. The 'λ' values calculated by Rayleigh models were much lower than the experimental values. Similar results, not shown here, were obtained by Maxwell model. This was expected since both Rayleigh and Maxwell models consider spherical fillers with negligible filler-filler interactions. Although, Rayleigh considered filler-filler interaction, for cubical arrangement these interactions are negligible even when the filler concentration is high [32]. Despite the fact that at high filler loading Bruggeman model gives good thermal conductivity predictions [62], here the model gave values lower than that of the experimental 'λ'. Comparatively, Agari and Lewis-Nielson models predicted the experimental 'λ' better. This was expected because these two models have two variables that can be subjected to fitting, thus giving a higher degree of freedom, and hence a better fitting. Nonetheless, the two models showed slight difference. The two models demonstrated good fitting for the MB-composites. In contrast, only Agari model exhibited good fitting for the BM composites. With that being said, Neilson model showed slight improvement in predicting the thermal conductivity at high h-BN loading (high 'λ'). The better performance of the Agari model might be ascribed to the ability of this model to account for the effect of both the polymer and the filler. The fitting parameters (C_m and C_f) of Agari model were found to depend on the composite's preparation methods. Among

the two parameters, parameter 'C_f', which determine the ability of the filler to form thermal bridges, showed greater variation with the processing method. The value of 'C_f' of the MB-composites was 1.02, whereas that of BM-composites was 1.97. This indicated that the fillers of the MB-composites formed thermal networks at relative ease compared to those of the BM-composites. However, the thermal conductivity of the BM-composites was higher than that of MB-composites, as shown previously in Fig. 42. Similar results was found by Zhang et al. [63]. Zhang's group found higher 'C_f' values for composites with higher 'λ' compared to those with lower 'λ'. They indicated that these was attributed to the composite fabrication method. Equivalently, the value of 'C_m' in the BM-composites was lower that of the MB-composites, supporting this argument. The little variation in the 'C_m' values was anticipated because the crystallinity of PE showed small variation with the h-BN loading, as will be discussed in section 4.3.3.

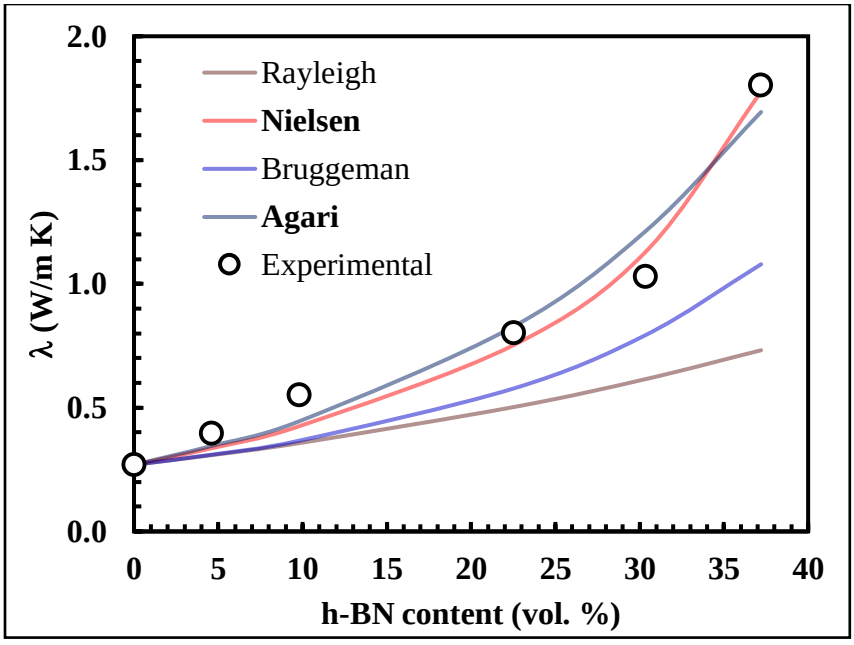

Fig. 54: The thermal conductivity of h-BN35/LLDPE composites at different h-BN loading; found experimentally (MB) and calculated using various models.

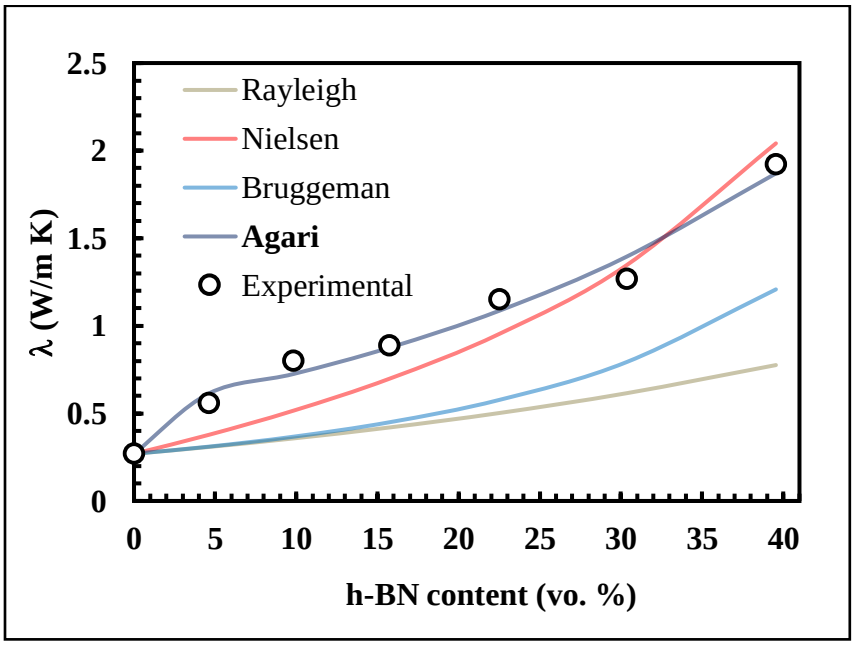

Fig. 55: The thermal conductivity of h-BN35/LLDPE composites at different h-BN loading; found experimentally (MB) and calculated using various models.

Table 10: 'C_m' and 'C_f' values of Agari model obtained by fitting the model to the experimental thermal conductivity.

Composites	C_m	C_f
MB-composites	0.64	1.02
BM-composites	0.45	1.97

4.3.3. Thermal Analysis

Thermal analysis was conducted using TGA, in which the weight change of the composite was measured as a function of time and temperature. Through this method, the non-oxidative thermal stability of h-BN/PE composites were thoroughly investigated. In addition, TGA was used to determine the actual h-BN loading in the composites.

Fig. 56 shows the TGA curves of h-BN35/LLDPE composites for several h-BN loading. The thermal decomposition temperature of these composites was enhanced with the incorporation of h-BN. For example, Fig. 57 shows T5 and T50 of the composites, which are the temperature at which 5 wt. % and 50 wt. % losses have happened, respectively. The T5 and T50 decomposition temperature showed improvement with the increase in h-BN loading. For instance, the T5 and T50 of pure LLDPE were 449 ℃ and 479 ℃, and that of 42 wt. % h-BN35/LLDPE were 452 ℃ and 489 ℃, respectively. This was expected knowing that h-BN possess a remarkable thermal stability and an unusual oxidation resistance. Ayoab *et al.* [142], reported that the thermal decomposition of h-BN/PE composites was enhanced upon the incorporation of h-BN. Similarly, Tanimoto *et al.* [185], stated that the thermal stability of polyimides improved with the addition of h-BN.

Fig. 58 compares the thermal decomposition of h-BN6/LLDPE and h-BN35/LLDPE composites. As shown earlier, the decomposition temperature of h-

BN/LLDPE composites increases with h-BN loading for both h-BN particle sizes. Among the two particle sizes, h-BN6 showed better enhancement in the thermal stability, as shown in Fig. B. 9. For instance, the T5 of 52 wt. % h-BN6/LLDPE was 456 ℃, whereas that of 54 wt. % h-BN35/LLDPE was 452 ℃. The higher performance of h-BN6 might be caused by their better dispersion. Jung et al. [141], reported higher decomposition temperature of nano-h-BN/HDPE relative to micro-h-BN/HDPE composites. Similarly, Alaei et al. [186], indicated that the thermal stability of silica/maleic anhydride grafted polypropylene composites was deteriorated when the silica particle size was increased.

Fig. 59 compares between the thermal decomposition behaviors of h-BN35/LLDPE composites prepared by MB and BM methods. The composites prepared by the MB method showed higher thermal decomposition temperature at all h-BN loading as compared to those prepared by BM method, see Fig. B. 10. The T5 temperature of the MB composites were 446 ℃ (20.4 wt. %) and 452 ℃ (42 wt. %), whereas that of BM composites were 426 ℃ (18.6 wt. %) and 436 ℃ (37.7 wt. %).

Fig. 60 shows the TGA curves of h-BN35/LLDPE and BMd-h-BN35/LLDPE composites. Also, a zoomed portion of Fig. 60 is shown in Fig. B. 11. The T5 of 20 wt. % and 46.1 wt. % BMd-h-BN35/LLDPE were 444 ℃and 442 ℃, while that of 20 wt. % and 42.5 wt. % h-BN35/LLDPE were 446 ℃ and 452 ℃, respectively. In addition, Fig. 61 shows an inverse functionality between T5 and h-BN concentration. The lower T5 values of the BMd-h-BN35/LLDPE composites was ascribed to the presence of oxygen group or absorbed moisture. For example, the onset temperature of 20 wt. % and 46.1 wt. % BMd-h-BN35/LLDPE composites was ~ 100 ℃, whereas that of pure LLDPE was ~ 369℃. At

369 ℃, the 20 wt. % and the 46.1 wt. % BMd-h-BN35/LLDPE composites had lost 1.38 % and 2.1 % of their weight, implying the loss of some functional groups related to BMd-h-BN (i.e. oxygen group). Riaz *et al.* [187], stated that TGA curve of graphene oxide showed 14.5 wt. % loss between the temperature values of 28 ℃ and 150 ℃. They assigned this mass loss to the physical desorption of moisture. Unlike the T5, the T50 of BMd-h-BN35/LLDPE composites demonstrated improvement compared to the T50 of pure LLDPE (Fig. 61). In addition, the T50 of BMd-h-BN35/LLDPE showed similar values as that of h-BN35/LLDPE. For instance, the T50 of 20 wt. % h-BN35/LLDPE and 20 wt. % BMd-h-BN35/LLDPE were 481.26 ℃ and 481.22 ℃, respectively.

Fig. 62 and Fig. B. 12 compare between the TGA profiles of h-BN35/LLDPE, BMd-h-BN35/LLDPE, and BMd-80%h-BN35/LLDPE composites. The TGA curves showed an improved T5 (450.36 ℃) of 43.9 wt. % BMd-80%h-BN35/LLDPE compared to that of 46.1 wt. % BMd-h-BN35/LLDPE (442 ℃). The relatively modified thermal stability of BMd-80%h-BN35/LLDPE composites was caused by the lower oxygen content in the BMd-80%h-BN35 (2 wt. %) compared to the BMd-h-BN35 (10 wt. %). For instance, the TGA profiles of BMd-80%h-BN35/LLDPE composites exhibited a trend similar to that of h-BN35/LLDPE composites.

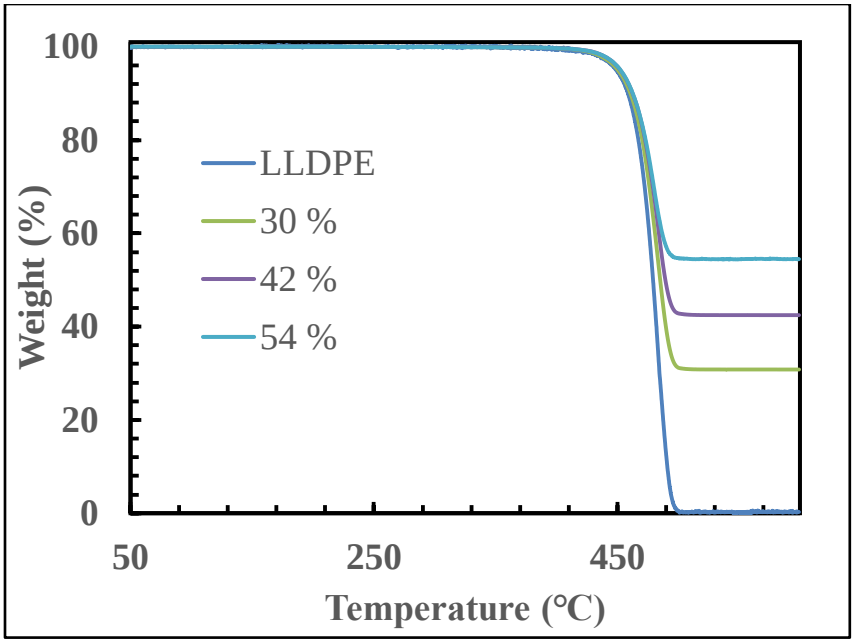

Fig. 56: TGA curves of pure LLDPE and h-BN35/LLDPE composites of various h-BN loading (wt. %).

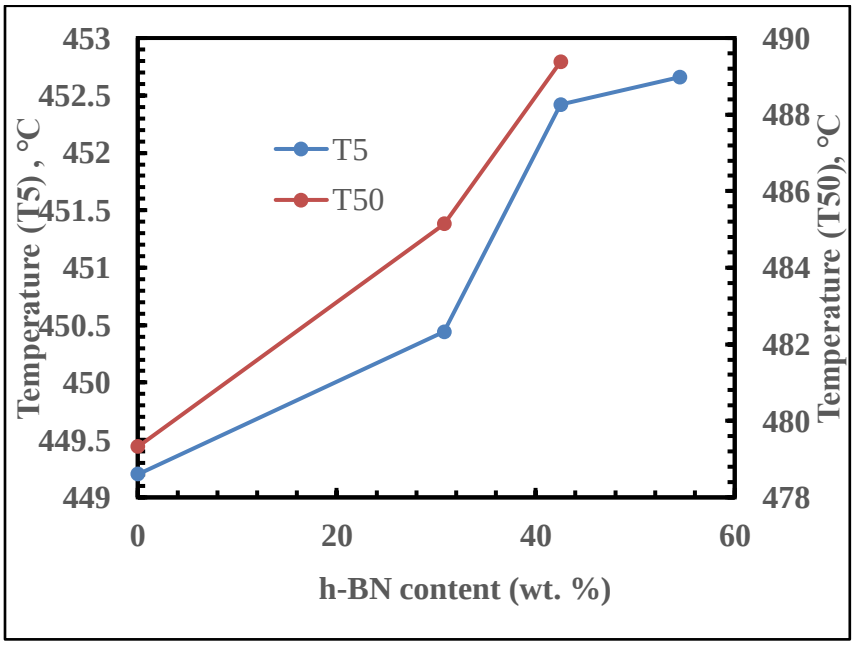

Fig. 57: T5 and T50 of h-BN35/LLDPE composites at different h-BN loading.

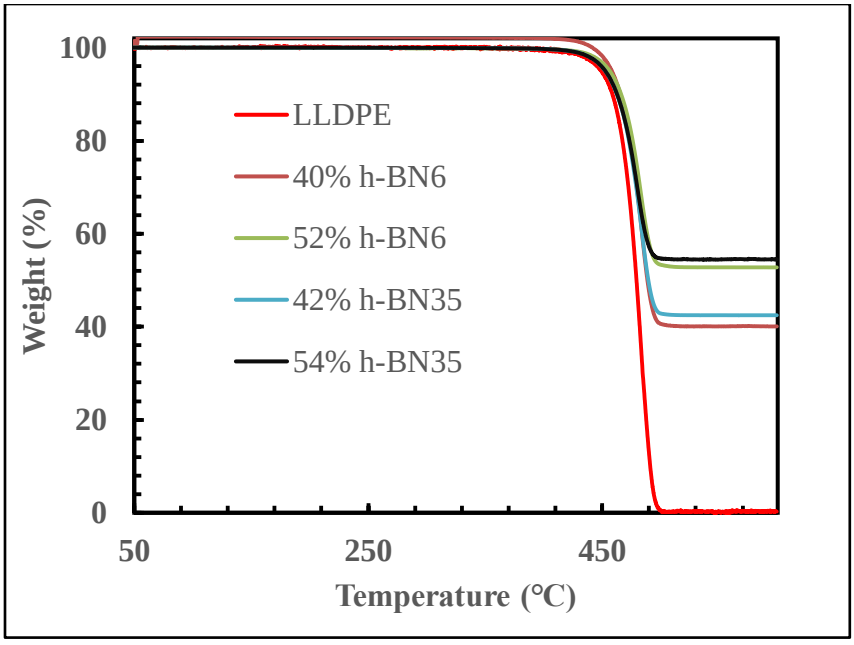

Fig. 58: TGA curves of h-BN6/LLDPE and h-BN35/LLDPE composites of different h-BN loading (wt. %).

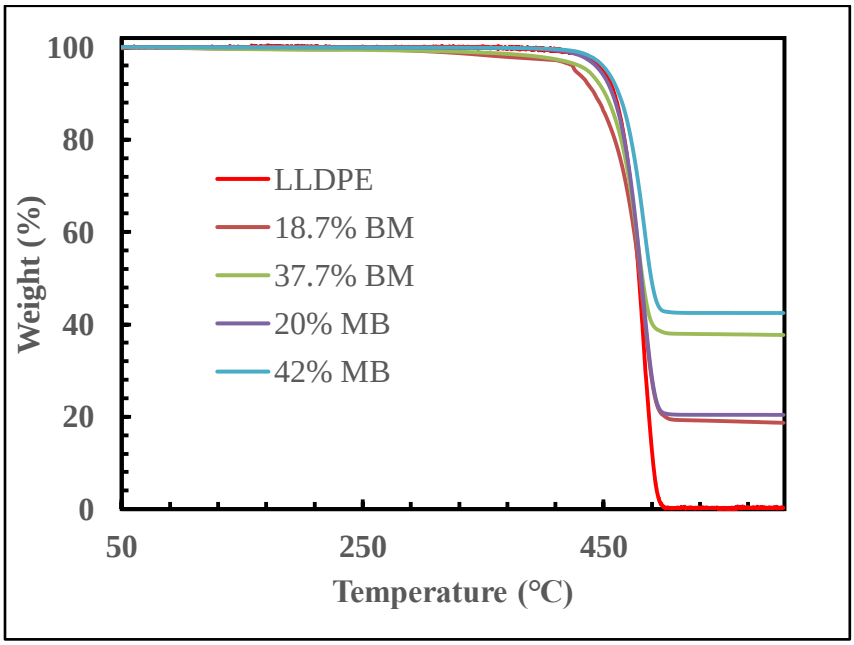

Fig. 59: TGA curves of h-BN35/LLDPE composites of different h-BN loading (wt. %); prepared by MB and BM methods.

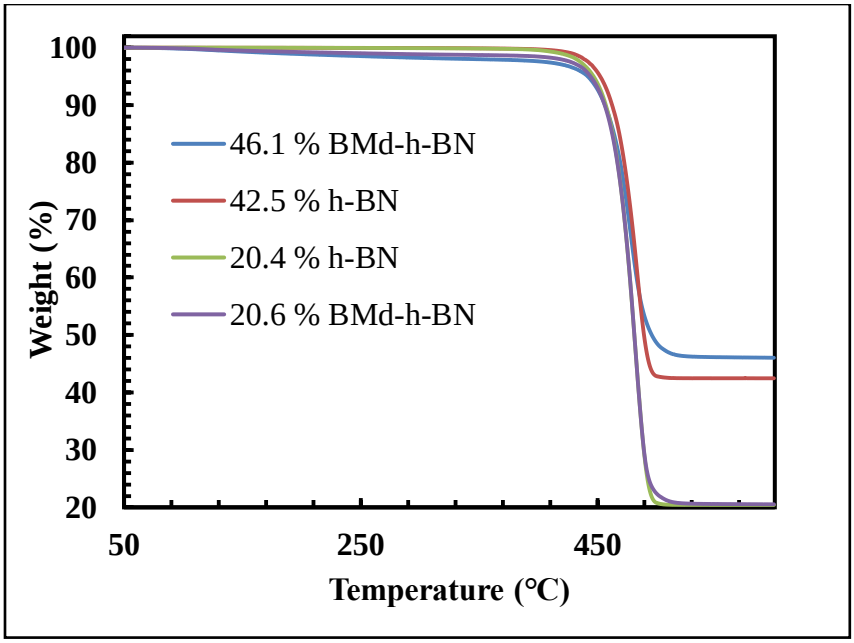

Fig. 60: TGA curves of h-BN35/LLDPE and BMd-h-BN35/LLDPE composites of several h-BN loading (wt. %).

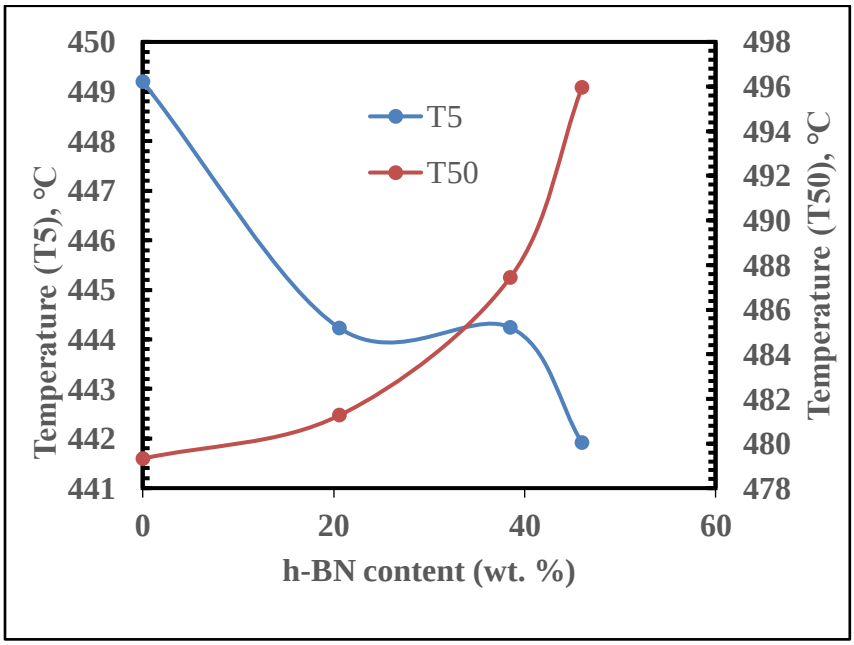

Fig. 61: T5 and T50 of BMd-h-BN35/LLDPE at different h-BN loading.

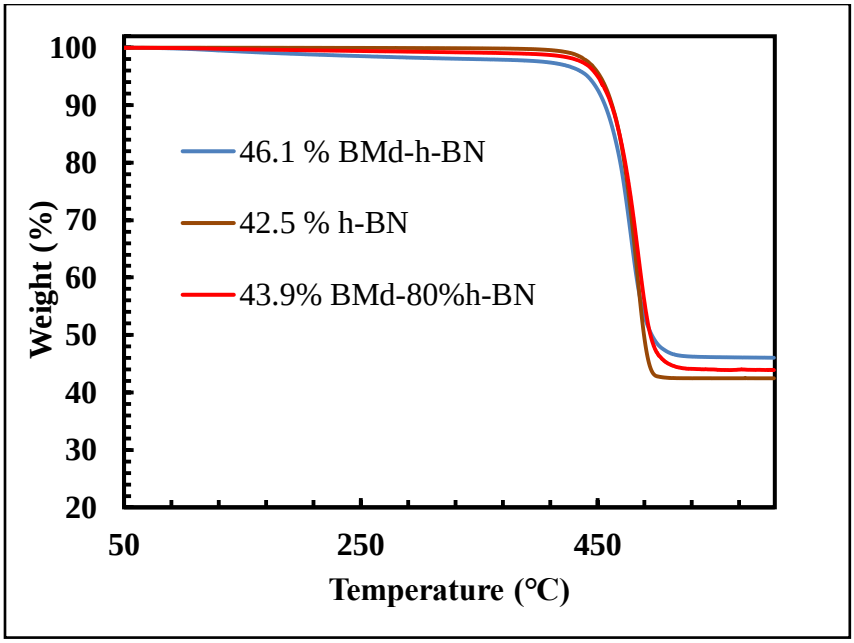

Fig. 62: TGA curves of h-BN35/LLDPE, BMd-h-BN35/LLDPE, and BMd-80%h-BN35/LLDPE composites of several h-BN loading (wt. %).

4.3.4. Thermal Transitions

In DSC the heat transfer of materials are measured as a function of time and temperature. DSC is a very strong technique in determining phase transition properties, such as glass transition temperature, crystalline phase transition temperatures, melting point, specific heat capacity, heat of fusion, and heat of vaporization [153]. In this thesis, DSC was used to determine the effect of h-BN on the phase transition properties of h-BN/PE composites, including specific heat capacity, heat of fusion, and melting point. Using the heat of fusion, the degree of crystallinity of the composites was calculated as follows:

$$\chi_c = \frac{\Delta H_f}{(1-w) \times \Delta H_f^0} \times 100 \qquad 4.1$$

where 'χ_c' is the degree of crystallinity (%), 'ΔH_f' is the heat of fusion of the h-BN/PE composite, 'w' is the h-BN weight fraction, and 'ΔH_f°' is the heat of fusion of 100 % crystalline PE polymer, which is 293.6 J/g [188].

Table 11 display the DSC thermal parameters of h-BN6/LDPE and h-BN35/LDPE composites. The crystallization temperature (T_m) of these composites demonstrated insignificant variation with h-BN loading and h-BN particle sizes. The percentage of crystallinity of these composites demonstrated a weak improvement at low h-BN loading, i.e. below 40 wt. %. However, at high loading, i.e. ~ 57 wt. %, the crystallinity reduced significantly. For instance, h-BN agglomeration tend to hinder the PE composites from crystallization up on cooling. Zhang *et al.* [143], found similar results in h-BN/HDPE systems. The improvement in the percent of crystallinity of h-BN/LDPE composites suggests that h-BN is a nucleating agent [142][180]. Thus, h-BN improves the crystallization behavior of LDPE by increasing their crystallization rate.

Table 11: Thermal transition parameters of h-BN/PE composites at various h-BN loading obtained from DSC analysis.

h-BN wt. %		T_m (°C)		ΔH_f (J/g)		χ_c(%)	
h-BN6	h-BN35	h-BN6	h-BN35	h-BN6	h-BN35	h-BN6	h-BN35
0	0	110.7		130.5		44.4	
6.9	9.4	109.0	109.1	122.4	133.7	44.8	50.3
18.4	19.4	108.8	108.4	111.6	123.7	46.6	52.2
36.9	39.6	109.2	108.5	83.32	90.7	45.0	51.1
56.5	57.8	107.8	108.5	51.91	49.1	40.7	39.6

4.3.5. Mechanical Properties

For the thermal management applications of PE, it is not only indispensable to enhance their thermal properties but also very vital to improve their mechanical properties. In general, the mechanical properties of polymers are commonly enhanced by the incorporation of inorganic fillers. Here, the mechanical properties of PE were modified by the addition of h-BN. Thereafter, the mechanical properties of h-BN/PE composites were investigated by tensile test.

Clearly, the tensile strength increases and the elongation at break decreases with the increase in the h-BN loading (Fig. 63). Being very ductile, the neat LLDPE showed the highest elongation at break. In addition, the pure polymer displayed the highest tensile strength at break. In contrast, with the increase in the h-BN content, the composites became brittle and broke at a lower strain values. Apparently, the neat LLDPE exhibited strain hardening. This phenomenon, strain hardening, is caused by the alignment of molecular chains during the deformation process, strengthening the polymer. Strain hardening is usually affected by the experimental conditions, such as strain rate, temperature, and specimen geometry [189][190][191]. In this work, the strain hardening might be cause by the low strain rate (10 mm/min) at which the tensile test was performed. Xu et al. showed that the elongation at break of PE polymers reduced with the increase in the strain rate [189].

Fig. 64 shows the stress-strain curves of h-BN35/LLDPE and BMd-80%h-BN35/LLDPE composites. Obviously, the BMd-80%h-BN35/LLDPE composites showed higher tensile strength compared to h-BN35/LLDPE composites. For instance, the stress

values of 10 wt. % BMd-8h-BN/LLDPE were higher than that of 23.9 wt. % h-BN35/LLDPE at all strain values. The highest tensile strength of 18.7 MPa was obtained at 43.9 wt. % of BMd-80%h-BN35/LLDPE.

4.3.5.1. Tensile Properties

Generally, the tensile strength of the bulk h-BN35/LLDPE, BMd-h-BN35/LLDPE, and BMd-80%h-BN35/LLDPE composites demonstrated a similar trend with no clear variation, as shown in Fig. 65. The tensile strength of these composites exhibited an unusual behavior compared to literatures [63][143]. For instance, the tensile strength decreased from 21.9 MPa at 0 wt. % (pure LLDPE) to a minimum (~ 12 MPa) at 20 wt. %, and then increased again at ~ 40 wt. %. As stated earlier, the neat LLDPE composites (Fig. 63) showed strain hardening which enhanced their tensile strength. Similarly, the strain hardening effect was also noticeable at low h-BN loading (< 10 wt. %), justifying their improved tensile strength compared to 20 wt. %. However, at high loading the effect of chain alignment was inhibited, and therefore the variation in the tensile strength was solely caused by the variation in the h-BN loading. This behavior was observed in all the composites, see Fig. B. 19 and Fig. B. 20. Thus, instead the yield stress was used to study the effect of h-BN loading for its high importance in engineering design.

Fig. 66, Fig. 67, and Fig. 68 show the yield stress, Young's modulus, and Elongation at break (%) of h-BN35/LLDPE, BMd-h-BN35/LLDPE, and BMd-80%h-BN35/LLDPE composites. The BMd-80%h-BN35 composites demonstrated higher yield stress and Young's modulus compared to the other two composites at all h-BN loading. The yield stress and Young's modulus of the bulk h-BN35 and the BMd-h-BN35

composites were low and presented similar values. Conversely, the elongation at break (%) of the BMd-h-BN35/LLDPE was higher than the other two composites. This can be ascribed to the comparatively lower Young's modulus of the BMd-h-BN35 composites. Fig. B. 5 and Fig. B. 6 show the SEM images of the three composites. Among these composites, BMd-80%h-BN35 composites displayed better dispersion, justifying their improved tensile properties. In contrast, the h-BN35 composites showed slightly random dispersion, whereas the BMd-h-BN35 composites showed h-BN agglomeration which might explain their relatively lower tensile properties.

Fig. 69, Fig. 70, and Fig. 71 study the effect of the composites fabrication methods, MB and BM, on the yield stress, Young's modulus, and elongation at break (%) of h-BN35/LLDPE composites. At 20 wt. % the composites prepared by both processing methods exhibited similar yield stress and Young's Modulus. However, at ~ 40 wt. %, the MB method presented better yield stress and Young's Modulus. In contrast, at low loading BM method exhibited higher elongation, meanwhile at high h-BN content it showed slightly low elongation at break. The slightly deteriorated tensile properties of the BM method might be cause by the presence of a relatively higher number of h-BN agglomerates, especially at high h-BN loading, in the composites prepared by this method. Agglomerates, aforementioned earlier, act as a source of mechanical failure. Kim et al. reported lower tensile properties in the composites prepared by a powder mixing method as compared to those prepared by a MB method [182].

Fig. 72, Fig. 73, and Fig. 74 study the effect of the h-BN particle size, h-BN6 and h-BN35, on the yield stress, Young's modulus, and elongation at break (%) of h-

BN/LLDPE composites. At low h-BN loading (~ 20 wt. %), no clear difference was observed in the yield stress and Young's modulus. Conversely, at high h-BN loading (~ 40 wt. %), the h-BN35 composites displayed higher yield stress and Young's Modulus. On the other hand, the elongation break of the h-BN6 composites was higher at all h-BN loading. As with the thermal conductivity, the formation of filler networks seem to enhance the tensile properties of h-BN35 composites. Cheewawuttipong et al. reported a higher mechanical properties of h-BN/ polypropylene composites filled with a big h-BN particle size compared to those filled with small particles, due to the formation of filler networks [192].

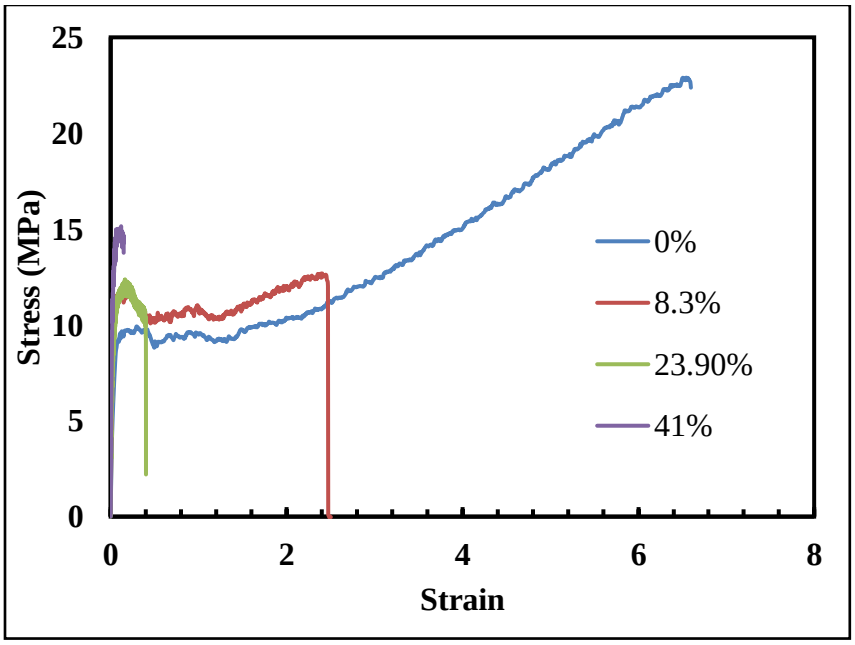

Fig. 63: Stress-Strain curves of h-BN35/LLDPE composites.

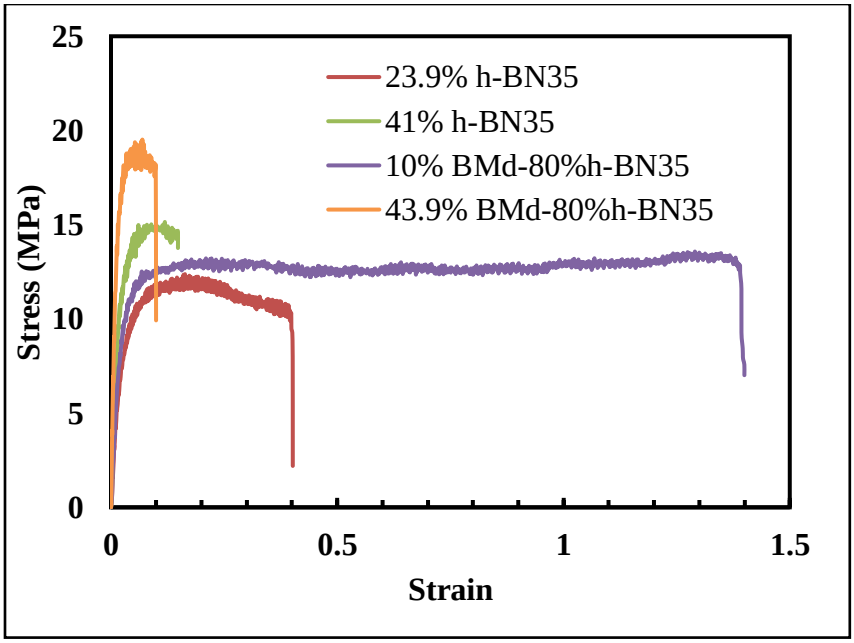

Fig. 64: Stress-Strain curves of h-BN35/LLDPE and BMd-80%h-BN35/LLDPE composites.

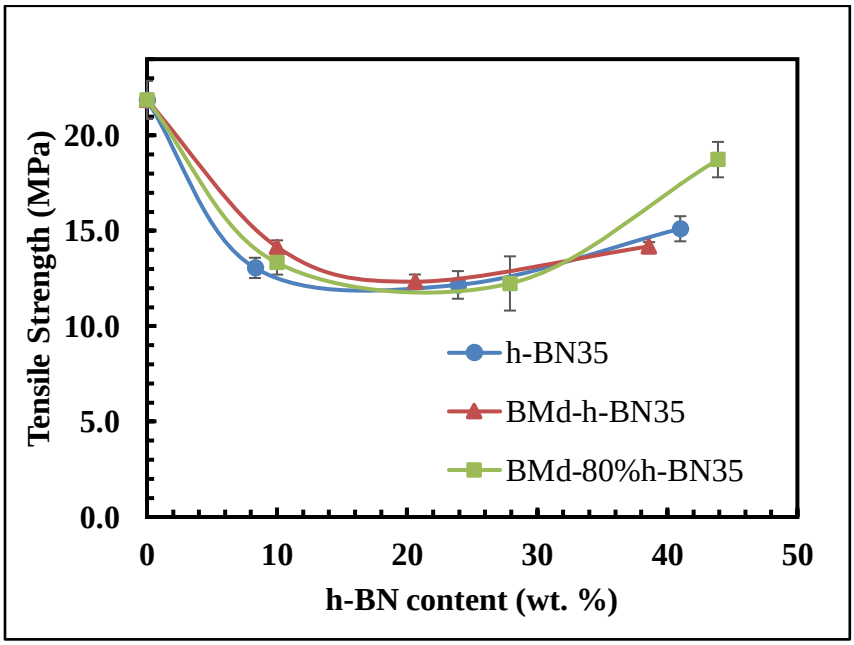

Fig. 65: The tensile strength of h-BN35/LLDPE, BMd-h-BN35/LLDPE, and BMd-80%h-BN35/LLPDE composites.

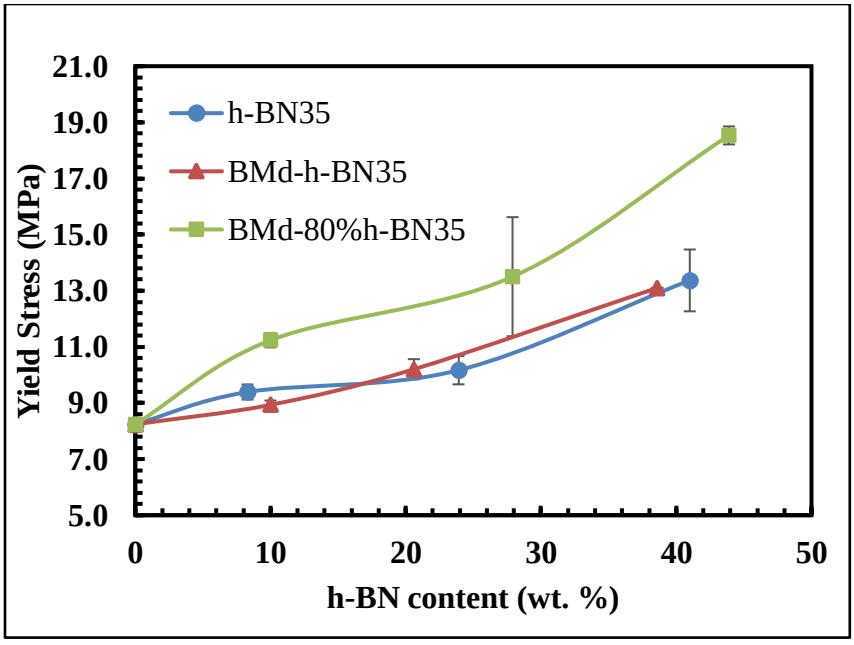

Fig. 66: The yield stress of h-BN35/LLDPE, BMd-h-BN35/LLDPE, and BMd-80%h-BN35/LLPDE composites.

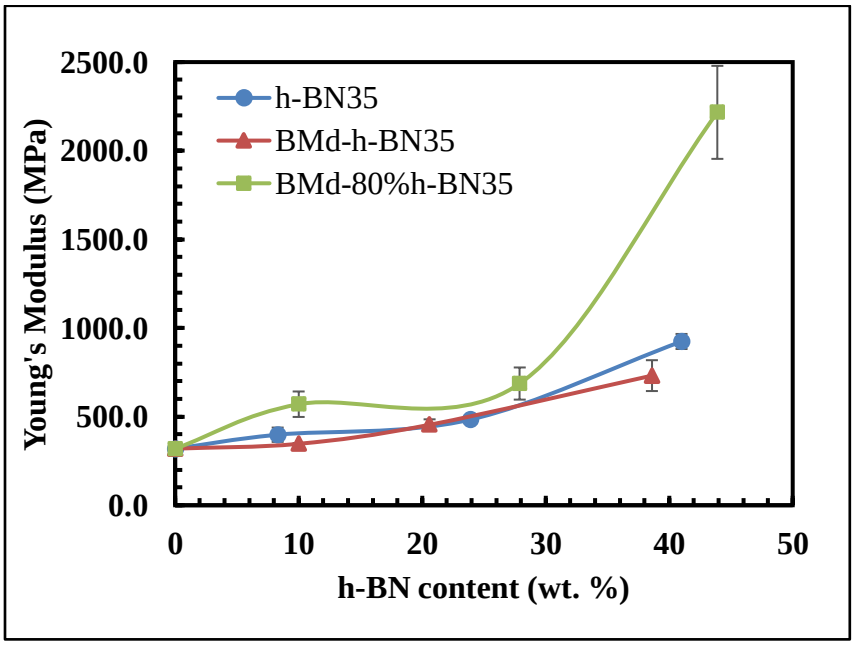

Fig. 67: The Young's modulus of h-BN35/LLDPE, BMd-h-BN35/LLDPE, and BMd-80%h-BN35/LLPDE composites.

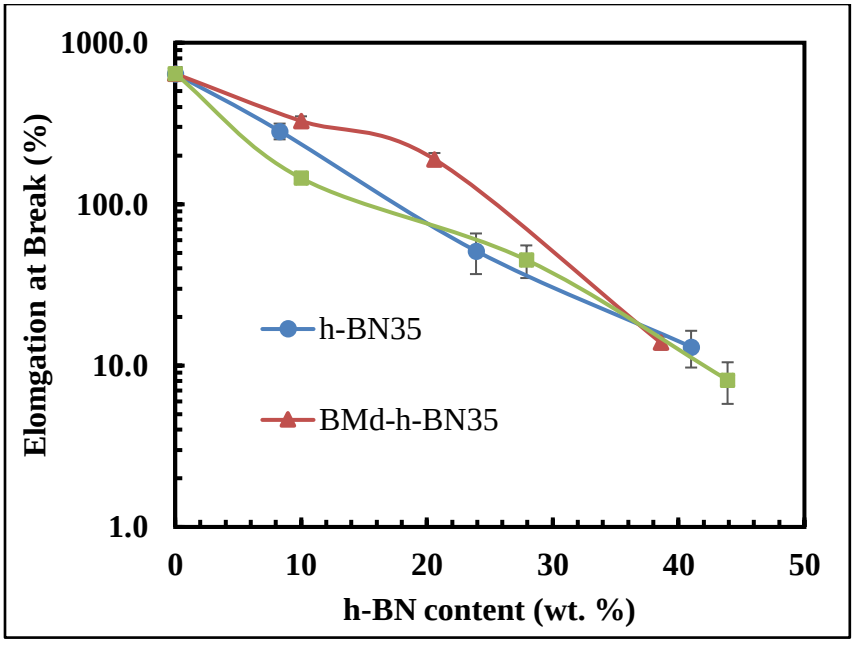

Fig. 68: The Elongation at break (%) of h-BN35/LLDPE, BMd-h-BN35/LLDPE, and BMd-80%h-BN35/LLPDE composites.

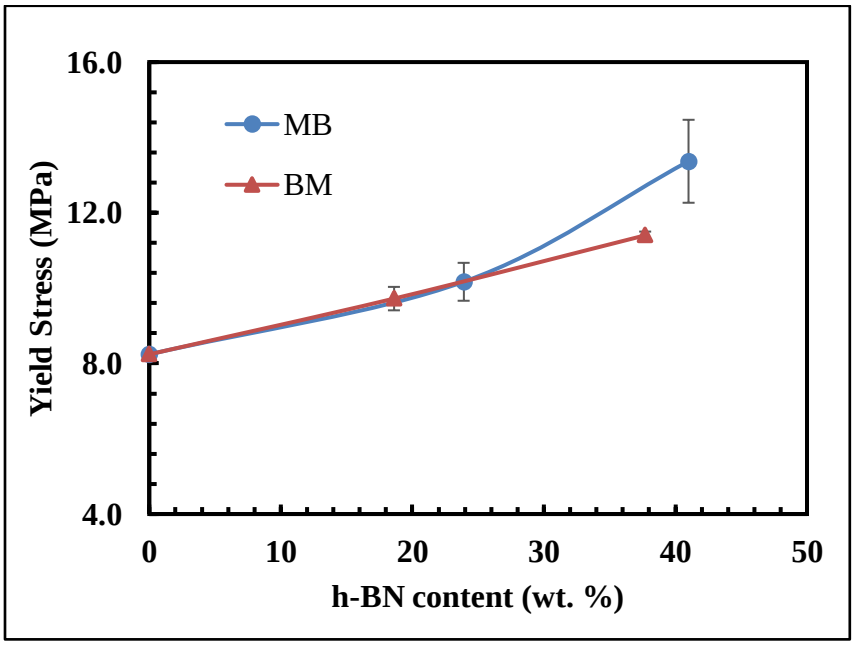

Fig. 69: The yield stress of h-BN35/LLDPE composites prepared by MB and BM methods.

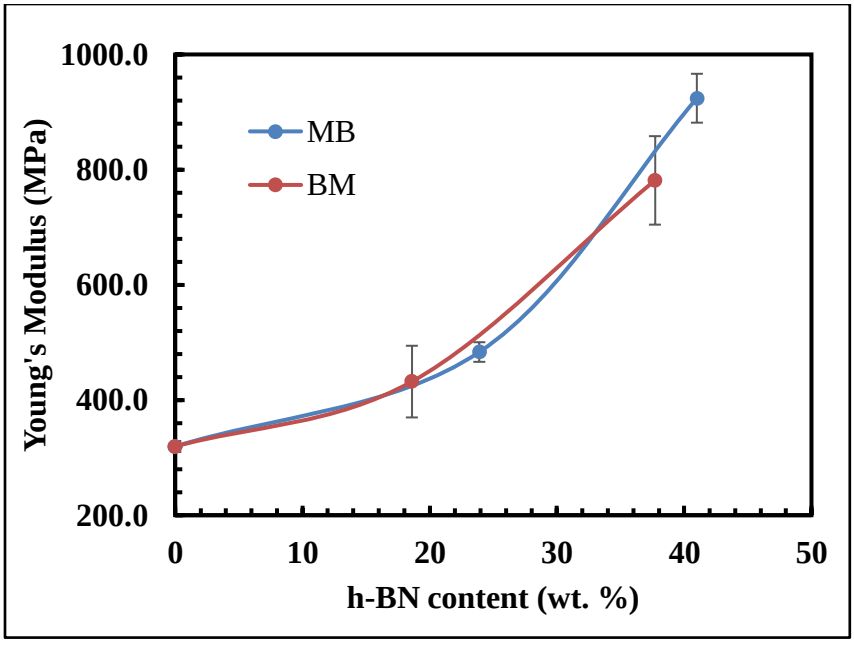

Fig. 70: The Young's modulus of h-BN35/LLDPE composites prepared by MB and BM methods.

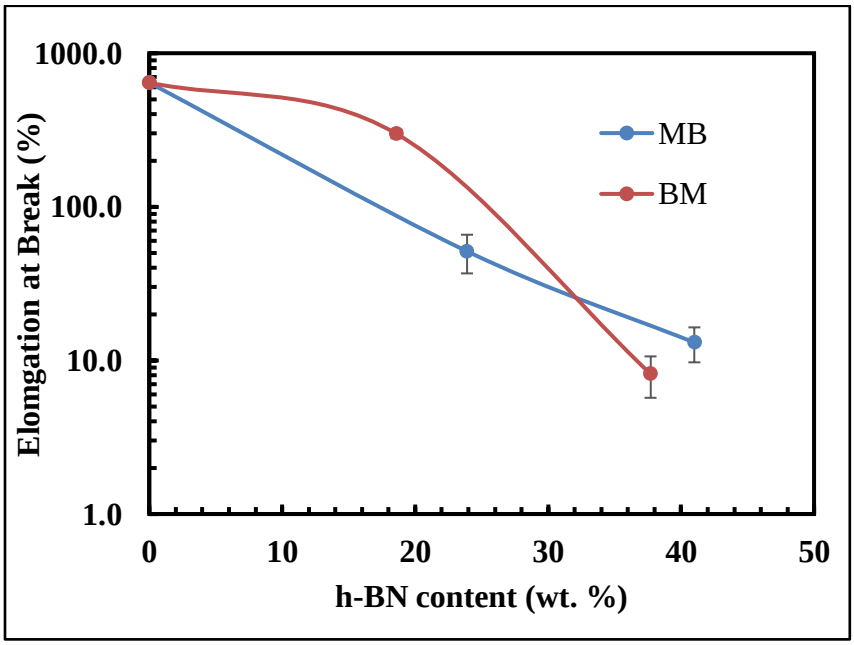

Fig. 71: The elongation at break (%) of h-BN35/LLDPE composites prepared by MB and BM methods.

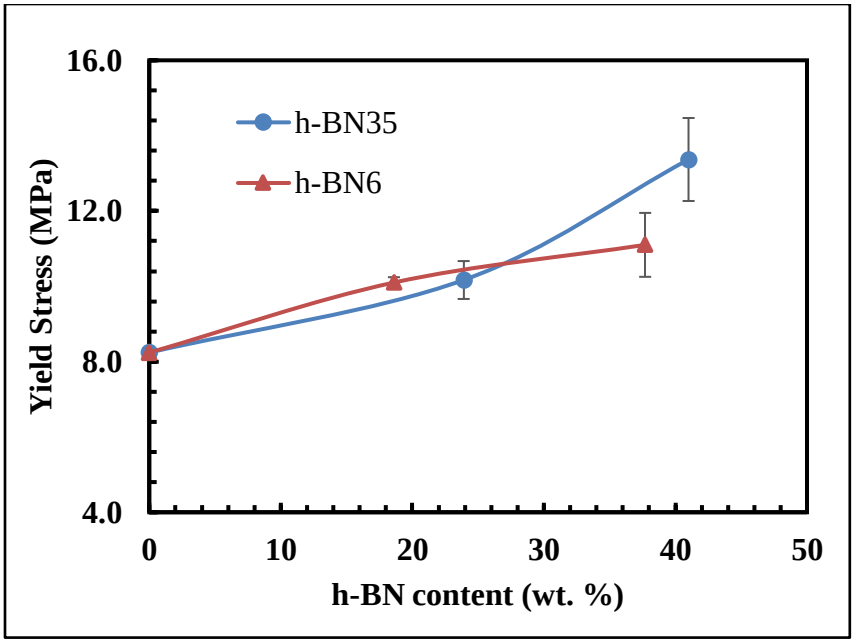

Fig. 72: The yield stress of h-BN35/LLDPE and h-BN6/LLDPE composites.

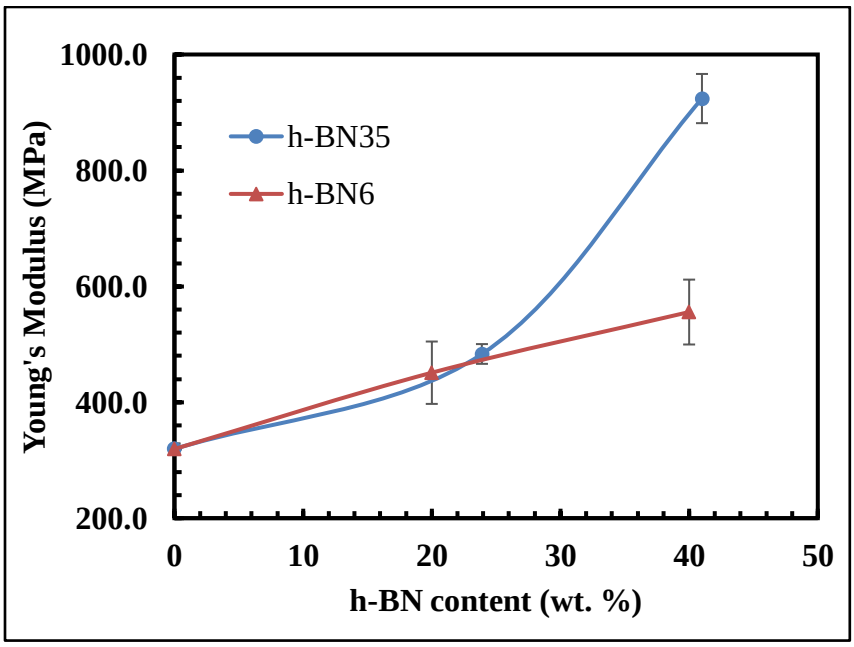

Fig. 73: The Young's Modulus of h-BN35/LLDPE and h-BN6/LLDPE composites.

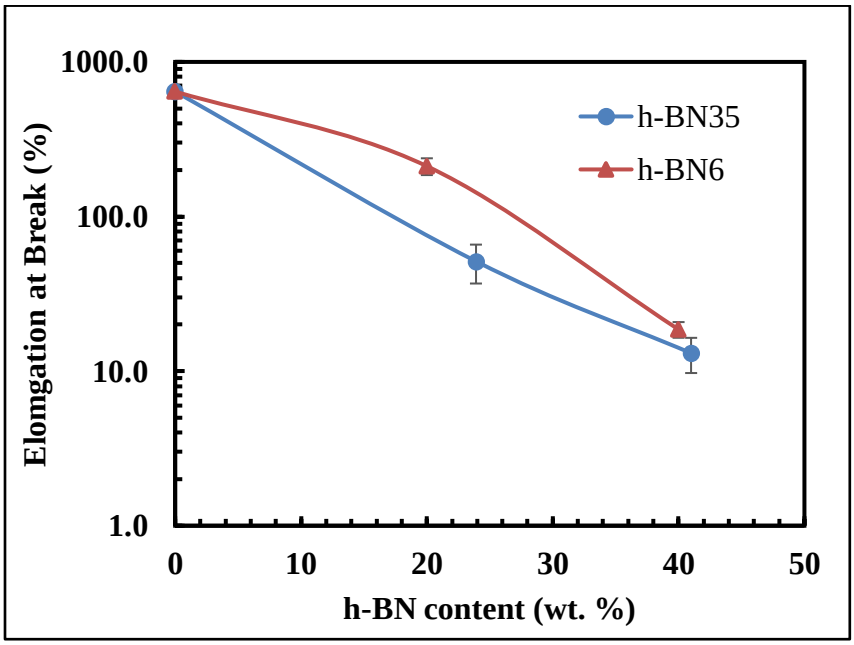

Fig. 74: The Elongation at break (%) of h-BN35/LLDPE and h-BN6/LLDPE composites.

4.3.6. Wettability

Wettability is a surface property of a material that determines the wetting ability of a liquid in contact with a solid surface. A fluid with good wettability will spread and form a low CA (< 90º) and vice versa. Being a surface property, wettability modification has significant impacts on the performance as a heat transfer surface. PE polymers comprising of only hydrogen and carbon have a very hydrophobic surface, and hence have poor wettability. For PE composites to be used as a heat transfer their wettability must be improved considerably. There are several techniques to improve the wettability of PE polymers, such as plasma treatment, corona discharge, and mechanical abrasion. Here,

the wettability of h-BN/PE composites were improved by plasma treatment. The wettability of the h-BN/PE composites were investigated by performing CA measurements, see Fig. 75.

Fig. 76 shows the CA of h-BN/PE composites at different h-BN loading. The CA showed functionality with h-BN loading. Apparently, the addition of h-BN increased the hydrophobicity of PE composites. Zahirifar et al. stated that the addition of h-BN reduced the wettability of polyvinylidene fluoride membrane by increasing the CA from 71 º at 0 wt. % to 130º at 2 wt. % h-BN loadings [193]. Conversely, Emrah et al. stated that the wettability of polyurethane was improved by the incorporation of h-BN [108]. They ascribed the hydrophilic nature of h-BN to its polarity and the presence of amine or hydroxyl functional groups on its surface. The CA of bulk h-BN varies significantly depending on the source of h-BN. For instance, Chen et al. reported a CA of untreated bulk h-BN of 108 º [194], meanwhile Wattankul et al. reported 86.8 º [195]. In this work, the h-BN acted as a hydrophobic compound reducing the wettability of PE composites. This argument is supported by the slightly higher CA of h-BN6/PE composites compared to h-BN35/PE composites. For instance, h-BN6 have more surface area compared to h-BN35 and hence more contact surface with water increasing the CA, hereby reducing the wettability.

The wettability of h-BN/PE composites was improved by plasma treatment. Plasma treatment, which contains ions, electrons, and neutral gases, is commonly used to change the surface properties of materials by changing the surface chemistry without affecting the bulk properties [170]. The CA of h-BN/PE composites before and after the plasma

treatment was measured. In addition, the aging behavior was also evaluated. Particularly, the CA of 50 wt. % h-BN/LLDPE composite reduce from 107.6º±2.57º in the untreated composite to 21.05º±2.34º at 0 h and 75.26º±5.3º after 1 month in the treated. Notably, the plasma treatment enormously enhanced the wettability of the composite by inducing polar functional groups on its surface. The deterioration in the properties after 1 month might be caused by the effect of pollutant changing the surface chemistry of the composite [170].

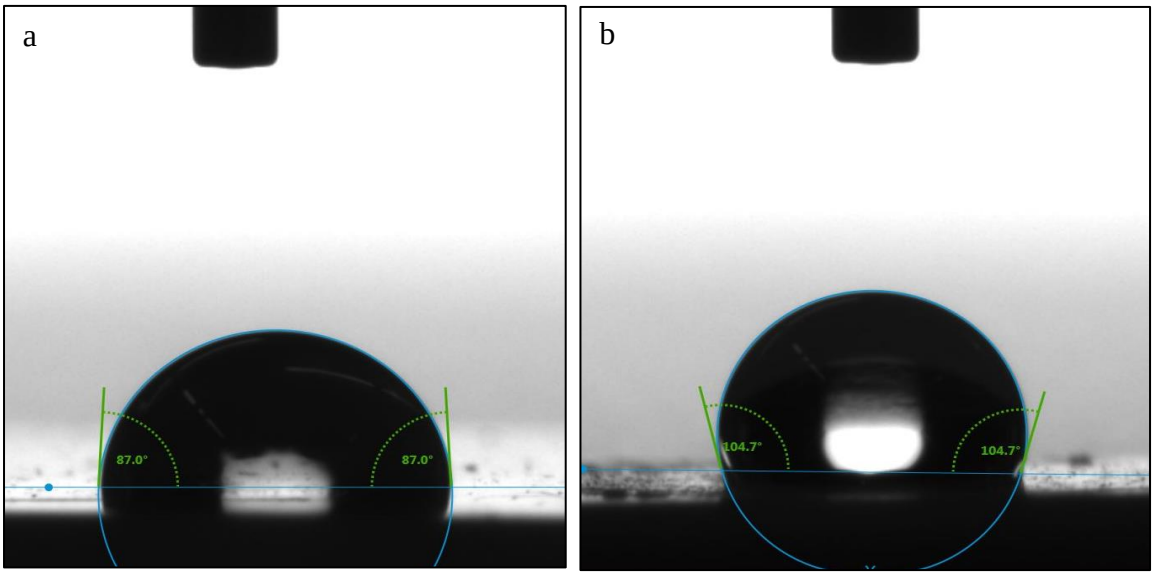

Fig. 75: The CA images of pure LDPE and 10 wt. % h-BN6/LDPE composite.

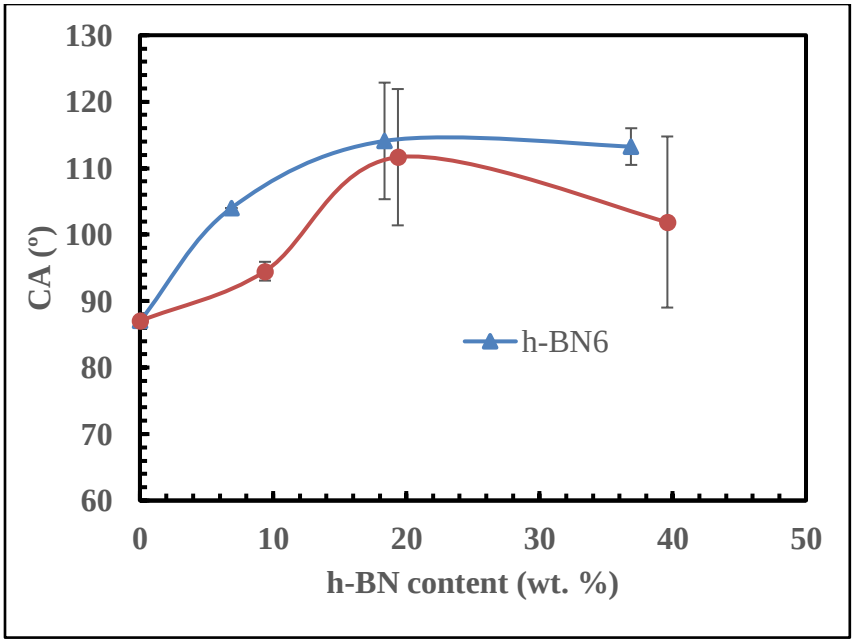

Fig. 76: The CA of water and h-BN/PE composites at different h-BN loading.

5. CONCLUSIONS AND RECOMMENDATIONS

In the first part of this thesis, h-BN was treated using a BM technique. The BMd-h-BN exhibited a remarkable stability and an unusually high yield of up to ~ 61 %, at a short BM time. The XRD analysis showed a clear shift and broadening of the (002) peak, implying exfoliation. The exfoliation was also supported by the significant reduction in their crystallite size of up to ~ 2.3 nm. The SEM analysis showed a substantial reduction in the average particle size. In addition, the TEM analysis showed few-layers h-BN sheets, clearly supporting the XRD and SEM results. The XPS and EDX analysis revealed a new peak ascribed to the oxidation of h-BN. In addition, the atomic oxygen concentration increased to 10 wt. %. Even though the BM treatment had shown high yield and stability, the h-BN particle size was reduced drastically. In addition, the BMd-h-BN showed signs of defects. Therefore, LLDPE was added to protect the h-BN particles during the BM treatment. The later was found to be beneficial in mitigating defect formation and amorphization, as well as improving the average particle size.

In the second part of the thesis, the thermo-mechanical properties of PE polymers were heightened by the inclusion of h-BN fillers. The effect of several factors, including h-BN particle size, composite processing method, composite sheet thickness, h-BN alignment, and h-BN exfoliation was systematically studied. The incorporation of h-BN increased the thermal and mechanical properties of PE composites. Owing to their bigger particle sizes, h-BN35 was found to form networks at low loading leading to a better 'λ' enhancement relative to h-BN6. The composites prepared by BM method displayed uneven h-BN distribution producing h-BN agglomerates and h-BN networks, leading to a higher 'λ'

compared to those prepared by MB method. The 0.5 mm thick composites exhibited orthogonal h-BN orientation, and hence low 'λ'. Afterward, the 'λ' was improved by increasing the sheet thickness to 2mm. Subsequently, the top and bottom layers of the 2 mm thick sheets were grinded and polished removing the layers where h-BN orientation is orthogonal to the heat flux leaving the center where the h-BN orientation is parallel to the heat flux. This resulted in a higher 'λ' of up to 2.7 W m^{-1} K^{-1} compared to 1.7 W m^{-1} K^{-1} in the original. Using this knowledge, h-BN was perfectly aligned parallel to the heat flux leading to a maximum 'λ' enhancement of over 1300 %. The BMd-80% h-BN/composites demonstrated better 'λ' enhancement compared to the bulk h-BN/composites. However, their processing was difficult limiting them to low loading only.

Having remarkable thermal stability, h-BN heightened the thermal stability of h-BN/PE composites. Small particle sized h-BN6 demonstrated better thermal stability enrichment compared to h-BN35, due to their better dispersion. Owing to their oxygen contents BMd-h-BN35 showed lower thermal stability compared to pure h-BN35 and BMd-80%h-BN35. The DSC results demonstrated nucleation ability of h-BN in the h-BN/PE composites leading to a higher percentage of crystallinity compared to the pure PE. However, at high h-BN concentration h-BN agglomerates deteriorating the percentage of crystallinity.

Similarly, the addition of h-BN enhanced the mechanical properties of h-BN/PE composites. Composites with good h-BN dispersion and less agglomeration was prepared by MB method leading to a better mechanical properties compared to the composites

prepared by BM method. Equivalently, BMd-80%h-BN35/LLDPE composites exhibited good and uniform h-BN dispersion leading to the highest yield stress and Young's Modulus values of 18.5 MPa and 22.2 GPa.

Oppositely, the addition of h-BN deteriorated the wettability of h-BN/PE composites showing CA in the range of 87 º- 113 º. Nonetheless, the wettability was improved by plasma treatment. Afterward, the effect of aging on the wettability was analyzed. For instance, the CA of 50 wt. % h-BN/LLDPE lowered from 107.6º±2.57º in the untreated composite to 21.05º±2.34º at 0 h. However, after one month the CA increased to 75.26º±5.3º showing slight weakening in the wettability due to the adsorption of impurities on the treated surface.

Based on the results discussed above it can be concluded that 30 vol. % BMd-80%h-BN35/LLDPE composites was found to exhibit optimum performance in terms of thermal conductivity, thermal stability, and mechanical properties. Moreover, it can be hypothesized that employing HDPE instead of LLDPE in these composites would result in better performance due to the higher crystallinity of HDPE relative to LLDPE.

The full potential of h-BN ability in improving the thermo-mechanical properties of PE composites can be further achieved by including h-BN surface modification [25]. The chemical nature of h-BN limits their ability to disperse inside the polymer matrix inducing interfacial thermal resistance. Organo-Silanes are commonly utilized as a surface modifier to enhance the interaction between the filler and the polymer matrix [29] [25]. The work of Fu et al [117] and Donnay *et al.* [125] have shown that the addition of surface modifier such as silane agent on h-BN have positive effect on the thermal conductivity of

h-BN/epoxy composites. The interfacial thermal resistance can also be reduced by grafting method. Jiang *et al.* [107], stated that grafting poly (glycidyl methacrylate) (PGM) on the surface of h-BN upgraded the thermal conductivity of h-BN/epoxy composites.

This work has shown that the h-BN alignment inside the polymer by far has the highest impact on 'λ'. For example, it was shown that the thermal conductivity of h-BN/PE composite was improved by ~ 600 % when the h-BN orientation was changed from horizontal to vertical. Similar work was reported by Yuan's and Sun's groups. Yuan *et al.* [123] used a magnetic field to orient BN platelets, meanwhile Sun *et al.* [124] used hot-pressing method to align h-BN. They reported significant improvement in the thermal conductivity due to these alignments. For instance, Sun's group reported a maximum 'λ' of 3.09 W m^{-1} K^{-1} at 18 vol. % BN loading. Therefore, inventing a simple method to align h-BN would not only improve the thermal conductivity but would also reduce the cost by lowering the h-BN loading.

The effect of plasma treatment on the bulk properties such as the thermal conductivity, thermal stability, and mechanical properties has not been studied in this work. Thus, it would be very enlightening if the effect of plasma treatment on these properties is investigated.

REFERENCES

[1] A. Pakdel, Y. Bando, and D. Golberg, “Nano boron nitride flatland,” *Chem. Soc. Rev.*, vol. 43, pp. 934–959, 2014.

[2] M. Schleberger and J. Kotakoski, “2D Material Science : Defect Engineering by Particle Irradiation,” *Materials (Basel).*, vol. 11, no. 10, pp. 1885–1913, 2018.

[3] R. Aradhana, S. Mohanty, and S. K. Nayak, “High performance electrically conductive epoxy / reduced graphene oxide adhesives for electronics packaging applications,” *J. Mater. Sci. Mater. Electron.*, vol. 30, no. 4, pp. 4296–4309, 2019.

[4] A. M. P. R. K. Goyal, “High performance polyetherketone-hexagonal boron nitride nanocomposites for electronic applications,” *J. Mater. Sci. Mater. Electron.*, vol. 30, no. 4, pp. 3899–3908, 2019.

[5] Y. Guo and S. N. Leung, “Thermally conductive polybutylene terephthalate / hexagonal boron nitride composites with bimodal fi ller size distribution,” *Mater. Chem. Phys.*, vol. 214, pp. 221–228, 2018.

[6] M. D. Ganji and R. Dodangeh, “Hydrogen purification performance of a nanoporous hexagonal boron nitride membrane : molecular dynamics and first-principle simulations,” *Phys. Chem. Chem. Phys.*, vol. 19, pp. 12032–12044, 2017.

[7] C. Buelke, A. Alshami, J. Casler, J. Lewis, M. Al-sayaghi, and M. A. Hickner, “Graphene oxide membranes for enhancing water purification in terrestrial and space-born applications: State of the ar,” *Desalination*, vol. 448, pp. 113–132,

2018.

[8] C. Xu, M. Miao, X. Jiang, and X. Wang, “Thermal conductive composites reinforced via advanced boron nitride nanomaterials,” *Compos. Commun.*, vol. 10, pp. 103–109, 2018.

[9] H. Fang, S. Bai, and C. P. Wong, “‘White graphene’– hexagonal boron nitride based polymeric composites and their application in thermal management,” *Compos. Commun.*, vol. 2, pp. 19–24, 2016.

[10] A. Pakdel, Y. Bando, and D. Golberg, “Nano boron nitride flatland,” *Chem. Soc. Rev.*, vol. 43, no. 3, pp. 934–959, 2014.

[11] K. Zhang, Y. Feng, F. Wang, Z. Yang, and J. Wang, “Two dimensional hexagonal boron nitride (2D-hBN): Synthesis, properties and applications,” *J. Mater. Chem. C*, vol. 5, no. 46, pp. 11992–12022, 2017.

[12] J. Bao, M. Edwards, S. Huang, Y. Zhang, and Y. Fu, “Two-dimensional hexagonal boron nitride as lateral heat spreader in electrically insulating packaging,” *Phys. D Appl. Phys.*, vol. 49, pp. 265501–265509, 2016.

[13] T. B. Wang, C. C. Jin, J. Yang, C. F. Hu, and T. Qiu, “Physical and mechanical properties of hexagonal boron nitride ceramic fabricated by pressureless sintering without additive,” vol. 114, no. 5, pp. 273–277, 2015.

[14] X. Duan *et al.*, “Review on the properties of hexagonal boron nitride matrix composite ceramics,” *J. Eur. Ceram. Soc.*, vol. 36, no. 15, pp. 3725–3737, 2016.

[15] Z. Lin, A. Mcnamara, Y. Liu, K. sik Moon, and C. P. Wong, “Exfoliated hexagonal boron nitride-based polymer nanocomposite with enhanced thermal

conductivity for electronic encapsulation," *Compos. Sci. Technol.*, vol. 90, pp. 123–128, 2014.

[16] S. Rudolph, "Composition and Application of Coatings Based on Boron Nitride," *Interceram*, vol. 42, no. 5, pp. 4–6, 1993.

[17] M. S. Charoo and M. F. Wani, "Tribological properties of h-BN nanoparticles as lubricant additive on cylinder liner and piston ring," *Lubr. Sci.*, vol. 29, no. 4, pp. 241–254, 2016.

[18] C. Su, J. Wang, C. Chen, K. Chu, and C. Lin, "Spherical Composite Powder by Coupling Polymethyl Methacrylate and Boron Nitride via Spray Drying for Cosmetic Application," *Materials (Basel).*, vol. 12, pp. 706–716, 2019.

[19] Z. Pawlak, T. Kaldonski, R. Pai, E. Bayraktar, and A. Oloyede, "A comparative study on the tribological behaviour of hexagonal boron nitride (h-BN) as lubricating micro-particles — An additive in porous sliding bearings for a car clutch," *Wear*, vol. 267, no. 5–8, pp. 1198–1202, 2009.

[20] H. M. Baalousha and O. K. M. Ouda, "Domestic water demand challenges in Qatar Domestic water demand challenges in Qatar," *Arab. J. Geosci.*, vol. 10, no. 24, pp. 537–549, 2017.

[21] H. Rahman and S. J. Zaidi, "Desalination in Qatar : Present Status and Future Prospects," *Civ. Eng. Res. J.*, vol. 6, no. 5, pp. 555700–555707, 2018.

[22] M. Alhaj, S. Mohammed, M. Darwish, and A. Hassan, "A review of Qatar ' s water resources , consumption and virtual water trade," *Desalin. Water Treat.*, vol. 70, pp. 70–85, 2017.

[23] J. G. Cevallos, A. E. Bergles, A. Bar-Cohen, P. Rodgers, and S. K. Gupta, "Polymer heat exchangers-history, opportunities, and challenges," *Heat Transf. Eng.*, vol. 33, no. 13, pp. 1075–1093, 2012.

[24] X. Chen, Y. Su, D. Reay, and S. Riffat, "Recent research developments in polymer heat exchangers – A review," *Renew. Sustain. Energy Rev.*, vol. 60, pp. 1367–1386, 2016.

[25] A. R. J. Hussain, A. A. Alahyari, S. A. Eastman, C. Thibaud-Erkey, S. Johnston, and M. J. Sobkowicz, "Review of polymers for heat exchanger applications: Factors concerning thermal conductivity," *Appl. Therm. Eng.*, vol. 113, pp. 1118–1127, 2017.

[26] A. J. Leao, "Polymer film heat transfer elements for multi - effect and vapour compression desalination," Faculty of Natural and Agricultural Science, University of Pretoria, Pretoria, South Africa, 2014.

[27] J. B. . Christman, L. J. Kratz, and H.-J. Bart, "Novel polymer film heat exchangers for seawater desalination," *Desalin. Water Treat.*, vol. 21, pp. 162–174, 2010.

[28] Robert J. Young; Peter A. Lovell, "Introduction To Polymers," in *Introduction to Polymers*, Third Edit., R. J. Y. P. A. Lovell, Ed. Boca Raton, Florida: CRC Press, 2011, pp. 3–469.

[29] H. Chen *et al.*, "Thermal conductivity of polymer-based composites: Fundamentals and applications," *Prog. Polym. Sci.*, vol. 59, pp. 41–85, 2016.

[30] X. Wang and P. Wu, "Preparation of Highly Thermally Conductive Polymer

Composite at Low Filler Content via a Self-Assembly Process between Polystyrene Microspheres and Boron Nitride Nanosheets," *ACS Appl. Mater. Interfaces*, vol. 9, no. 23, pp. 19934–19944, 2017.

[31] D. M. Bigg, "Thermal conductivity of heterophase polymer compositions," *Adv. Polym. Sci.*, vol. 119, pp. 1–30, 1995.

[32] E. N. L. Byron Bird, Warren E. Stewart, *Transport Phenomena*, 2nd ed., vol. 5, no. 10–11. John Wiley & Sons, Inc., 2000.

[33] V. Guerra, C. Wan, and T. Mcnally, "Progress in Materials Science Thermal conductivity of 2D nano-structured boron nitride (BN) and its composites with polymers," *Prog. Mater. Sci.*, vol. 100, pp. 170–186, 2019.

[34] Terry M. Tritt, *Thermal Conductivity Theory, Properties, and Applications*. New York: Kluwer Academic, 2004.

[35] N. Burger, A. Laachachi, M. Ferriol, M. Lutz, V. Toniazzo, and D. Ruch, "Review of thermal conductivity in composites: Mechanisms, parameters and theory," *Prog. Polym. Sci.*, vol. 61, pp. 1–28, 2016.

[36] X. Xu, J. Chen, J. Zhou, and B. Li, "Thermal Conductivity of Polymers and Their Nanocomposites," *Adv. Mater.*, vol. 30, no. 17, pp. 1705544–1705554, 2018.

[37] N. Mehra *et al.*, "Thermal transport in polymeric materials and across composite interfaces," *Appl. Mater. Today*, vol. 12, pp. 92–130, 2018.

[38] C. Huang, X. Qianb, and R. Yang, "Thermal conductivity of polymers and polymer nanocomposites," *Mater. Sci. Eng. R*, vol. 132, pp. 1–22, 2018.

[39] N. Burger, A. Laachachi, M. Ferriol, M. Lutz, V. Toniazzo, and D. Ruch,

"Progress in Polymer Science Review of thermal conductivity in composites : Mechanisms , parameters and theory," *Prog. Polym. Sci.*, vol. 61, pp. 1–28, 2016.

[40] A. B. Robbins and A. J. Minnich, "Crystalline polymers with exceptionally low thermal conductivity studied using molecular dynamics," *Appl. Phys. Lett.*, vol. 107, no. 20, 2015.

[41] C. Huang, X. Qian, and R. Yang, "Thermal conductivity of polymers and polymer nanocomposites," *Mater. Sci. Eng. R Reports*, vol. 132, no. July, pp. 1–22, 2018.

[42] X. Huang, P. Jiang, and T. Tanaka, "A review of dielectric polymer composites with high thermal conductivity," *IEEE Electr. Insul. Mag.*, vol. 27, no. 4, pp. 8–16, 2011.

[43] X. Huang, P. Jiang, and T. Tanaka, "A Review of Dielectric Polymer Composites With High Thermal," *IEEE Electr. Insul. Mag.*, vol. 27, no. 4, pp. 8–16, 2011.

[44] G. W. Lee, M. Park, J. Kim, J. I. Lee, and H. G. Yoon, "Enhanced thermal conductivity of polymer composites filled with hybrid filler," *Compos. Part A Appl. Sci. Manuf.*, vol. 37, no. 5, pp. 727–734, 2006.

[45] K. Wattanakul, H. Manuspiya, and N. Yanumet, "Thermal conductivity and mechanical properties of BN-filled epoxy composite: Effects of filler content, mixing conditions, and BN agglomerate size," *J. Compos. Mater.*, vol. 45, no. 19, pp. 1967–1980, 2011.

[46] Y. K. Shin, W. S. Lee, M. J. Yoo, and E. S. Kim, "Effect of BN filler on thermal properties of HDPE matrix composites," *Ceram. Int.*, vol. 39, pp. S569–S573, 2013.

[47] F. Kargar *et al.*, "Thermal Percolation Threshold and Thermal Properties of Composites with Graphene and Boron Nitride Fillers," *ACS Appl. Mater. Interfaces*, vol. 10, no. 43, pp. 37555–37565, 2018.

[48] A. Li, C. Zhang, and Y. F. Zhang, "Thermal conductivity of graphene-polymer composites: Mechanisms, properties, and applications," *Polymers (Basel).*, vol. 9, no. 9, pp. 1–18, 2017.

[49] D. M. Bigg, "Conductive Polymeric Compositions," *Polym. Eng. Sci.*, vol. 17, no. 12, pp. 842–847, 1977.

[50] Maxwell, "A treatise on electricity and magnetism," *Oxford Univ. Press*, vol. 1, p. 500, 1904.

[51] L. R. Strutt, J.W., "On the instability of cylindrical fluid surfaces," *Philos. Mag.*, vol. 34, no. 207, pp. 177–180, 1892.

[52] D. P. H. Hasselman and L. F. Johnson, "Effective Thermal Conductivity of Composites with Interfacial Thermal Barrier Resistance," *J. Compos. Mater.*, vol. 21, no. 6, pp. 508–515, 1987.

[53] J. Ordóñez-Miranda, J. J. Alvarado-Gil, and R. Medina-Ezquivel, "Generalized Bruggeman formula for the effective thermal conductivity of particulate composites with an interface layer," *Int. J. Thermophys.*, vol. 31, no. 4–5, pp. 975–986, 2010.

[54] J. P. Angle, Z. Wang, C. Dames, and M. L. Mecartney, "Comparison of Two-Phase Thermal Conductivity Models with Experiments on Dilute Ceramic Composites," *J. Am. Ceram. Soc.*, vol. 96, no. 9, pp. 2935–2942, 2013.

[55] N. M. R., “Thermal Conduction in Polymeric Nanofluids and Nanosolids Controlled by Interfacial Scattering : Solutions to Some Selected Problems Department of Instrumentation,” Ph.D dissertation, Cochin University of Science and Technology, Kochi, Kerala, 2011. Accesed on: September 1, 2019. [Online]. Available: https://pdfs.semanticscholar.org/a9b7/50131a1f6af0ff7995d21977b7bb88b6fdc9.pdf.

[56] R. Pal, “On the Lewis-Nielsen model for thermal/electrical conductivity of composites,” *Compos. Part A Appl. Sci. Manuf.*, vol. 39, no. 5, pp. 718–726, 2008.

[57] Y. Agar, T. Uno, and O. Municipal, “Estimation on Thermal Conductivities of Filled Polymers,” *J. Appl. Polym. Sci.*, vol. 32, no. 7, pp. 5705–5712, 1986.

[58] Y. Agari, A. Ueda, and S. Nacal, “Thermal Conductivity of a Polymer Composite,” *J. Appl. Polym. Sci.*, vol. 49, no. 9, pp. 1625–1634, 1993.

[59] K. Pietrak and T. S. Winiewski, “A review of models for effective thermal conductivity of composite materials,” *J. J. Power Technol.*, vol. 95, no. 1, pp. 14–24, 2015.

[60] L. E. Nielsen, “The Thermal and Electrical Conductivity of Two-Phase Systems,” *Ind. Eng. Chem. Fundam.*, vol. 13, no. 1, pp. 17–20, 1974.

[61] S. Nie, X. Zhang, J. Luo, Y. Liu, and W. Yan, “Synergistic Effect of Boron Nitride and Tetrapod-Shaped Zinc Oxide Whisker Hybrid Fillers on Filler Networks in Thermal Conductive HDPE Composites,” *Polym. Compos.*, vol. 38,

no. 9, pp. 1902–1909, 2017.

[62] W. Zhou, S. Qi, H. Li, and S. Shao, “Study on insulating thermal conductive BN/HDPE composites,” *Thermochim. Acta*, vol. 452, no. 1, pp. 36–42, 2007.

[63] X. Zhang, L. Shen, H. Wu, and S. Guo, “Enhanced thermally conductivity and mechanical properties of polyethylene (PE)/boron nitride (BN) composites through multistage stretching extrusion,” *Compos. Sci. Technol.*, vol. 89, pp. 24–28, 2013.

[64] C. Yu, J. Zhang, W. Tian, and Y. Yao, “Polymer composites based on hexagonal boron nitride and their application in thermally conductive composites,” *R. Soc. Chem.*, vol. 8, no. 39, pp. 21948–21967, 2018.

[65] B. Ertuğ, “Powder Preparation , Properties and Industrial Applications of Hexagonal Boron Nitride,” in *Sintering Applications*, Intech, 2013, pp. 33–55.

[66] S. Bernard and P. Miele, “Polymer-Derived Boron Nitride: A Review on the Chemistry, Shaping and Ceramic Conversion of Borazine Derivatives,” *Materials (Basel).*, vol. 7, pp. 7436–7459, 2014.

[67] M. A. Vadivelu, C. R. Kumar, and G. M. Joshi, “Polymer composites for thermal management: a review,” *Compos. Interfaces*, vol. 23, no. 9, pp. 847–872, 2016.

[68] Z. Han, J. Wood, and H. Herman, “Thermal properties of composites filled with different fillers,” *Int. Symp. Electr. Insul.*, pp. 497–501, 2008.

[69] L. Podila, Ramakrishna and Rao, Apparao and Puneet, Pooja and Bhattacharya, Sriparna and Mallineni, Sai Sunil Kumar and Srivastava, Anurag and Liu, Fengjiao and Taha-Tijerina, Jaime and Peña-Parás, Laura and Maldonado-Cortes,

Demofilo and Qin, Guangzhao and , “2D-Based Nanofluids: Materials Evaluation and Performance,” in *Two-dimensional Materials - Synthesis, Characterization and Potential Applications*, Intech, 2016, pp. 1–46.

[70] L. H. Li and Y. Chen, “Atomically Thin Boron Nitride: Unique Properties and Applications,” *Adv. Funct. Mater.*, vol. 26, no. 16, pp. 2594–2608, 2016.

[71] C. Y. Zhi, Y. Bando, T. Terao, C. Tang, and D. Golberg, “Dielectric and thermal properties of epoxy/boron nitride nanotube composites,” *Pure Appl. Chem.*, vol. 82, no. 11, pp. 2175–2183, 2010.

[72] J. Lee *et al.*, “Boron Nitride Nanosheets (BNNSs) Chemically Modified by ‘Grafting-From’ Polymerization of Poly(caprolactone) for Thermally Conductive Polymer Composites,” *Chem. - An Asian J.*, vol. 11, no. 13, pp. 1921–1928, 2016.

[73] J. Meng, N. Tajaddod, S. W. Cranford, and M. L. Minus, “Polyethylene-Assisted Exfoliation of Hexagonal Boron Nitride in Composite Fibers: A Combined Experimental and Computational Study,” *Macromol. Chem. Phys.*, vol. 216, no. 8, pp. 847–855, 2015.

[74] D. Lee, B. Lee, K. H. Park, H. J. Ryu, S. Jeon, and S. H. Hong, “Scalable exfoliation process for highly soluble boron nitride nanoplatelets by hydroxide-assisted ball milling,” *Nano Lett.*, vol. 15, no. 2, pp. 1238–1244, 2015.

[75] B. Zhang *et al.*, “High-Efficient Liquid Exfoliation of Boron Nitride Nanosheets Using Aqueous Solution of Alkanolamine,” *Nanoscale Res. Lett.*, vol. 12, no. 1, p. 596, 2017.

[76] W. Y. Ko, C. Y. Chen, W. H. Chen, and K. J. Lin, “Fabrication of Hexagonal

Boron Nitride Nanosheets by Using a Simple Thermal Exfoliation Process," *J. Chinese Chem. Soc.*, vol. 63, no. 3, pp. 303–307, 2016.

[77] D. Paciĺ, J. C. Meyer, Ç. Girit, and A. Zettl, "The two-dimensional phase of boron nitride: Few-atomic-layer sheets and suspended membranes," *Appl. Phys. Lett.*, vol. 92, no. 13, pp. 2–5, 2008.

[78] Y. Tominaga, K. Sato, D. Shimamoto, Y. Imai, and Y. Hotta, "Development of High Aspect Ratio Hexagonal Boron Nitride Filler by Mechanical Exfoliation," in *Advanced Processing and Manufacturing Technologies for Nanostructured and Multifunctional Materials II*, John Wiley & Sons, Ltd, 2015, pp. 91–100.

[79] W. Q. Han, L. Wu, Y. Zhu, K. Watanabe, and T. Taniguchi, "Structure of chemically derived mono- and few-atomic-layer boron nitride sheets," *Appl. Phys. Lett.*, vol. 93, no. 22, pp. 3–6, 2008.

[80] J. N. Coleman *et al.*, "Supporting Online Material for Two-Dimensional Nanosheets Produced by Liquid Exfoliation of Layered Materials Two-dimensional nano-sheets produced by liquid exfoliation of layered materials," *Science (80-.).*, vol. 331, no. 568, pp. 568–571, 2011.

[81] H. X. Jiang and J. Y. Lin, "Review — Hexagonal Boron Nitride Epilayers : Growth , Optical Properties and Device Applications," *J. Solid State Sci. Technol.*, vol. 6, no. 2, pp. Q3012–Q3021, 2017.

[82] S. Gao, B. Li, D. Li, C. Zhang, R. Liu, and S. Wang, "Micromorphology and structure of pyrolytic boron nitride synthesized by chemical vapor deposition from borazine," *Ceram. Int.*, vol. 44, no. 10, pp. 11424–11430, 2018.

[83] B. Zhong, “A Novel Polymeric Precursor for Boron Nitride Ceramics : Synthesis , Characterization , and Ceramic Conversion,” *Int. J. Appl. Ceram. Technol.*, vol. 13, no. 5, pp. 929–937, 2016.

[84] H. Wu, M. Chen, X. Wei, M. Ge, and W. Zhang, “Applied Surface Science Deposition of BN interphase coatings from B-trichloroborazine and its effects on the mechanical properties of SiC / SiC composites,” *Appl. Surf. Sci.*, vol. 257, no. 4, pp. 1276–1281, 2010.

[85] H. O. Pierson, “Boron Nitride Composites By Chemical Vapor Deposition,” *J. Compos. Mater.*, vol. 9, pp. 228–240, 1975.

[86] N. V. C. A. S. Rozenberg, Yu. A. Sinenko, “Regularities of pyrolytic boron nitride coating formation on a graphite matrix,” *J. Mater. Sci.*, vol. 28, no. 20, pp. 5528–5533, 1993.

[87] J. Liu, R. G. Kutty, and Z. Liu, “Controlled Synthesis of Atomically Layered Hexagonal Boron Nitride via Chemical Vapor Deposition,” *Molecules*, vol. 21, no. 12, pp. 1636–1643, 2016.

[88] J. Park *et al.*, “Large-Area Monolayer Hexagonal Boron Nitride on Pt Foil,” *ACS Nano*, vol. 8, no. 8, pp. 8520–8528, 2014.

[89] P. Sutter, J. Lahiri, P. Albrecht, and E. Sutter, “Chemical Vapor Deposition and Etching of High-Quality Monolayer Hexagonal Boron Nitride Films,” *ACS Nano*, vol. 5, no. 9, pp. 7303–7309, 2011.

[90] S. Nakhaie, J. M. Wofford, T. Schumann, U. Jahn, M. Ramsteiner, and M. Hanke, “Synthesis of atomically thin hexagonal boron nitride films on nickel foils by

molecular beam epitaxy," *Appl. Phys. Lett.*, vol. 106, no. 21, pp. 213108–21313, 2018.

[91] K. K. Kim *et al.*, "Synthesis of Monolayer Hexagonal Boron Nitride on Cu Foil Using Chemical Vapor Deposition," *Nano Lett.*, vol. 12, no. 1, pp. 161–166, 2012.

[92] W. Joshi, Sushobhan; Ecija, David; Koitz, Ralph; Iannuzzi, Marcella; Seitsonen, Ari P; Hutter, Juerg; Sachdev, Hermann; Vijayaraghavan, Saranyan; Bischoff, Felix; Seufert, Knud; Barth, Johannes V; Auwaerter and Abstract:, "Boron nitride on Cu (111): An electronically corrugated monolayer," *Nano Lett.*, vol. 12, no. 11, pp. 5821–5828, 2012.

[93] M. Morscher, M. Corso, T. Greber, and J. Osterwalder, "Formation of single layer h-BN on Pd (1 1 1)," *Surf. Sci.*, vol. 600, no. 16, pp. 3280–3284, 2006.

[94] S. M. Kim *et al.*, "Synthesis of large-area multilayer hexagonal boron nitride for high material performance," *Nat. Commun.*, vol. 8662, no. 6, 2015.

[95] M. P. Allan, S. Berner, M. Corso, T. Grebar, and O. Jurg, "Tunable self-assembly of one-dimensional nanostructures with orthogonal directions," *Nanoscale Res. Lett.*, vol. 2, no. 2, pp. 94–99, 2007.

[96] F. H. Farwick *et al.*, "Structure and Growth of Hexagonal Boron Nitride on Ir(111)," *ACS Nano*, vol. 10, no. 12, pp. 11012–11026, 2016.

[97] C. Vapor and D. Cvd, "The Transition Metal Surface Passivated Edges of Hexagonal Boron Nitride (h- hexagonal boron nitride (h-BN) and the mechanism," *Phys. Chem. Chem. Phys.*, vol. 17, pp. 29327–29334, 2015.

[98] A. P. Farkas, P. Török, F. Solymosi, J. Kiss, and Z. Kónya, “Applied Surface Science Investigation of the adsorption properties of borazine and characterisation of boron nitride on Rh (1 1 1) by electron spectroscopic methods,” *Appl. Surf. Sci.*, vol. 354, pp. 367–372, 2015.

[99] P. Papin. and R. T. Paine. M. T. Paffett, R.J. Simonson, “Borazine Adsorption and Decomposition at Pt(111) And Ru(Oo1) Surfaces,” *Surf. Sci.*, vol. 232, no. 3, pp. 286–296, 1990.

[100] Z. Cui, A. J. Oyer, A. J. Glover, H. C. Schniepp, and D. H. Adamson, “Large scale thermal exfoliation and functionalization of boron nitride,” *Small*, vol. 10, no. 12, pp. 2352–2355, 2014.

[101] B. Yu *et al.*, “Thermal exfoliation of hexagonal boron nitride for effective enhancements on thermal stability, flame retardancy and smoke suppression of epoxy resin nanocomposites: Via sol-gel process,” *J. Mater. Chem. A*, vol. 4, no. 19, pp. 7330–7340, 2016.

[102] W. A. Khan, “Polymer nanocomposites–synthesis techniques, classification and properties,” *Sci. Appl. Tailored Nanostructures, one Cent. Press*, pp. 50–67, 2016.

[103] M. Amin, “Methods for preparation of nano-composites for outdoor insulation applications,” *Rev. Adv. Mater. Sci.*, vol. 34, no. 2, pp. 173–184, 2013.

[104] V. Mittal, “Synthesis of Polymer Nanocomposites,” *Polymer (Guildf).*, pp. 1–26, 2015.

[105] M. Oliveira and A. V Machado, “Preparation of polymer-based nanocomposites by different routes,” *Nanocomposites Synth. Charact. Appl.*, pp. 1–22, 2013.

[106] M. Sadej, H. Gojzewski, P. Gajewski, G. J. Vancso, and E. Andrzejewska, "Photocurable acrylate-based composites with enhanced thermal conductivity containing boron and silicon nitrides," *Express Polym. Lett.*, vol. 12, no. 9, pp. 790–807, 2018.

[107] Y. Jiang, X. Shi, Y. Feng, S. Li, X. Zhou, and X. Xie, "Enhanced thermal conductivity and ideal dielectric properties of epoxy composites containing polymer modified hexagonal boron nitride," *Compos. Part A Appl. Sci. Manuf.*, vol. 107, pp. 657–664, 2018.

[108] A. Durmus and M. V. Kahraman, "Preparation and Characterization of Thermally Conductive Thermoplastic Polyurethane / h-BN Nanocomposites," *Polym. Compos.*, vol. 35, no. 3, pp. 530–538, 2014.

[109] Z. Zhu *et al.*, "Densely Packed Polymer / Boron Nitride Composite for Superior Anisotropic Thermal Conductivity," *Polym. Compos.*, vol. 39, no. S3, pp. E1653–E1658, 2018.

[110] M. Wang *et al.*, "Enhanced thermal conductivity of poly (vinylidene fluoride)/ boron nitride nanosheet composites at low filler content," *Compos. Part A Appl. Sci. Manuf.*, vol. 109, pp. 321–329, 2018.

[111] S. S. Ray and M. Okamoto, "Polymer / Layered Silicate Nanocomposites : a review from preparation to processing," *Prog. Polym. Sci.*, vol. 28, no. 11, pp. 1539–1641, 2003.

[112] S. Pavlidou and C. D. Papaspyrides, "A review on polymer-layered silicate nanocomposites," *Prog. Polym. Sci.*, vol. 33, no. 12, pp. 1119–1198, 2008.

[113] W. Zhou, J. Zuo, X. Zhang, and A. Zhou, “Thermal, electrical, and mechanical properties of hexagonal boron nitride-reinforced epoxy composites,” *J. Compos. Mater.*, vol. 48, no. 20, pp. 2517–2526, 2014.

[114] K. Sato, H. Horibe, T. Shirai, Y. Hotta, H. Nakano, and H. Nagai, “Thermally conductive composite films of hexagonal boron nitride and polyimide with affinity-enhanced interfaces,” *J. Mater. Chem.*, vol. 20, no. 14, pp. 2749–2752, 2010.

[115] Z. Kuang, Y. Chen, Y. Lu, L. Liu, S. Hu, and S. Wen, “Fabrication of Highly Oriented Hexagonal Boron Nitride Nanosheet / Elastomer Nanocomposites with High Thermal Conductivity,” *Small*, vol. 11, no. 14, pp. 1655–1659, 2015.

[116] T.-L. Li and S. L.-C. Hsu, “Enhanced thermal conductivity of polyimide films via a hybrid of micro-and nano-sized boron nitride,” *J. Phys. Chem. B*, vol. 114, no. 20, pp. 6825–6829, 2010.

[117] J. Fu, L. Shi, D. Zhang, Q. Zhong, and Y. Chen, “Effect of Nanoparticles on the Performane of Thermally Conductive Epoxy Adhesives,” *Polym. Eng. Sci.*, vol. 47, pp. 1809–1820, 2010.

[118] J. K. Wenying Zhou, Shuhua Qi, Chunchao Tu, Hongzhen Zhao, Caifeng Wang, “Effect of the Particle Size of Al2O3 on the Properties of Filled Heat-Conductive Silicone Rubber,” *J. Appl. Polym. Sci.*, vol. 104, no. 7, pp. 1312–1318, 2007.

[119] C. Liu, M. Chen, D. Zhou, D. Wu, and W. Yu, “Effect of Filler Shape on the Thermal Conductivity of Thermal Functional Composites,” *J. Nanomater.*, vol. 2017, 2017.

[120] I. A. Tsekmes, R. Kochetov, P. H. F. Morshuis, and J. J. Smit, "Thermal conductivity of polymeric composites: A review," *2013 IEEE Int. Conf. Solid Dielectr.*, pp. 678–681, 2013.

[121] L. Huang *et al.*, "Spherical and flake-like BN filled epoxy composites: morphological effect on the thermal conductivity, thermo-mechanical and dielectric properties," *J. Mater. Sci. Mater. Electron.*, vol. 26, no. 6, pp. 3564–3572, 2015.

[122] H. J. Ahn, S. H. Cha, W. S. Lee, and E. S. Kim, "Effects of amphiphilic agent on thermal conductivity of boron nitride/poly(vinyl butyral) composites," *Thermochim. Acta*, vol. 591, pp. 96–100, 2014.

[123] C. Yuan, B. Duan, L. Li, B. Xie, M. Huang, and X. Luo, "Thermal Conductivity of Polymer-Based Composites with Magnetic Aligned Hexagonal Boron Nitride Platelets," *ACS Appl. Mater. Interfaces*, vol. 7, no. 23, pp. 13000–13006, 2015.

[124] N. Sun *et al.*, "Hot-pressing induced orientation of boron nitride in polycarbonate composites with enhanced thermal conductivity," *Compos. Part A Appl. Sci. Manuf.*, vol. 110, pp. 45–52, 2018.

[125] M. Donnay, S. Tzavalas, and E. Logakis, "Boron nitride filled epoxy with improved thermal conductivity and dielectric breakdown strength," *Compos. Sci. Technol.*, vol. 110, pp. 152–158, 2015.

[126] A. Falin *et al.*, "nitride and the role of interlayer interactions," *Nat. Commun.*, vol. 8, pp. 1–9, 2017.

[127] X. Jiang *et al.*, "Journal of Materials Science & Technology Recent Progress on

Fabrications and Applications of Boron Nitride Nanomaterials : A Review," *J. Mater. Sci. Technol.*, vol. 31, no. 6, pp. 589–598, 2015.

[128] H. Y. Ng, X. Lu, and S. K. Lau, "Thermal conductivity, electrical resistivity, mechanical, and rheological properties of thermoplastic composites filled with boron nitride and carbon fiber," *Polym. Compos.*, vol. 26, no. 1, pp. 66–73, 2005.

[129] X. Cui, P. Ding, N. Zhuang, L. Shi, N. Song, and S. Tang, "Thermal Conductive and Mechanical Properties of Polymeric Composites Based on Solution-Exfoliated Boron Nitride and Graphene Nanosheets: A Morphology-Promoted Synergistic Effect," *ACS Appl. Mater. Interfaces*, vol. 7, no. 34, pp. 19068–19075, 2015.

[130] A. J. Peacock, *Handbook Of Polyethylene Structures, Properties, and Applications*. New York: Marcel Dekker, Inc., 2000.

[131] A. Graziano, S. Jaffer, and M. Sain, "Review on modification strategies of polyethylene / polypropylene immiscible thermoplastic polymer blends for enhancing their mechanical behavior," *J. Elastomers Plast.*, vol. 51, no. 4, pp. 291–336, 2018.

[132] X. Zhong, X. Zhao, Y. Qian, and Y. Zou, "Polyethylene plastic production process," *Insight - Mater. Sci.*, vol. 1, no. 1, pp. 1–11, 2018.

[133] P. N. Khanam and M. A. A. AlMaadeed, "Processing and characterization of polyethylene-based composites," *Adv. Manuf. Polym. Compos. Sci.*, vol. 1, no. 2, pp. 63–79, 2015.

[134] P. M. Visakh and M. J. Martínez Morlanes, "Characterization Methods for

Polyethylene-Based Composites and Nanocomposites," in *Polyethylene Based Blends, Composites, and Nanocomposities*, John Wiley & Sons, Incorporated, 2015, pp. 281–298.

[135] G. Wypych, "LDPE low density polyethylene," in *Handbook of Polymers*, 2nd ed., Toronto: Chem Tec, 2012, pp. 172–177.

[136] G. Wypych, "LLDPE linear low density polyethylene," in *Handbook of Polymers*, 2nd ed., Toronto: Chem Tec, 2012, pp. 178–183.

[137] G. Wypych, "HDPE high density polyethylene," in *Handbook of Polymers*, 2nd ed., Toronto: Chem Tec, 2012, pp. 150–156.

[138] F. Ren, P. Ren, Y. Di, D. Chen, and G. Liu, "Thermal , Mechanical and Electrical Properties of Linear Low-Density Polyethylene Composites Filled with Different Dimensional SiC Particles Thermal , Mechanical and Electrical Properties of Linear Low-Density Polyethylene Composites Filled with Different," *Polym. Plast. Technol. Eng.*, vol. 50, no. 8, pp. 791–796, 2011.

[139] S. N. Leung, "Thermally conductive polymer composites and nanocomposites : Processing- structure-property relationships," *Compos. Part B*, vol. 150, no. May, pp. 78–92, 2018.

[140] M. Kenny, S. E. Barbosa, R. E. Martini, S. La Tegola, and A. Terenzi, "Polyethylene-Based Nanocomposite Films : Structure / Properties Relationship," *Polym. Eng. Sci.*, vol. 54, no. 8, pp. 1931–1940, 2014.

[141] J. Jung *et al.*, "Preparations and thermal properties of micro- and nano-BN dispersed HDPE composites," *Thermochim. Acta*, vol. 499, no. 1–2, pp. 8–14,

2010.

[142] R. Ayoob, “Enhanced dielectric properties of polyethylene / hexagonal boron nitride nanocomposites,” *J. Mater. Sci.*, vol. 53, no. 5, pp. 3427–3442, 2018.

[143] X. Zhang, H. Wu, and S. Guo, “Effect of Interfacial Interaction on Morphology and Properties of Polyethylene / Boron Nitride Thermally Conductive Composites Effect of Interfacial Interaction on Morphology and Properties of Polyethylene / Boron Nitride Thermally Conductive Composites,” *LPTE*, vol. 54, no. 11, pp. 1097–1105, 2015.

[144] D. S. Muratov, A. A. Stepashkin, S. M. Anshin, and D. V Kuznetsov, “Controlling thermal conductivity of high density polyethylene fi lled with modi fi ed hexagonal boron nitride (hBN),” *J. Alloys Compd.*, vol. 735, pp. 1200–1205, 2018.

[145] J. Li *et al.*, “Microstructure evolution effect on high-temperature thermal conductivity of LDPE / BNNS investigated by in-situ SAXS,” *Mater. Lett.*, vol. 234, pp. 74–78, 2019.

[146] E. Chan, S. N. Leung, M. O. Khan, H. Naguib, F. Dawson, and V. Adinkrah, “Fabrication and characterization of thermoplastics composites with enhanced multifunctional properties,” *J. Thermoplast. Compos. Mater.*, vol. 27, no. 4, pp. 541–557, 2014.

[147] H. Ding, Y. Guo, and S. N. Leung, “Development of thermally conductive polymer matrix composites by foaming-assisted networking of micron- and submicron-scale hexagonal boron nitride,” *J. Appl. Polym. Sci.*, vol. 133, no. 4,

pp. 42910–412911, 2016.

[148] J. Ding, H. Zhao, and H. Yu, “High-yield synthesis of extremely high concentrated and few-layered boron nitride nanosheet dispersions High-yield synthesis of extremely high concentrated and few-layered boron nitride nanosheet dispersions,” *2D Mater.*, vol. 5, no. 4, pp. 045015–045021, 2018.

[149] V. N. Mochalin, D. Liu, S. Qin, Y. Gogotsi, W. Lei, and Y. Chen, “Boron nitride colloidal solutions, ultralight aerogels and freestanding membranes through one-step exfoliation and functionalization,” *Nat. Commun.*, vol. 6, pp. 1–8, 2015.

[150] J. Y. Huang, H. Yasuda, and H. Mori, “HRTEM and EELS Studies on the Amorphization of Hexagonal Boron Nitride Induced by Ball Milling,” *J. Am. Ceram. Soc.*, vol. 83, no. 2, pp. 403–409, 2000.

[151] J. O. Cross, R. L. Opila, I. W. Boyd, and E. N. Kaufmann, “Materials characterization and the evolution of materials,” *MRS Bull.*, vol. 40, no. 12, pp. 1019–1034, 2015.

[152] R. B. Prime *et al.*, “Thermogravimetric Analysis (TGA),” in *Thermal Analysis of Polymers*, J. D. Menczel, A. Laboratories, F. W. TX, R. B. Prime, and C. San Jose, Eds. Hoboken, New Jersey: John Wiley & Sons, Inc., 2009, pp. 250–317.

[153] H. Bhadeshia, “Differential scanning calorimetry,” *Methods Mol. Biol.*, vol. 40, pp. 191–218, 1995.

[154] D. Zhao, X. Qian, X. Gu, S. A. Jajja, and R. Yang, “Measurement Techniques for Thermal Conductivity and Interfacial Thermal Conductance of Bulk and Thin

Film Materials," *J. Electron. Packag.*, vol. 138, no. 4, pp. 040802–040820, 2016.

[155] S. Oswald, "X-ray Photoelectron Spectroscopy in Analysis of Surfaces," in *Encyclopedia of Analytical Chemistry*, American Cancer Society, 2013, pp. 1–49.

[156] S. Ebnesajjad, "Chapter 4 - Surface and Material Characterization Techniques," in *Surface Treatment of Materials for Adhesive Bonding (Second Edition)*, Second Edition., S. Ebnesajjad, Ed. Oxford: William Andrew Publishing, 2014, pp. 39–75.

[157] A. A. Bunaciu, E. gabriela Udriştioiu, and H. Y. Aboul-Enein, "X-Ray Diffraction: Instrumentation and Applications," *Crit. Rev. Anal. Chem.*, vol. 45, no. 4, pp. 289–299, 2015.

[158] J. I. Langford and A. J. C. Wilson, "Scherrer after sixty years: A survey and some new results in the determination of crystallite size," *J. Appl. Crystallogr.*, vol. 11, no. 2, pp. 102–113, 2002.

[159] A. Monshi, M. R. Foroughi, and M. R. Monshi, "Modified Scherrer Equation to Estimate More Accurately Nano-Crystallite Size Using XRD," *World J. Nano Sci. Eng.*, vol. 02, no. 03, pp. 154–160, 2012.

[160] O. P. Choudhary and Priyanka, "Scanning Electron Microscope: Advantages and Disadvantages in Imaging Components," *Int. J. Curr. Microbiol. Appl. Sci.*, vol. 6, no. 5, 2017.

[161] K. Akhtar, S. A. Khan, and S. B. Khan, "Scanning Electron Microscopy : Principle and Applications in Nanomaterials Scanning Electron Microscopy : Principle and Applications in Nanomaterials Characterization," in *Handbook of*

Materials Characterization, S. K. Sharma, Ed. Cham: Springer International Publishing, 2019, pp. 113–145.

[162] Priyanka and O. P. Choudhary, "Uses of Transmission Electron Microscope in Microscopy and its Advantages and Disadvantages," vol. 7, no. 05, pp. 743–747, 2018.

[163] T. Walther, "Transmission Electron Microscopy of Nanostructures," in *Microscopy Methods in Nanomaterials Characterization*, R. K. M. Sabu Thomas, Raju Thomas, Ajesh K. Zachariah, Ed. Elsevier, 2017, pp. 105–134.

[164] R. Jagtap and A. Ambre, "Atomic force microscopy (AFM): Basics and its important applications for polymer characterization : An overview Overview literature on atomic force microscopy (AFM): Basics and its important applications for polymer characterization," *Indian J. Eng. Mater. Sci.*, vol. 13, pp. 368–384, 2006.

[165] S. Ryu, K. Kim, and J. Kim, "Silane surface treatment of boron nitride to improve the thermal conductivity of polyethylene naphthalate requiring high temperature molding," *Polym. Compos.*, vol. 39, pp. E1692–E1700, 2018.

[166] P. S. Nikola Slepickova Kasalkova and Z. K. and V. Svorcik, "Wettability and Other Surface Properties of Modified Polymers," *InTech Open Sci.*, 2015.

[167] J. Cui and Y. Cui, "Effects of Surface Wettability and Roughness on the Heat Transfer Performance of Fluid Flowing through Microchannels," *Energies*, vol. 8, no. 6, pp. 5704–5724, 2015.

[168] C. Choi and M. Kim, "Wettability Effects on Heat Transfer," in *Two Phase Flow,*

Phase Change and Numerical Modeling, A. Ahsan, Ed. Intech, 2011, pp. 312–340.

[169] M. Edalatpour, L. Liu, A. M. Jacobi, K. F. Eid, and A. D. Sommers, "Managing water on heat transfer surfaces : A critical review of techniques to modify surface wettability for applications with condensation or evaporation Managing water on heat transfer surfaces : A critical review of techniques to modify surface wettability for applications with condensation or evaporation," *Appl. Energy*, vol. 222, no. May, pp. 967–992, 2018.

[170] N. Encinas, J. Abenojar, and M. A. Martínez, "Surface & Coatings Technology Extreme durability of wettability changes on polyole fi n surfaces by atmospheric pressure plasma torch," *Surf. Coat. Technol.*, vol. 205, no. 2, pp. 396–402, 2010.

[171] R. K. a and S. T. O. Shoichiro Namba, Atsushi Takagaki, Keiko Jimura, Shigenobu Hayashi, "Effects of ball-milling treatment on physicochemical properties and solid base activity of hexagonal boron nitrides," *Catal. Sci. Technol.*, vol. 9, no. 2, pp. 302–309, 2019.

[172] D. G. Ortiz, C. Pochat-bohatier, J. Cambedouzou, M. Bechelany, and P. Miele, "Exfoliation of Hexagonal Boron Nitride (h-BN) in Liquide Phase by Ion Intercalation," *Nanomaterials*, vol. 8, no. 9, pp. 716–727, 2018.

[173] O. Y. Posudievsky, O. A. Khazieieva, V. V Cherepanov, G. I. Dovbeshko, V. G. K. And, and V. D. Pokhodenkoa, "Efficient dispersant-free liquid exfoliation down to the graphene-like state of solvent-free mechanochemically delaminated bulk hexagonal boron nitride," *RSC Adv.*, vol. 6, no. 52, pp. 47112–47119, 2016.

[174] J. Sahu, K. Panda, B. Gupta, and N. Kumar, “Enhanced tribo-chemical properties of oxygen functionalized mechanically exfoliated hexagonal boron nitride nanolubricant additives,” *Mater. Chem. Phys.*, vol. 207, pp. 412–422, 2018.

[175] E. Evin, M. Aksoy, E.Evin, and Ö. Guler, “The effect of milling parameters on synthesis of high yield boron nitride nanotube,” *Journals Optoelectron. Adv. Mater.*, vol. 16, no. 7–8, pp. 831–836, 2014.

[176] E. Evin, V. Selen, S. H. Guler, V. Selen, S. Yardimici, and A. Keles, “Synthesis of C-BN Hybride Nano Structures,” *J. Optoeletronics Adv. Mater.*, vol. 17, no. 5–6, pp. 795–798, 2015.

[177] Abhinav K, Venkata and Rao R, Venkata Krishna and Karthik, P. S. and Singh, Surya Prakash, “Copper Conductive Inks : Synthesis and Utilization in Flexible Electronics,” *RSC Adv.*, vol. 5, pp. 63985–64030, 2015.

[178] M. Shafiq, T. Yasin, and S. Saeed, “Synthesis and Characterization of Linear Low- Density Polyethylene / Sepiolite Nanocomposites Synthesis and Characterization of Linear Low-Density Polyethylene / Sepiolite Nanocomposites,” *J. Appl. Polym. Sci.*, vol. 123, pp. 1718–1723, 2012.

[179] L. Li, Y. I. Chen, and H. Zhang, “Large-scale mechanical peeling of boron nitride nanosheets by low-energy ball milling,” *J. Mater. Chem.*, vol. 21, pp. 11862–11866, 2011.

[180] T. Zhao and X. Zhang, “Enhanced Thermal Conductivity of PE / BN Composites Through Controlling Crystallization Behavior of PE Matrix,” *Polym. Compos.*, vol. 38, no. 12, pp. 2806–2813, 2017.

[181] S. Yang, Y. Huang, J. Lei, L. Zhu, and Z. Li, “Composites : Part A Enhanced thermal conductivity of polyethylene / boron nitride multilayer sheets through annealing,” *Compos. Part A*, vol. 107, pp. 135–143, 2018.

[182] K. Kim and J. Kim, “Core-shell structured BN / PPS composite fi lm for high thermal conductivity with low filler concentration,” *Compos. Sci. Technol.*, vol. 134, pp. 209–216, 2016.

[183] D. R. Cooper *et al.*, “Experimental Review of Graphene,” *ISRN Condens. Matter Phys.*, vol. 2012, pp. 1–56, 2012.

[184] G. A. Slack, L. J. Schowalter, D. Morelli, and J. A. Freitas, “Some effects of oxygen impurities on AlN and GaN,” *J. Cryst. Growth*, vol. 246, pp. 287–298, 2002.

[185] M. Tanimoto, T. Yamagata, K. Miyata, and S. Ando, “Anisotropic Thermal Di ff usivity of Hexagonal Boron Nitride-Filled Polyimide Films: Effects of Filler Particle Size, Aggregation, Orientation, and Polymer Chain Rigidity,” *ACS*, vol. 5, pp. 4374–4382, 2013.

[186] M. H. Alaei *et al.*, “Effect of particle size on thermomechanical properties of particulate polymer composite,” *Iran. Polym. J.*, vol. 22, no. 11, pp. 853–863, 2013.

[187] S. Riaz and S. Park, “Thermal and Mechanical Interfacial Behaviors of Graphene Oxide-Reinforced Epoxy Composites Cured by Thermal Latent Catalyst,” *Materials (Basel).*, vol. 12, pp. 1354–1357, 2019.

[188] T. Soitong, “Mechanical and thermal properties of hemp fiber reinforced high

density polyethylene composites," *Key Eng. Mater.*, vol. 659, pp. 441–445, 2015.

[189] M. Xu, G. Huang, S. Feng, G. J. Mcshane, and W. J. Stronge, "Static and Dynamic Properties of Semi-Crystalline Polyethylene," *Polymers (Basel).*, vol. 8, no. 4, pp. 77–90, 2016.

[190] D. J. A. Senden, "Strain hardening and anisotropy in solid polymers Strain Hardening and Anisotropy in Solid Polymers," Ph.D dissertation, Eindhoevn University of Technology, Eindhoevn, 2013. Accesed on: September 10, 2019. [Online]. Available: https://research.tue.nl/en/publications/strain-hardening-and-anisotropy-in-solid-polymers.

[191] R. N. Haward, "Strain Hardening of High Density Polyethylene," *J. Polym. Sci. Part B Polym. Phys.*, vol. 45, no. 9, pp. 1090–1099, 2007.

[192] W. Cheewawuttipong, D. Fuoka, S. Tanoue, H. Uematsu, and Y. Iemoto, "Thermal and Mechanical Properties of Polypropylene / Boron Nitride Composites," *Energy Procedia*, vol. 34, pp. 808–817, 2013.

[193] J. Zahirifar, A. Hadi, J. Karimi-sabet, and A. Dastbaz, "Influence of hexagonal boron nitride nanosheets as the additives on the characteristics and performance of PVDF for air gap membrane distillation Influence of hexagonal boron nitride nanosheets as the additives on the characteristics and performance of ," *Desalination*, vol. 460, pp. 81–91, 2019.

[194] L. Chen *et al.*, "Thermal Conductivity Performance of Polypropylene Composites Filled with Polydopamine-Functionalized Hexagonal Boron Nitride," *PLoS One*, vol. 12, no. 1, pp. 1–16, 2017.

[195] K. Wattanakul, H. Manuspiya, and N. Yanumet, “Effective Surface Treatments for Enhancing the Thermal Conductivity of BN-Filled Epoxy Composite,” *J. Appl. Polym. Sci.*, vol. 119, pp. 3234–3243, 2010.

[196] X. Wang, Y. Yang, G. Jiang, Z. Yuan, and S. Yuan, “A facile synthesis of boron nitride nanosheets and their potential application in dye adsorption,” *Diam. Relat. Mater.*, vol. 81, pp. 89–95, 2018.

[197] P. K. Ojha, R. Maji, and S. Karmakar, “Effect of crystallinity on droplet regression and disruptive burning characteristics of nanofuel droplets containing amorphous and crystalline boron nanoparticles Effect of crystallinity on droplet regression and disruptive burning characteristics of nano,” *Combust. Flame*, vol. 188, pp. 412–427, 2017.

[198] B. H. Tran, K. Tieu, S. Wan, and H. Zhu, “Understanding the tribological impacts of alkali element on lubrication of binary borate melt †,” *RSC Adv.*, vol. 8, pp. 28847–28860, 2018.

[199] O. M. Moon, B. Kang, S. Lee, and J. Boo, “Temperature effect on structural properties of boron oxide thin films deposited by MOCVD method,” *Thin Solid Films*, vol. 464–465, pp. 164–169, 2004.

APPENDIX A

h-BN Exfoliation

Liquid Exfoliation

Liquid exfoliation was done using (a) bath and (b) probe sonicators. (a) Pristine h-BN6 was mixed with several solvents, such as IPA, DMF, MEA, NMP, and DI water, at a ratio of 2.5 mg/ml. Afterwards, the mixture was sonicated for 24 hours in an ultrasonic bath sonicator (Branson 5210), see Fig. A. (1). The bath solution (water) was replaced every 90 min, and the maximum bath temperature was held at 50 ℃. Then, the mixture was centrifuged for 5 min in a SIGMA 3-18KS centrifuge using 12159-H rotor. Finally, the supernatant was collected by a vacuum filtration and dried overnight in a vacuum oven at 100 ℃. (b) Pristine h-BN was mixed with several solvent at a ratio of 4 mg/ml and sonicated in a probe sonicator (Q700 Qsonica Sonicator) for 90 min, see Fig. A. (2). The sonication was done in an interval of 2 min on and 1 min off pulses, and the maximum temperature was held at 50 ℃. Then, the mixture was centrifuged at 1500 rpm for 5 min in a SIGMA 3-18KS centrifuge using 12159-H rotor. Finally, the supernatant was collected by a vacuum filtration and dried overnight in a vacuum oven at 100 ℃.

Fig. A. 1: Branson 5210 Bath Sonicator.

Fig. A. 2: Q700 Qsonica Sonicator Probe Sonicator.

Thermal Exfoliation

Thermal Exfoliation was done using Thermolyne muffle furnace (Thermo SCIENTIFIC), see Fig. A. (3). h-BN was heated at a temperature of 1000 °C and a heating rate of 50 °C/ min for 1 hour, 3 hours, and 5 hours. Afterwards, h-BN was mixed with water (4 mg/ml) and dispersed in a bath sonicator. Afterward, the mixture was centrifuged at 3500 rpm for 5 minutes in SIGMA 3-18KS centrifuge (11180 rotor). The supernatant was collected, dried, and prepared for characterization.

Fig. A. 3: Thermolyne Muffle Furnace (Thermo SCIENTIFIC).

Liquid Exfoliation Results and Discussion

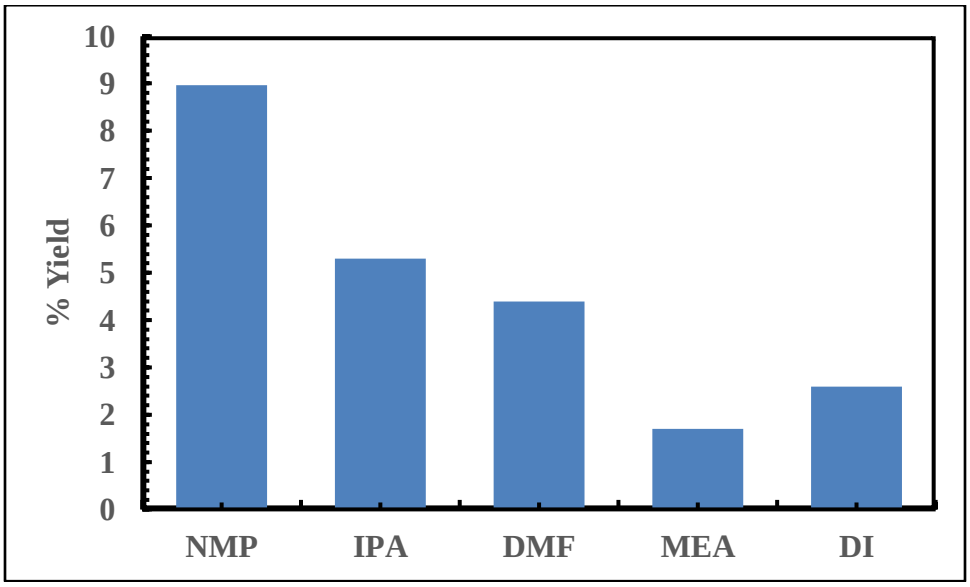

Fig. A. 4: Yield of h-BNNS prepared by liquid Exfoliation (Probe Sonicator).

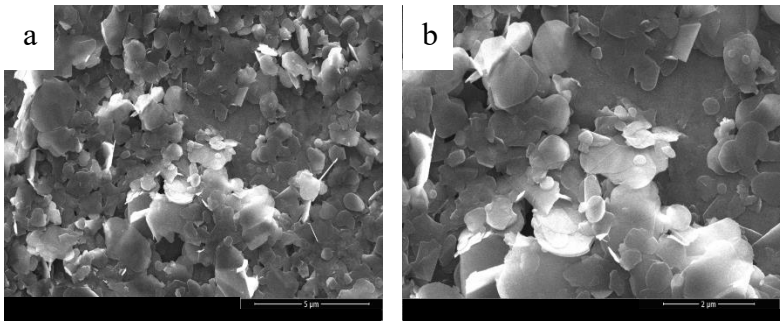

Fig. A. 5: SEM images of h-BN exfoliated in NMP solvents.

Fig. A. 4 displays the yield of h-BNNS prepared using several solvents. As was expected, the h-BNNS yield from the liquid exfoliation method was low, i.e. less than 10 %, which is the usual case of liquid exfoliation [75][196]. NMP solvent demonstrated the highest yield of ~ 9 %, followed by IPA ~ 5.3 % and then DMF ~ 4.4%. Meanwhile, MEA and DI water showed very low yields. Fig. A. 5 shows the SEM images of h-BNNS

exfoliated by NMP solvent. The image shows h-BNNS agglomerates with particle sizes varying from nanometers to less than ~ 5 um. Compared to the BM method, liquid exfoliation produced h-BNNS with bigger particle sizes and less defects. However, the yield of h-BNNS was comparatively very low making their utilization in a large scale for nanocomposites fabrication impractical.

Thermal Exfoliation Results and Discussion

Table. A.1 shows the yield (supernatant) and the percent of weight increased due to the thermal treatment. The weight of h-BN showed functionality with the thermal treatment time. For instance the weight of h-BN increased by 10.6 %, 22.1 %, and 25.6 % at 1, 2, and 3 h, respectively. The increase in mass was caused by the addition of oxygen group, i.e. h-BN oxidize at ~ 800 ℃ [76][100][101].

Table. A. 1: Thermal treatment of h-BN at 1000 ℃.

Heating time (h)	Weight Increase (%)	Yield (%)
1	10.6	10
2	22.1	25
3	25.6	70

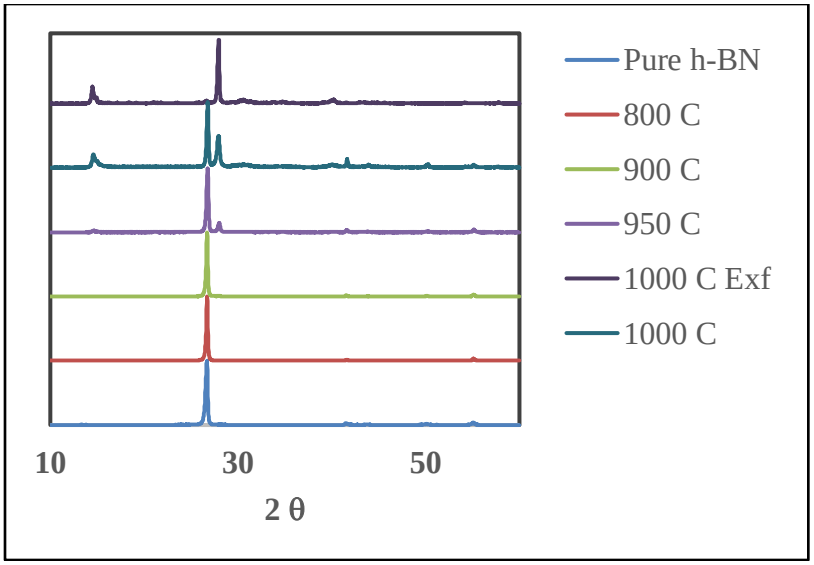

Fig. A. 6: XRD patterns of h-BN heated for 5 hours at various temperature. Where 'Exf' represents supernatant.

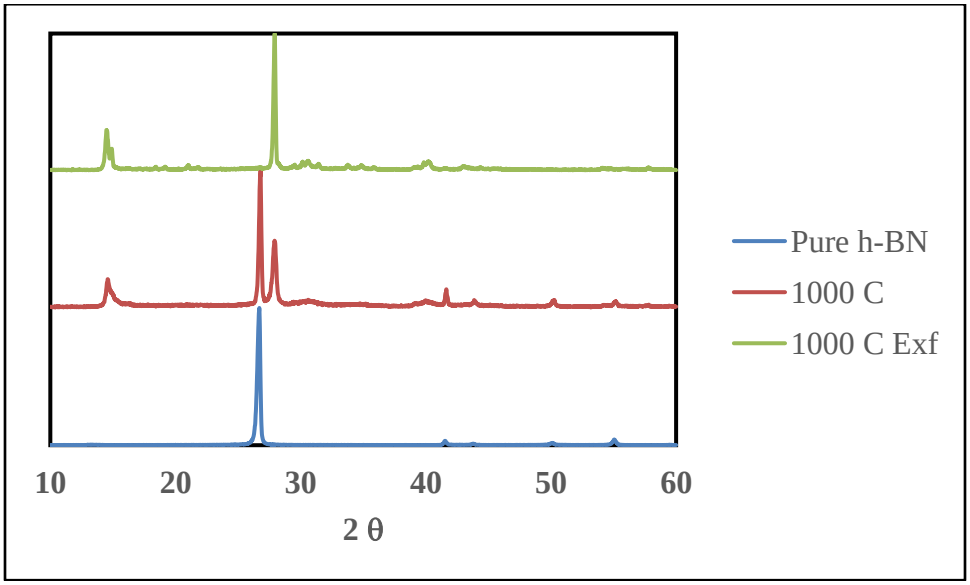

Fig. A. 7: XRD patterns of h-BN thermally treated at 1000 ℃ for 5 hours. Where 'Exf' represents supernatant.

Fig. A. 6 shows the XRD spectra of thermal treated h-BN at several temperatures.

The pure h-BN and the h-BN treated at 800 ℃ and 900℃ manifested no change, implying

no or low h-BN oxidation. Whereas, the h-BN treated at 950 ℃ and 1000 ℃ exhibited two more peaks, in addition to the bulk h-BN XRD peaks, at 2θ values of 14.6º and 28º which were assigned to the oxidation product. Fig. A. 7 shows the XRD spectra of pure h-BN, the h-BN treated at 1000 ℃ before and after the separation of the h-BN supernatant. As above, treated h-BN displayed two peaks in addition to the pure h-BN peaks. However, the pure h-BN peaks disappeared in the supernatant. Thus, the two new peaks, at 2θ values of 14.6º and 28º, were related with the XRD peaks of boron trioxide (B_2O_3) [197][198][199]. B_2O_3 is a common oxidation product of h-BN. Fig. A. 8 shows the XRD spectra of h-BN treated at 1000 ℃ for 1 h, 3h, and 5h. As in the 5h treatment, the two peaks were also present at 1h and 3h thermal treatments with the absence of pure h-BN peaks, indicating that the oxidation product was only B_2O_3. Table. A. 2 summarizes the atomic concentration of the pure h-BN and of the thermally treated h-BN before and after separating the h-BN supernatant. The pure h-BN consisted of approximately equal number of boron and nitrogen making their ratio ~ 1. After the 3h of thermal treatment this ratio increased to ~ 1.6, i.e. the percent of nitrogen reduced significantly while that of boron decreased marginally, suggesting the evaporation of nitrogen oxides. In addition, the percent of oxygen increased from 2.26 % to 25.6 % as a result of the thermal oxidation. The h-BN supernatant showed a huge decline in the nitrogen concentration, where the ratio of boron to nitrogen reached 6.7. Moreover, the oxygen concentration increased to 52.52 %. At 3h, the ratio of oxygen to boron was ~ 1.6, which is very close to the ratio of oxygen to boron (1.5) in B_2O_3. Finally, the supernatant was heated to 200 ℃, and then to 450 ℃. There was no change at 200 ℃, above the melting point of boric acid (170.9 ℃),

eliminating the presence of boric acid. However, at 450 °C, which is the melting point of B_2O_3, the supernatant melted, as shown in Fig. A. 8. This prove that at the followed experimental conditions h-BN oxidize to B_2O_3 but does not exfoliate.

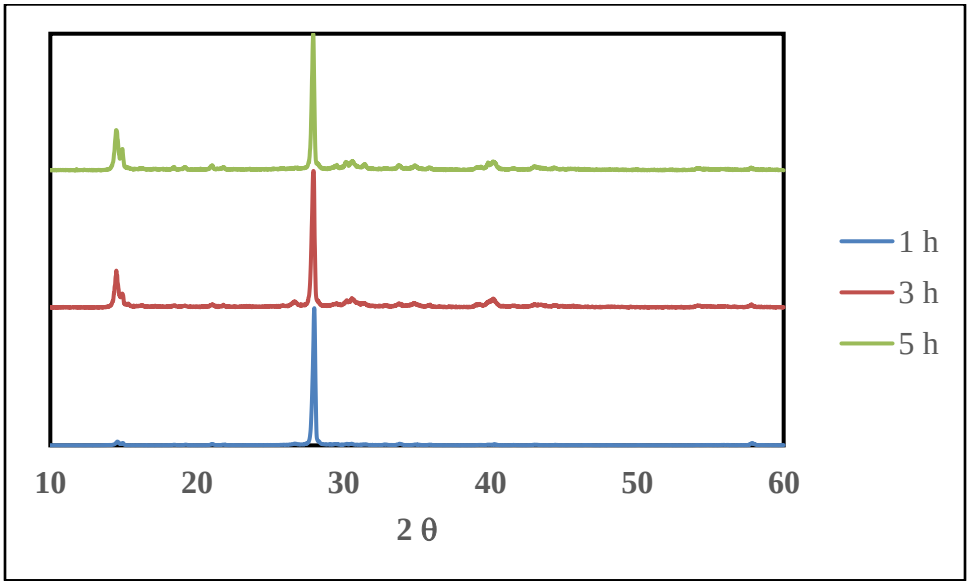

Fig. A. 8: XRD pattern of the h-BN (supernatant) thermally treated at 1000 °C for various hours.

Table. A. 2: Atomic concentration of pure h-BN and of the thermally treated (1000 °C) h-BN before and after separating the supernatant. Where the 'Exf' means the h-BN supernatant.

Atomic concentration (%)	0 h	3-h	3-h-Exf	5-h-Exf
Carbon	4.06	5.8	9.17	8.43
Oxygen	2.26	25.6	52.52	54.83
Nitrogen	45.2	26.56	4.99	2.73
Boron	48.48	42.05	33.32	34.01

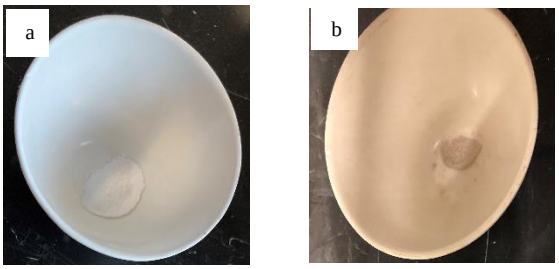

Fig. A. 9: B_2O_3 before (a) and after (b) melting.

APPENDIX B

Composites

XRD Analysis

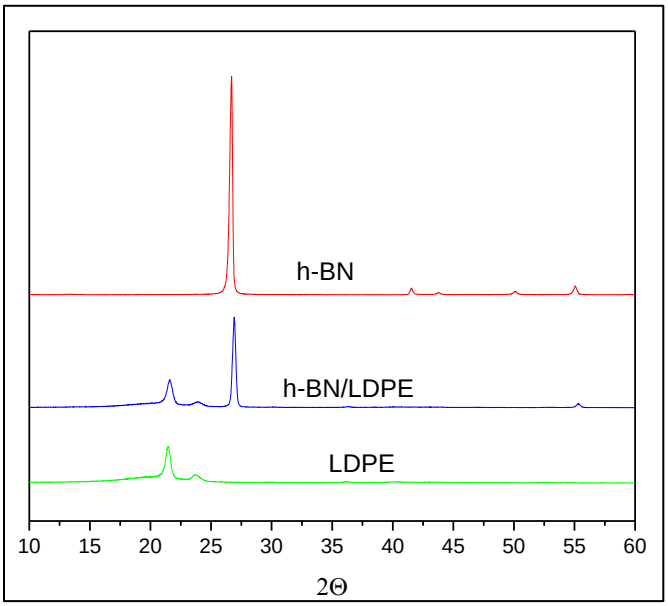

Fig. B. 1: XRD spectra of LDPE, h-BN, and h-BN/LDPE composite.

SEM Analysis

Composites Fabrication Methods

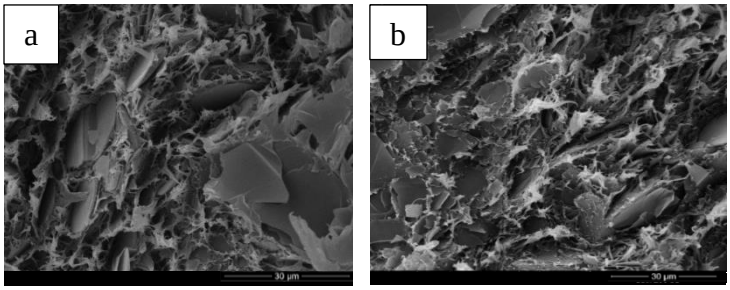

Fig. B. 2: SEM images of 30.4 vol. % h-BN35/LLDPE prepared by (a) MB method and (b) BM method.

Sheet Thickness

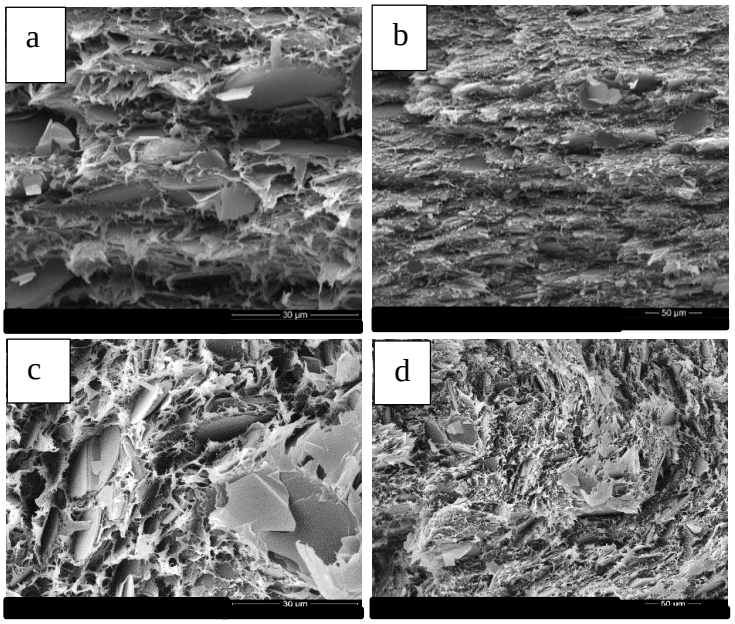

Fig. B. 3: SEM images of 30.4 vol. % h-BN35/LLDPE composites prepared by MB method. (a and b) 0.5 mm thick samples and (c and d) 2 mm thick samples.

Effect of Exfoliation and Defect Mitigation

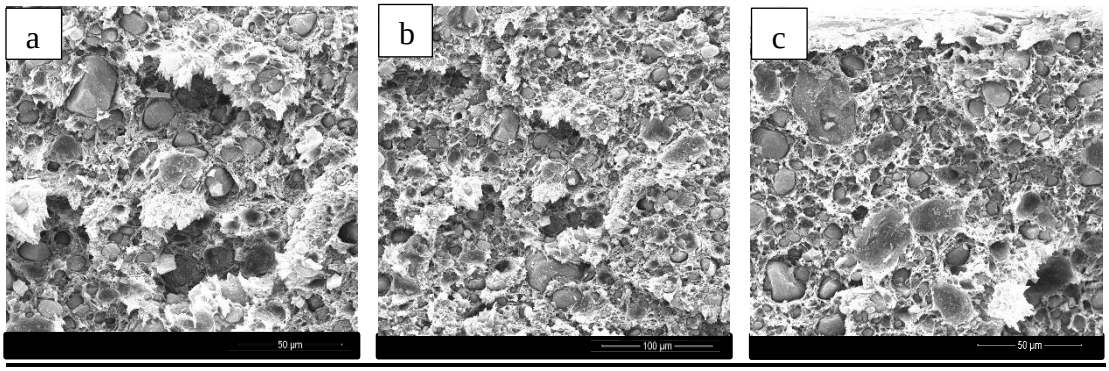

Fig. B. 4: SEM images of 30.4 vol. % BMd-h-BN35/LLDPE composites. Specimen center (a) and (b) and Specimen edge (c)

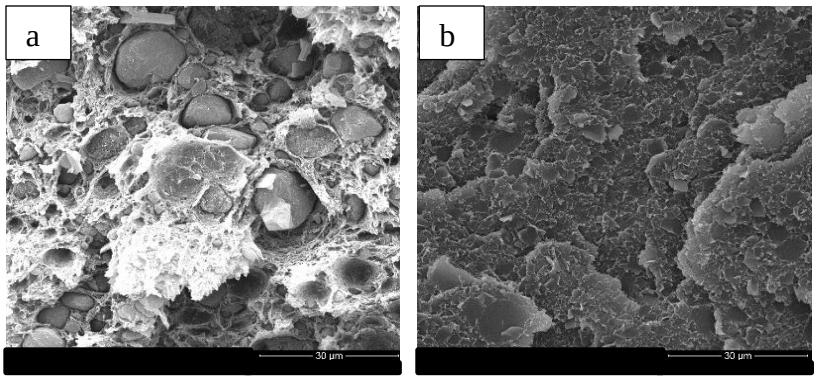

Fig. B. 5: SEM images of 30.4 vol. % h-BN35/LLDPE prepared by MB method; where the h-BN was subjected to BM treatment. (a) h-BN35 BMd for 90 min and (b) 80%h-BN35 BMd for 90 min.

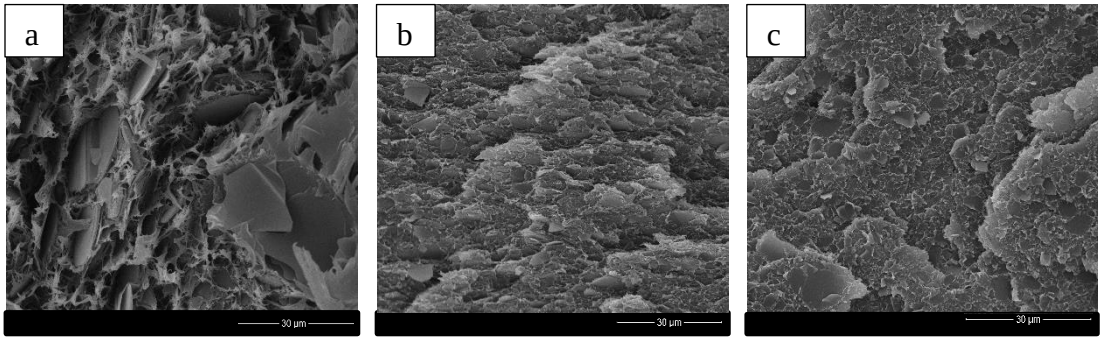

Fig. B. 6: SEM images of 30.4 vol. % 80%h-BN35/LLDPE composites in which h-BN was BMd with PE powder prior to the composite fabrications at various milling time. (a) 0 h, (b) 45 min, and (c) 90 min.

Effect of Specimen Thickness and h-BN Alignment

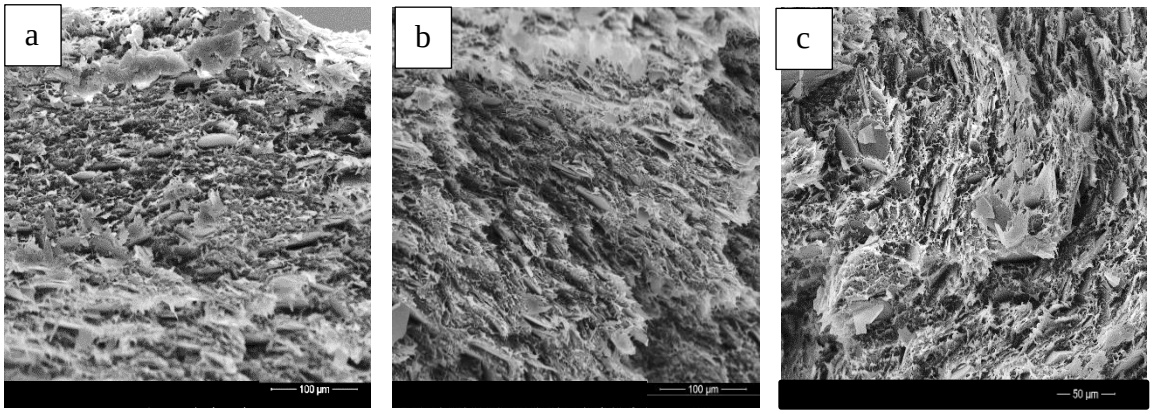

Fig. B. 7: SEM images of 30.4 vol. % h-BN35/LLDPE with specimen thickness of 2 mm at different location starting from the edge to the middle of the specimen. (a) Edge, (b) Intermediate, and (c) Middle.

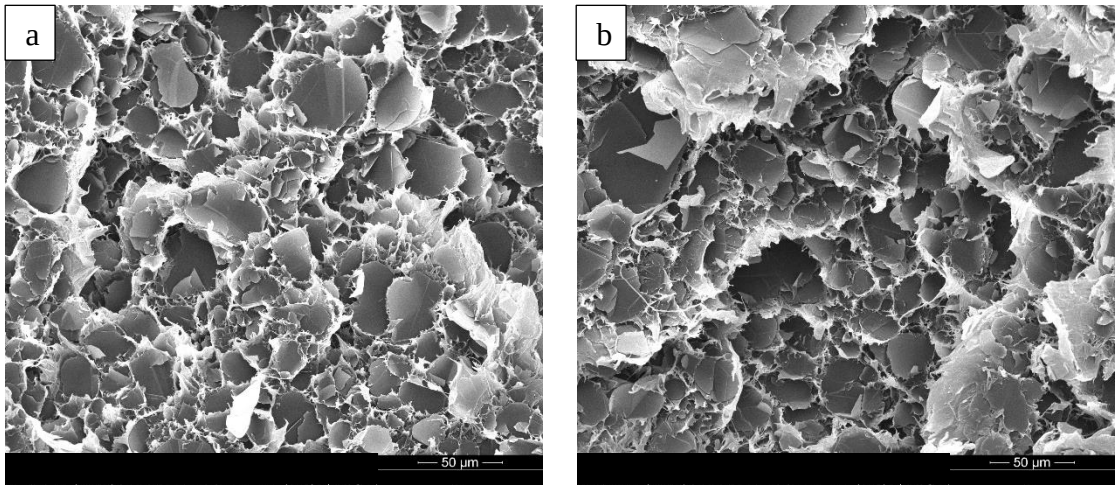

Fig. B. 8: SEM images of 22.5 vol. % h-BN35/LLDPE (cross-section) with specimen thickness of 2 mm. (a) Middle of the specimen and (b) Edge of the specimen.

Thermal Analysis

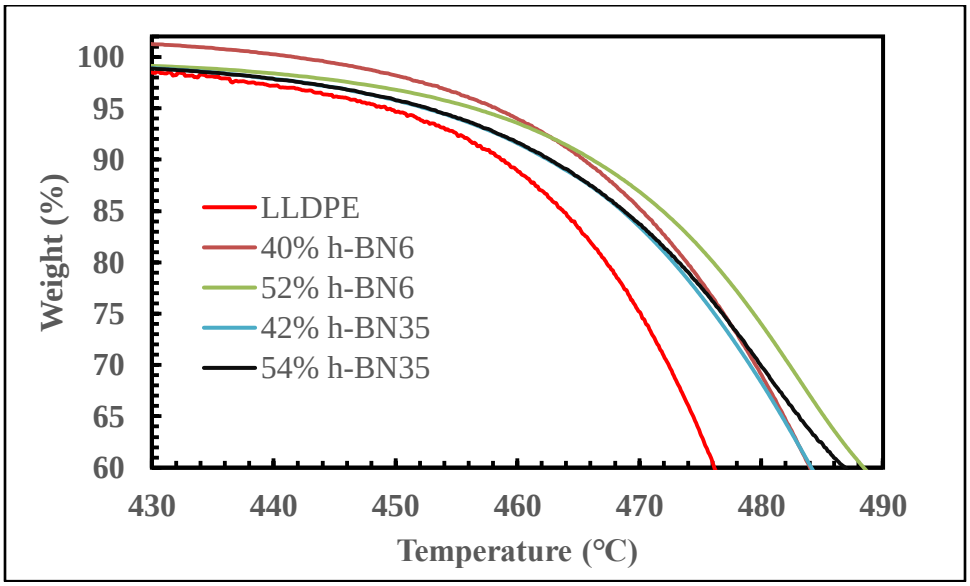

Fig. B. 9: Zoomed TGA curves of h-BN6 and h-BN35/LLDPE composites of various h-BN loading (wt. %).

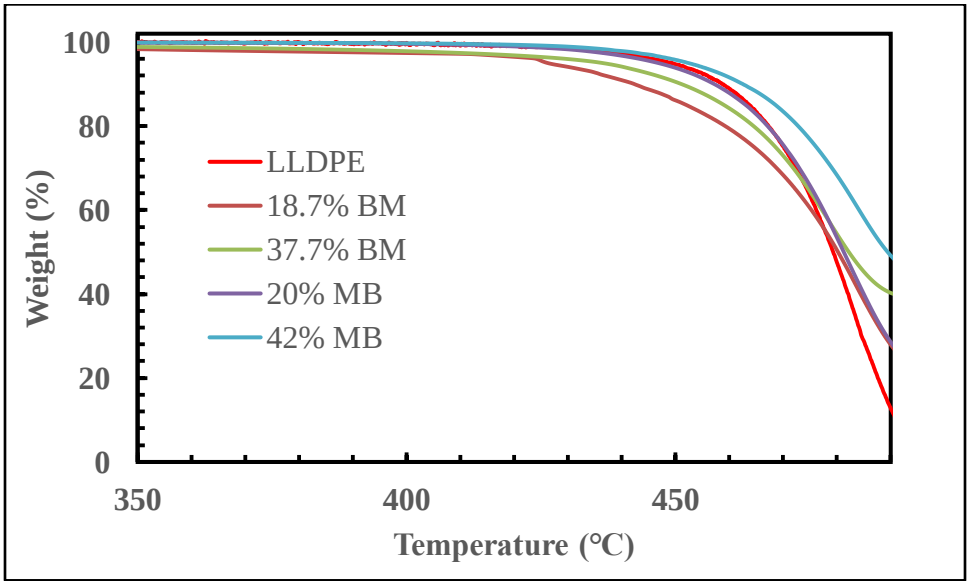

Fig. B. 10: Zoomed TGA curves of h-BN35/LLDPE composites, prepared by MB and BM methods, of several h-BN loading (wt. %).

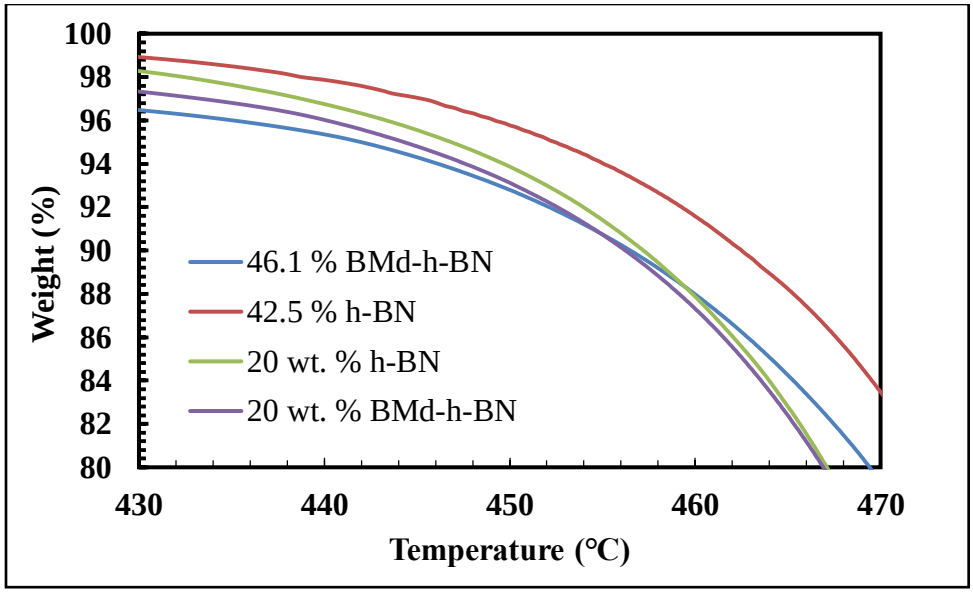

Fig. B. 11: Zoomed TGA curves of h-BN35 and BMd-h-BN35/LLDPE composites of different h-BN loading (wt. %).

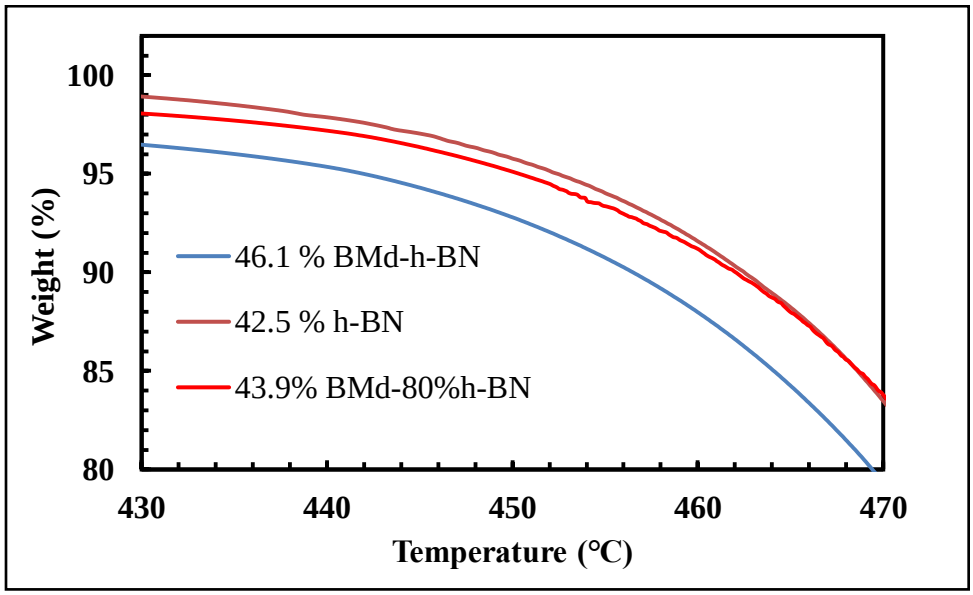

Fig. B. 12: Zoomed TGA curves of h-BN35, BMd-h-BN35, and BMd-80%h-BN35/LLDPE composites of different h-BN loading (wt. %).

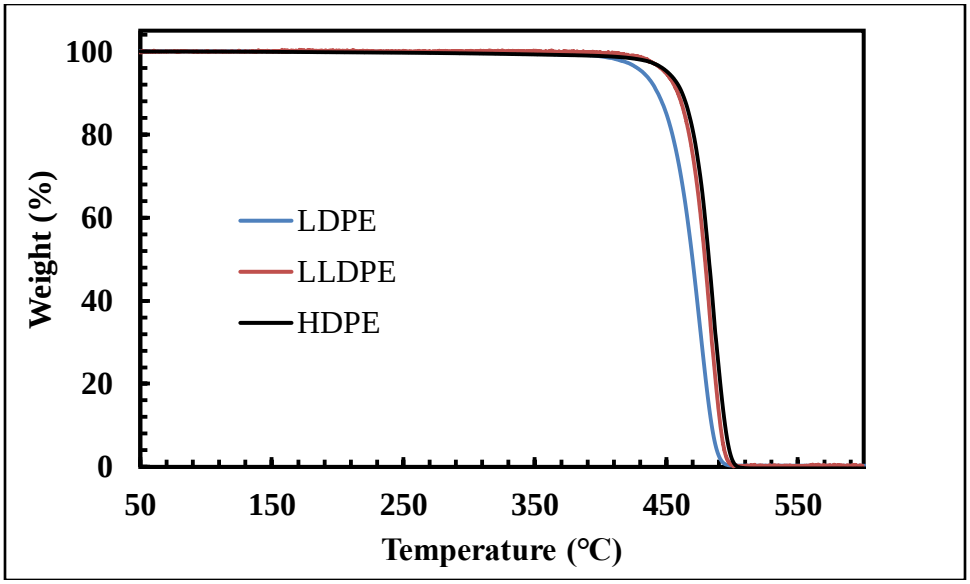

Fig. B. 13: TGA curves of LDPE, LLDPE, and HDPE.

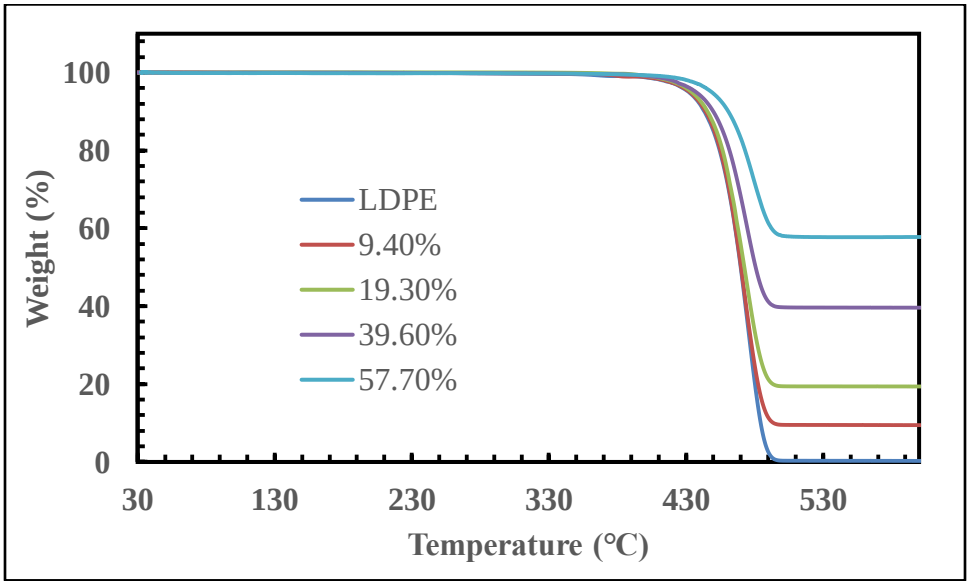

Fig. B. 14: TGA curves of h-BN35/LDPE composites of different h-BN loading (wt. %).

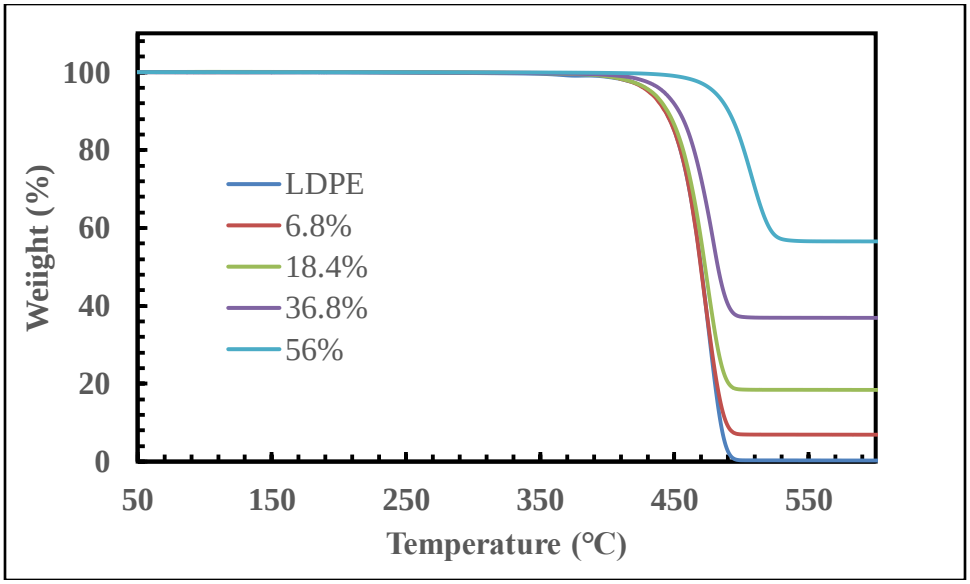

Fig. B. 15: TGA curves of h-BN6/LDPE composites of different h-BN loading (wt. %).

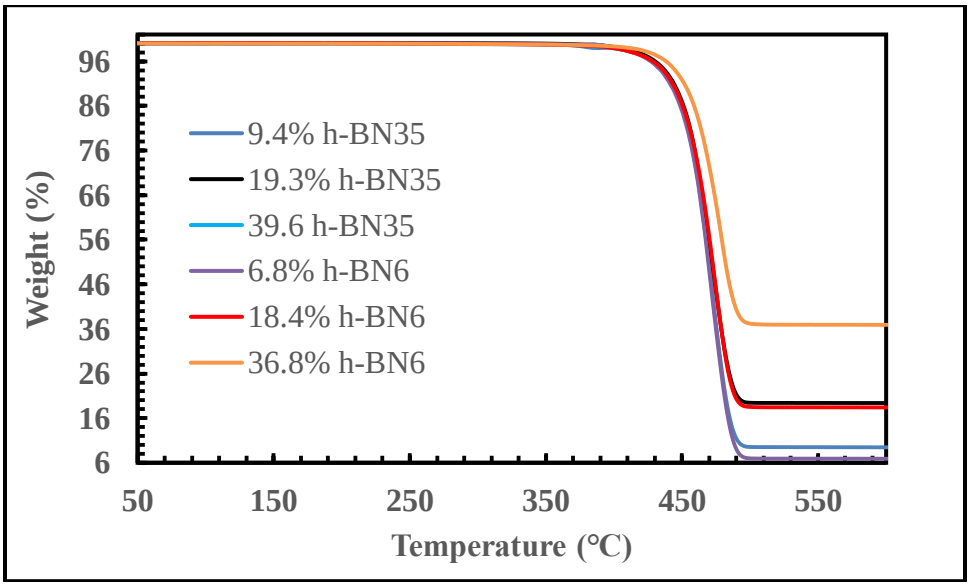

Fig. B. 16: TGA curves of h-BN6/LDPE and h-BN35/LDPE composites of several h-BN loading (wt. %).

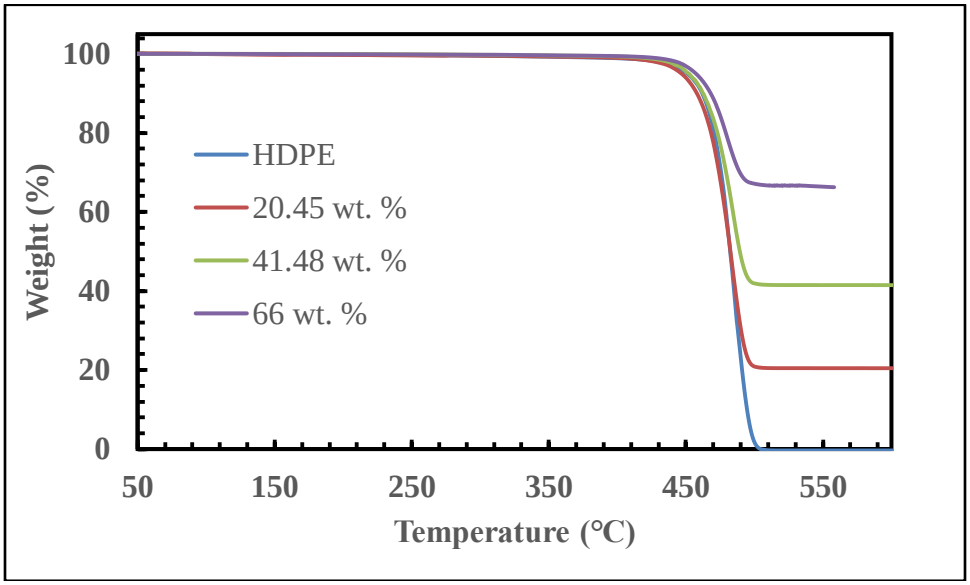

Fig. B. 17: TGA curves of h-BN35/HDPE composites of several h-BN loading (wt. %).

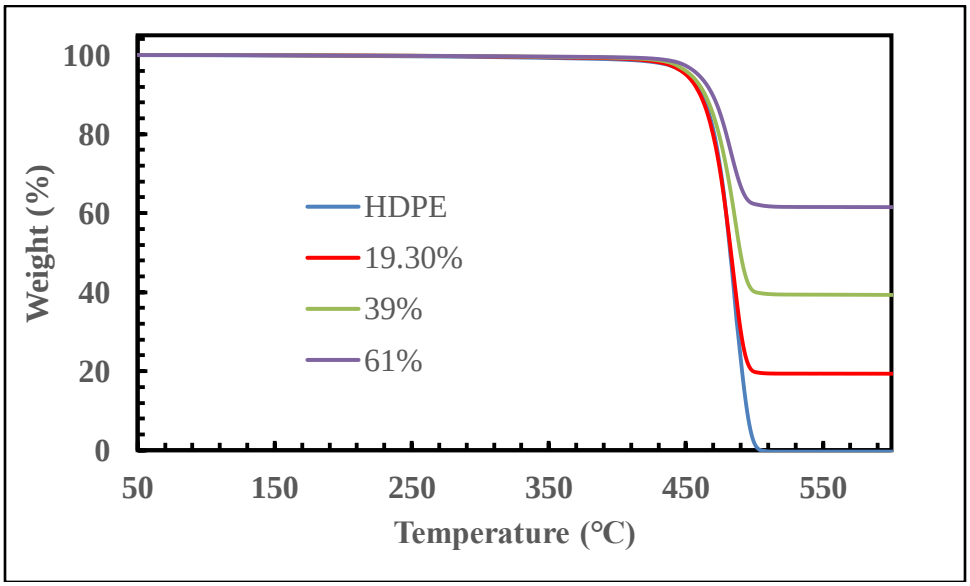

Fig. B. 18: TGA profiles of h-BN6/HDPE composites of various h-BN loading (wt. %).

Mechanical Properties

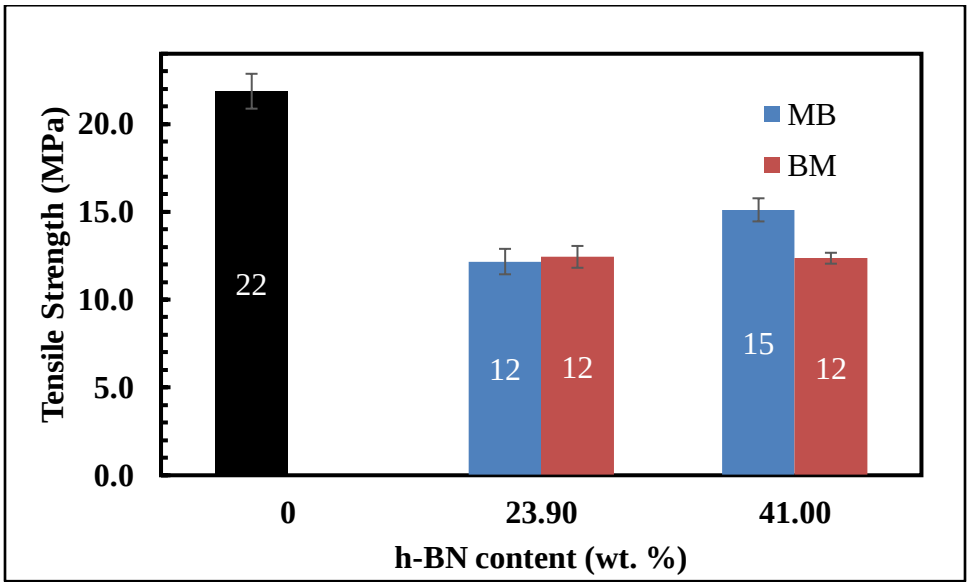

Fig. B. 19: The tensile strength of h-BN35/LLDPE composites prepared by MB and BM methods.

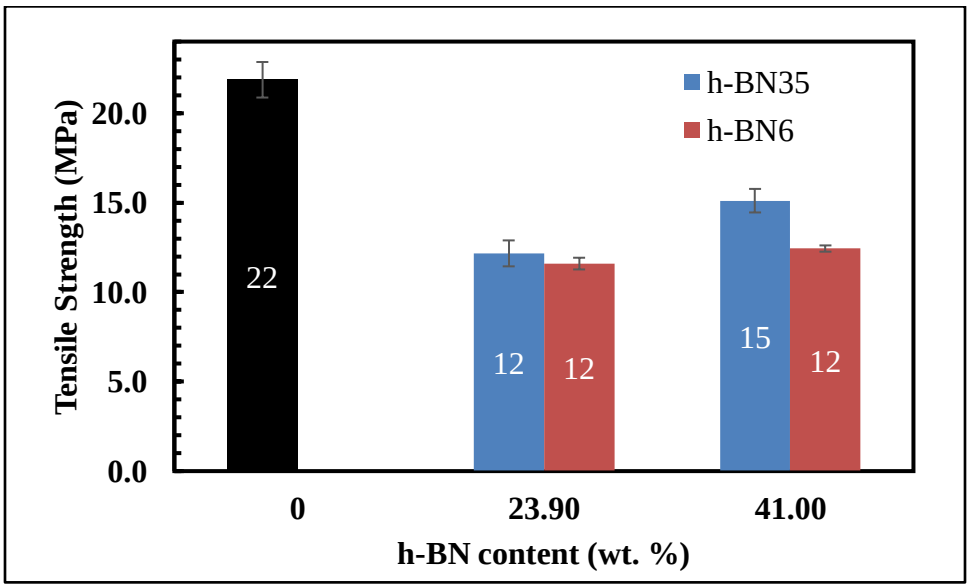

Fig. B. 20: The tensile strength of h-BN35/LLDPE and h-BN6/LLDPE composites.